Development of CRISPR/Cas9 Mediated *In Vivo* Gene-Editing Therapy for Cardiovascular Disease

by

Zhuoying Ren

A dissertation submitted in partial fulfillment
of the requirements for the degree of
Doctor of Philosophy
(Pharmacology)
in the University of Michigan
2026

Doctoral Committee:

Professor Y Eugene Chen, Co-Chair
Professor Jie Xu, Co-Chair
Assistant Professor Matthew Brody
Professor Liangyou Rui

Zhuoying Ren

zhuoyren@umich.edu

ORCID iD: 0000-0003-2217-8232

© Zhuoying Ren 2026

Acknowledgements

Undertaking a PhD has been the most intellectually challenging and personally transformative journey of my life. I am truly grateful to all the remarkable individuals who have supported me along the way.

First, I would like to thank my advisors Dr. Y Eugene Chen and Dr. Jie Xu for their dedicated mentorship throughout my PhD. They provided comprehensive and rigorous training covering every stage of doing research: from experimental design and troubleshooting to data analysis and scientific writing. I have benefited a lot from their profound knowledge, professional guidance and patience.

My dissertation committee members, Dr. Matthew Brody, Dr. Liangyou Rui and Dr. Charles Bisgaier have supported me throughout my doctoral studies over the years. I am grateful for their sustained commitment and insightful feedback that elevated the quality of my research.

I want to acknowledge my lab mates for creating a collaborative environment. A special thanks to Dr. Jifeng Zhang and Dr. Yanhong Guo for their tremendous help with the cardiovascular disease research that forms a substantial part of this thesis. Their generosity with their time and knowledge is appreciated. I also want to thank Dr. Guizhen Zhao, Dr. Yang Zhao, Dr. Yaozhong Liu, Ying Zhao, Dr. Linyuan Ma, Dr. Dongshan Yang, Jun Zhou, Dr. Zhuying Wei and Dr. Zhenguo Wang for their diverse expertise that contributed to my projects.

The collective kindness from the entire Department of Pharmacology played a significant role in my academic and personal growth. I am grateful to Dr. Lori Isom, our department Chair,

for her consistent leadership and support over the years. I would like to thank both current and past PhD program coordinators Dr. Paul Jenkins, Dr. Emily Jutkiewicz and Dr. Margaret E. Gnegy for their help to overcome many of the challenges I faced during my PhD studies. My appreciation goes to Dr. Stephen Fisher for his warm encouragement and support since my master's studies and continued. I would also like to thank Sondra Auerbach for her administrative support and her willingness to patiently answer countless questions.

Finally, I am deeply thankful to my family for their steadfast love, encouragement and support throughout not only the pursuit of this degree but my entire life.

Table of Contents

Acknowledgements ii

List of Tables ix

List of Figures x

Abstract xiii

Chapter 1 Introduction 1

1.1 Acknowledgement 1

1.2 Overview 1

1.3 Gene editing tools 5

1.3.1 Zinc-finger nucleases 7

1.3.2 Transcription activator-like effector nucleases 7

1.3.3 CRISPR/Cas9 7

1.3.4 Nuclease-inactive Cas9 variants 8

1.3.5 Base editors 8

1.3.6 PRIME editors 11

1.4 GETx Strategies 13

1.4.1 Gene disruption 15

1.4.2 Point mutation 15

1.4.3 Large size gene knock-In 16

1.5 Delivery considerations 17

1.5.1 Adeno-associated Virus 19

1.5.2 Lentivirus 20

1.5.3 Adenovirus 21
1.5.4 Lipid Nanoparticles 22
1.5.5 Virus Like Particles 25
1.6 Genes of interest in LivGETx-CVD 25
1.6.1 PCSK9 29
1.6.2 ANGPTL3 34
1.6.3 CETP 37
1.6.4 ApoC3 39
1.6.5 ASGR1 42
1.6.6 LPA 44
1.6.7 IDOL 46
1.6.8 General limitations of these trials 48
1.7 Conclusions 49
Chapter 2 ASGR1 Knockdown via CRISPR/Cas9 Improves Glucose Homeostasis and Reduces Atherosclerosis in *ApoE*$^{-/-}$ Mice 50
2.1 Introduction 50
2.2 Materials and methods 51
2.2.1 Animals 51
2.2.2 Cell culture and transfection 52
2.2.3 Generation of Adenovirus particles and administration into mice 52
2.2.4 PCR and primers 53
2.2.5 T7EI assay 53
2.2.6 Deep sequencing (deep-seq) and analysis 54
2.2.7 Quantitative real-time PCR (qPCR) analysis 54
2.2.8 Droplet Digital PCR (ddPCR) 57
2.2.9 Western blot analysis 57

2.2.10 Serum analysis 58

2.2.11 Liver cholesterol and triglycerides measurement 58

2.2.12 Insulin tolerance and glucose tolerance test 59

2.2.13 Oil Red O (ORO) staining of the aorta trees 59

2.2.14 Statistical Analysis 60

2.3 Results 60

2.3.1 In vitro validation of Asgr1-targeting gRNAs 60

2.3.2 Construction of Adv-Cas9-Asgr1 to disrupt Asgr1 in vivo 64

2.3.3 Adv-Cas9-Asgr1 effectively knockdown ASGR1 in ApoE$^{-/-}$ mice 65

2.3.4 Adv-Cas9-Asgr1 led to reduction of total cholesterol levels 69

2.3.5 Adv-Cas9-Asgr1 mediated ASGR1 knockdown attenuated atherosclerosis in ApoE$^{-/-}$ mice 73

2.3.6 Adv-Cas9-Asgr1 mediated ASGR1 knockdown improves insulin sensitivity 77

2.3.7 Adv-Cas9-Asgr1 mediated ASGR1 knockdown reduces body weight and adipose tissue mass 82

2.3.8 Minimal liver toxicity by Adv-Cas9-Asgr1 treated animals 85

2.4 Discussion 88

Chapter 3 AAV-Mediated *Idol* Gene Disruption Does Not Confer Atheroprotection in *ApoE*$^{-/-}$ Mice 91

3.1 Introduction 91

3.2 Materials and methods 93

3.2.1 Animals 93

3.2.2 Plasmid construction 93

3.2.3 Generation of AAV particles and administration into mice 93

3.2.4 Cell culture and transfection 94

3.2.5 PCR and primers 95

3.2.6 T7EI assay 96
3.2.7 Deep sequencing (deep-seq) and analysis 96
3.2.8 TA cloning 96
3.2.9 Quantitative real-time PCR (qPCR) analysis 97
3.2.10 Western blot analysis 97
3.2.11 Serum analysis 98
3.2.12 Oil Red O (ORO) staining of the aorta trees 98
3.2.13 Fluorescence microscopy 99
3.2.14 Statistical Analysis 99
3.3 Results 100
3.3.1 In vitro validation of Idol-targeting gRNAs 100
3.3.2 Effects of dual AAV vectors mediated Idol disruption in C57 mice 106
3.3.3 Effects of single AAV vector mediated Idol disruption in Rosa26-spCas9 KI mice 110
3.3.4 Efficacy evaluations of AAV8-U6-msgL3-msgR3 to target Idol in ApoE$^{-/-}$/Cas9-KI mice 112
3.3.5 Safety evaluations of AAV8-U6-msgL3-msgR3 to target Idol in ApoE$^{-/-}$/Cas9-KI mice 122
3.4 Discussion 126
Chapter 4 Summary and Perspectives 129
4.1 A summary of ASGR1 and IDOL projects 129
4.2 Promises of GETx-CVD informed by the ASGR1, IDOL projects, and the literature 134
4.3 Technical challenges for GETx-CVD 136
4.4 Ethical considerations: from individual to civilization 138
4.5 Lessons learned and future directions, the next 5, 10, and 20 years from 2026 140
4.6 Concluding remarks 142

Bibliography 143

List of Tables

Table 1.1: Primary features of major potential delivery systems to achieve LivGETx-CVD. 18

Table 1.2: Summary of loss of function effects of targeted genes. 24

Table 1.3: Summary of active LivGETx-CVD trials as of November 1, 2025. 28

Table 2.1: PCR primer sequences. 53

Table 2.2: qPCR primer sequences. 56

Table 2.3: Information of off-target sites by sg1 and sg3. 62

Table 3.1: PCR primer sequences. 95

Table 3.2: qPCR primer sequences. 97

Table 3.3: *In vivo* off-target activity analysis. 123

Table 4.1: Comparison of targeting strategies of ASGR1 and IDOL 132

List of Figures

Figure 1.1: Illustration of LivGETx-CVD. 4

Figure 1.2: Illustration of ZFN, TALEN and CRISPR-Cas9 and their shared downstream DNA repair pathways: HDR and NHEJ. 6

Figure 1.3: Illustration of Adenine base editor (ABE) and Cytosine base editor (CBE). 10

Figure 1.4: Illustration of PRIME editor. 12

Figure 1.5: Illustration of therapeutic strategies: gene disruption, point mutation, and large size gene knock-in. 14

Figure 1.6: Illustration of key targets and their mechanistic pathways in LivGETx-CVD. 27

Figure 2.1: Validation of *Asgr1* targeting guide RNAs. 63

Figure 2.2: Illustration of the *in vivo* experiment. 66

Figure 2.3: Adv-Cas9-Asgr1 mediated ASGR1 knockdown at $3x10^{10}$ vg/animal dose *in vivo*.. 67

Figure 2.4: Adv-Cas9-Asgr1 mediated ASGR1 knockdown at $5x10^{9}$ vg/animal dose *in vivo*. .. 68

Figure 2.5: Adv-Cas9-Asgr1 treatment at $3x10^{10}$ vg/animal dose reduced total cholesterol (TC) levels in *ApoE*$^{-/-}$ mice. 70

Figure 2.6: Adv-Cas9-Asgr1 treatment at $5x10^{9}$ vg/animal dose reduced total cholesterol (TC) levels in *ApoE*$^{-/-}$ mice. 71

Figure 2.7: Effects of Adv-Cas9-Asgr1 on the levels of triglycerides (TG) in *ApoE*$^{-/-}$ mice. 72

Figure 2.8: Adv-Cas9-Asgr1 at $3x10^{10}$ vg/animal dose reduced the extent of atherosclerosis in *ApoE*$^{-/-}$ mice. 74

Figure 2.9: Adv-Cas9-Asgr1 treatment at $5x10^{9}$ vg/animal dose reduced the extent of atherosclerosis in *ApoE*$^{-/-}$ mice. 75

Figure 2.10: Effects of Adv-Cas9-Asgr1 on atherosclerosis related gene expressions in the liver of *ApoE*$^{-/-}$ mice. 76

Figure 2.11: Adv-Cas9-Asgr1 treatment at $3x10^{10}$ vg/animal dose improved insulin sensitivity in *ApoE*$^{-/-}$ mice. 79

Figure 2.12: Adv-Cas9-Asgr1 treatment at $5x10^9$ vg/animal dose improved insulin sensitivity in *ApoE*$^{-/-}$ mice. 80

Figure 2.13: Effects of Adv-Cas9-Asgr1 on insulin sensitivity related protein expressions. 81

Figure 2.14: Adv-Cas9-Asgr1 treatment at $3x10^{10}$ vg/animal dose reduced body weight and adipose tissue mass in *ApoE*$^{-/-}$ mice. 83

Figure 2.15: Adv-Cas9-Asgr1 treatment at $5x10^9$ vg/animal dose reduced body weights of *ApoE*$^{-/-}$ mice. 84

Figure 2.16: Minimal liver toxicity by Adv-Cas9-Asgr1 at $3x10^{10}$ vg/animal dose in *ApoE*$^{-/-}$ mice. 86

Figure 2.17: Minimal liver toxicity by Adv-Cas9-Asgr1 treatment at $5x10^9$ vg/animal dose to *ApoE*$^{-/-}$ mice. 87

Figure 3.1: *In vitro* validation of *IDOL*-targeting gRNAs in human cells. 103

Figure 3.2: *In vitro* validation of *Idol*-targeting gRNAs in rabbit cells. 104

Figure 3.3: *In vitro* validation of *Idol*-targeting gRNAs in mouse cells. 105

Figure 3.4: Optimization of *in vivo* AAV delivery strategy by comparing different AAV serotypes and promoters. 108

Figure 3.5: Effects of dual AAV vectors mediated *Idol* disruption in C57 mice. 109

Figure 3.6: Editing outcomes of single AAV vector mediated *Idol* disruption in *ApoE*$^{-/-}$/Cas9-KI mice 111

Figure 3.7: Genotyping of *ApoE*$^{-/-}$/Cas9-KI mice. 115

Figure 3.8: Evaluations of AAV8-U6-msgL3-msgR3 mediated *Idol* gene disruption in *ApoE*$^{-/-}$/Cas9-KI mice. 116

Figure 3.9: IDOL target proteins expression levels. 118

Figure 3.10: Total cholesterol (TC) and triglyceride (TG) levels of AAV8-U6-msgL3-msgR3 mediated *Idol* disruption in *ApoE*$^{-/-}$/Cas9-KI mice. 119

Figure 3.11: LDL and HDL levels of AAV8-U6-msgL3-msgR3 mediated *Idol* disruption in *ApoE*$^{-/-}$/Cas9-KI mice. 120

Figure 3.12: Evaluation of the extent of atherosclerosis development in the female animals treated with AAV8-U6-msgL3-msgR3 121

Figure 3.13: Liver and renal toxicity analysis. 124

Figure 3.14: Safety evaluations of AAV8-U6-msgL3-msgR3 to target *Idol* in *ApoE*$^{-/-}$/Cas9-KI mice. 125

Abstract

Cardiovascular disease (CVD) remains a leading cause of morbidity and mortality worldwide. Recent advances in gene editing technologies offer potentially curative and preventative therapies for its management. State-of-the-art gene editing tools including zinc finger nucleases (ZFNs), transcription activator-like effector nucleases (TALENs), CRISPR/Cas9 systems, base editors, and prime editors have enabled precise modulation of lipid metabolic pathways central to CVD pathogenesis. Key therapeutic targets such as *PCSK9, ANGPTL3, CETP, APOC3, ASGR1, LPA*, and *IDOL* have been identified, with promising results in human genetics, preclinical models, and early clinical trials. Liver-targeted *in vivo* editing modalities (LivGETx-CVD) employing advanced delivery vehicles such as adeno-associated viruses (AAVs), lipid nanoparticles (LNPs), lentiviruses, and virus-like particles (VLPs) have accelerated translation of research towards clinical trials.

In this thesis, two gene editing strategies were explored for therapeutic impact in mouse models of atherosclerosis. First, CRISPR/Cas9-based disruption of hepatic *Asgr1*, delivered via adenoviral vectors, conferred robust therapeutic benefits in ApoE knockout ($ApoE^{-/-}$) mice on a Western diet. Up to 80% reduction in ASGR1 protein led to marked decreases in serum and hepatic cholesterol, reduction in aortic plaque burden, improved insulin sensitivity and adiposity. Importantly, the approach demonstrated a favorable safety profile, with no overt liver toxicity or adverse effects on organ function.

By contrast, AAV8 mediated CRISPR/Cas9 disruption of *Idol* in an *ApoE*$^{-/-}$ mouse line that consecutively expresses Cas9 (*ApoE*$^{-/-}$/Cas9-KI) resulted in efficient hepatic gene disruption; however, such genetic editing did not increase LDL receptor expression or significantly reduce plasma cholesterol and triglycerides, nor did it substantially decrease atherosclerotic plaque burden. Liver safety assessments indicated minimal off-target effects and no toxicity, suggesting that hepatic *Idol* disruption alone may be insufficient for atheroprotection in mice, likely reflecting species-specific differences in IDOL function.

Together, these findings highlight both the promise and complexity of gene editing therapy for CVD. While some targets yielded ineffective atheroprotection upon disruption (as observed with *Idol*), others such as *Asgr1* offered multi-dimensional benefits for lipid and metabolic regulation, as well as atheroprotection. These results support continued refinement and translational development of liver-directed gene editing strategies, emphasizing careful target selection and preclinical validation. Collectively, gene editing holds great potential to redefine the prevention and long-term management of CVD.

Chapter 1 Introduction

1.1 Acknowledgement

This chapter contains work previously published in the *Cells* under the Creative Commons Attribution (CC BY) license.[1]

J.X. and Y.E.C. conceived the idea. Z.R., J. Zhou, D.Y., Y.G., J. Zhang, J.X. and Y.E.C. wrote the manuscript.

1.2 Overview

The past decade has witnessed rapid advances in gene editing technologies. In 2020, the Nobel Prize in Chemistry is awarded to Drs. Charpentier and Doudna for their contributions in the development of CRISPR/Cas9 (Clustered Regularly Interspaced Short Palindromic Repeats/CRISPR-associated protein-9), the dominant gene editing nuclease (GENs) that is used nowadays (*1*). Today, gene editing is widely used in research and is being explored in therapeutics. Gene editing therapy, referred to as GETx in this article, offers new options for treating, and maybe curing many diseases, including genetic diseases, infectious diseases, and cancer.

Cardiovascular disease (CVD) remains one of the most significant health challenges worldwide, accounting for one-third of all global deaths and resulting in more than 17 million

[1]Ren Z, Zhou J, Yang D, Guo Y, Zhang J, Xu J, Chen YE. Gene Editing Therapies Targeting Lipid Metabolism for Cardiovascular Disease: Tools, Delivery Strategies, and Clinical Progress. *Cells*. 2026; 15(2):134. PMID: 41597209.

fatalities annually (*2*). Elevated levels of circulating low-density lipoprotein cholesterol (LDL-C) have been identified as a major risk factor for CVD, as established by the Framingham Heart Study, a landmark longitudinal investigation into cardiovascular risk factors (*3*). Similarly, elevated triglyceride (TG) levels are positively associated with an increased risk of atherosclerosis and cardiovascular diseases (*4*). While current first-line therapies such as statins and emerging medicines such as PCSK9 (proprotein convertase subtilisin/kexin type 9) monoclonal antibodies, are effective in slowing the progression of coronary artery disease in many (*5*-*7*), a considerable subset of patients do not benefit, due to reasons such as drug intolerance, fear of side effects, genetic factors affecting drug response, and non-adherence driven by prior medication experiences or aversion to drugs. As a result, there is a critical unmet need for innovative cardiovascular treatments that can more effectively lower disease risk while minimizing the burden of long-term medication adherence. New technologies such as gene editing, as we will see soon, are paving the way toward solutions that require fewer doses, offering hope for more sustained protection and improved patient quality of life.

Gene editing tools, represented by CRISPR/Cas9, hold promise for delivering new therapeutic solutions for many human diseases. The question whether GETx can be employed for treating cardiovascular diseases (GETx-CVD) was raised in 2014, one year after Cas9 debuted (*8*). CVD, like many other diseases, is genetically predisposed; hence, modifying the gene(s) "for the good" may bring therapeutic benefits (*9, 10*). The approach is conceptually simple: (i) first, identify a gene whose loss-of-function mutation provides cardioprotective effects; these genes are often involved in lipid metabolism (*9*). (ii) Next, employ gene editing technologies such as CRISPR/Cas9, or its advanced iterations like base or prime editors or other editing tools, to introduce these beneficial mutations. (iii) Such intervention confers a lasting reduction in

cardiovascular disease risks. Analogous to vaccination, a single administration ideally provides long-term protection, leading some to refer to such strategy as a form of “CVD vaccination” (*11*), as illustrated in Figure 1.1.

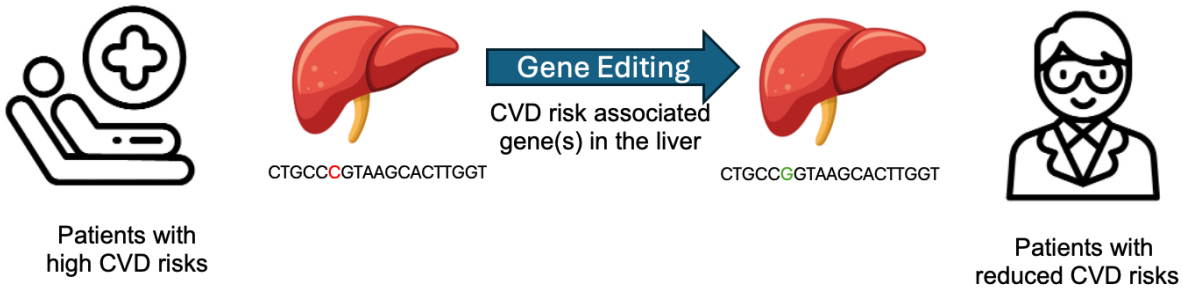


Figure 1.1: Illustration of LivGETx-CVD.

Gene editing on CVD risk associated gene(s) in the liver is a “one-shot, one cure” therapy. A single administration is expected to provide long-term therapeutic protection.

In this review, we first introduce the major gene editing tools and recent advances in *in vivo* delivery platforms. We then highlight key genetic targets for GETx-CVD. One of the best-characterized domains in cardiovascular genetics is how genes that regulate cholesterol and triglyceride metabolism and homeostasis drive atherosclerosis and downstream cardiovascular diseases. Principal players include low-density lipoprotein receptor (*LDLR*), proprotein convertase subtilisin/kexin type 9 (*PCSK9*), apolipoprotein B (*APOB*), inducible degrader of LDLR (*IDOL*), asialoglycoprotein receptor 1 (*ASGR1*), angiopoietin-like 3 (*ANGPTL3*), apolipoprotein C3 (*APOC3*), and lipoprotein(a) (*LPA*), which are all liver-specific or liver-relevant. We refer to GETx-CVD strategies directed at these hepatic lipid-metabolism genes as LivGETx-CVD and provide a focused review of their biological rationale and therapeutic potential. Finally, we summarize ongoing LivGETx-CVD clinical trials targeting these pathways.

1.3 Gene editing tools

Gene editing nucleases (GENs), represented by Zinc Finger Nuclease (ZFN), Transcription Activator-Like Effector Nuclease (TALEN), and CRISPR/Cas9 have become major tools in biomedical research (*12*). ZFN, TALEN and CRISPR/Cas9 are all capable in generating double-strand breaks (DSB) at specific genomic loci in a programmable (so-called customizable) manner (Figure 1.2). These tools opened the era of gene editing. In recent years, base editors (BEs) and PRIME editors (PEs) have emerged as prominent tools in both research and clinical applications. Here we provide a brief introduction of these tools. Comprehensive reviews of gene editing tools, including other recent developments, are available elsewhere (*13, 14*).

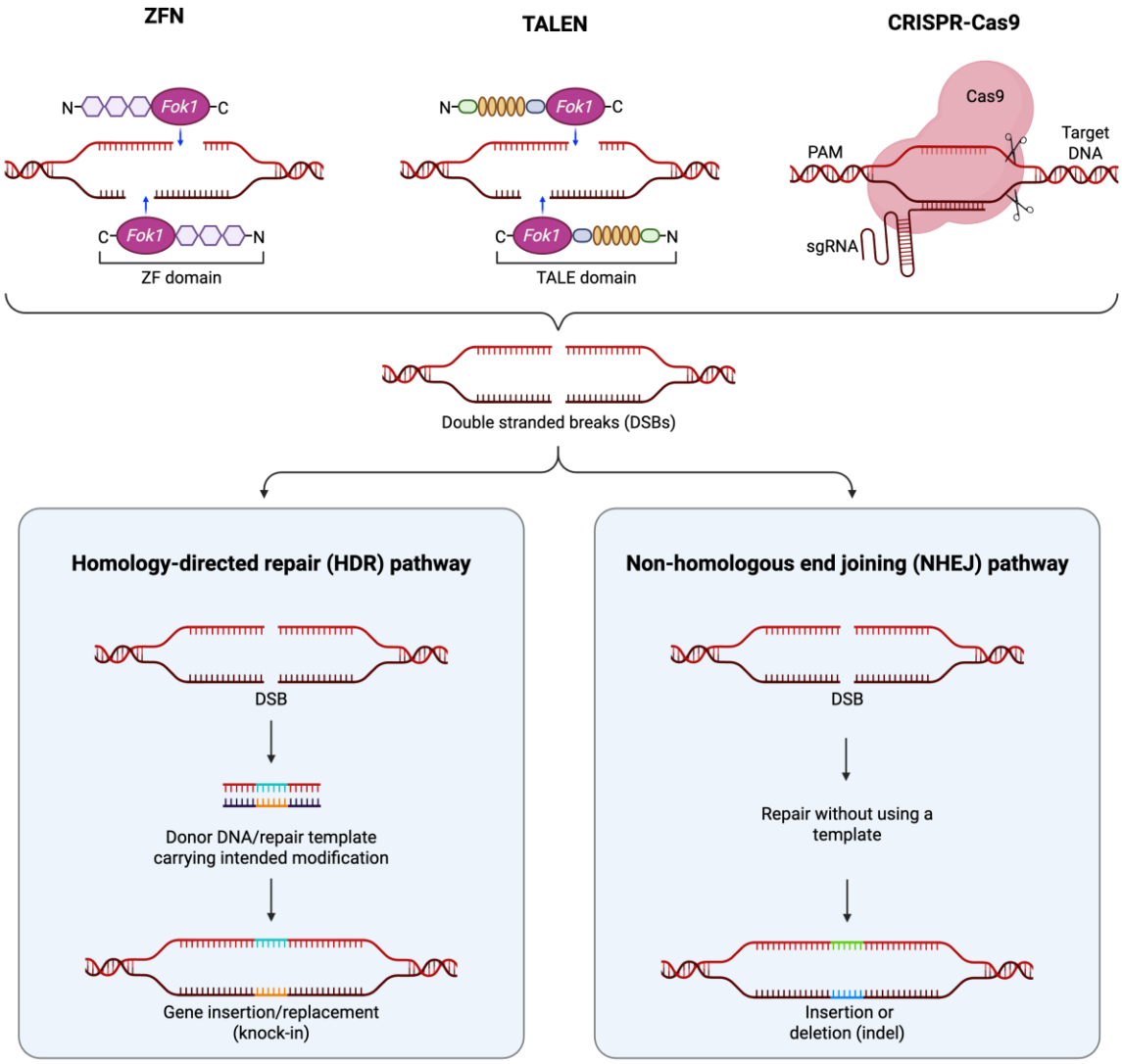


Figure 1.2: Illustration of ZFN, TALEN and CRISPR-Cas9 and their shared downstream DNA repair pathways: HDR and NHEJ.

ZFN, TALEN and CRISPR-Cas9 are all capable of generating DNA double stranded breaks (DSBs), which are repaired by two major pathways: the homology directed repair (HDR) utilizing endogenous or user-supplied donor template for precise repair; and the non-homologous end joining (NHEJ) which is error-prone and introduces insertion and deletion (indel) edits. Modified from reference (*15, 16*) and created in BioRender. Xu, J. (2025).

1.3.1 Zinc-finger nucleases

ZFN is the first generation GEN, which became commercially available in the early 2000s. A ZFN pair are comprised of two different zinc finger proteins (DNA-binding domains) each linked with a Fok I endonuclease domain (*17*). In the most common practice, a zinc finger domain would consist of 6 tandem fingers, each recognizing 3 bp of DNA, to recognize an 18 bp long sequence. The two zinc finger domains lie in inverted orientation, such that the two FokI endonuclease domains would form a functional dimer to cleave the target DNA sequence.

1.3.2 Transcription activator-like effector nucleases

The TALEN is considered an upgraded version of programmable nucleases. Like ZFN, TALEN recognizes targeted DNA sequence through programmable protein domains, so called transcription activator-like effectors (TALEs), which were derived from Xanthomonas spp. bacteria (*18, 19*), and also uses the FokI pair as DNA scissors. Each TALE contains a repeated highly conserved 33–34 amino acid sequence with Repeat Variable Diresidue (RVD) at the 12th and 13th amino acid positions. The RVDs recognize specific nucleotides, for example, NN for guanine, NI for adenine, HD for cytosine and NG for thymine, etc. This straightforward relationship between amino acid sequence and DNA recognition in TALEN design has allowed for easier engineering of sequence specific binding domains than with ZFNs (*15, 16*).

1.3.3 CRISPR/Cas9

The CRISPR/Cas9 technology is the most recent version of the programmable genome editing nucleases. In its most popular format, the CRISPR/Cas9 ribonuclease complex consists of

a spCas9 protein and a single guide RNA (sgRNA). spCas9 recognizes and binds to a protospacer adjacent motif (PAM) sequence on the target DNA, initiating local DNA unwinding that allows the guide RNA to form a complementary RNA-DNA hybrid (R-loop) with the target sequence; upon complete base pairing, conformational changes activate the HNH and RuvC nuclease domains of spCas9, resulting in site-specific cleavage of both DNA strands three base pairs upstream of the PAM. One distinction of CRISPR/Cas9 from ZFN and TALEN is that CRISPR/Cas9 recognizes the target sequence through the RNA-DNA complementation. This feature makes CRISPR/Cas9 much easier and faster to design and engineer than the two prior versions which rely on protein-DNA recognitions.

1.3.4 Nuclease-inactive Cas9 variants

ZFN, TALEN and CRISPR/Cas9 are capable of generating DSBs. The DSBs are subsequently repaired by different pathways, with non-homologous end joining (NHEJ) as the dominant one, along with others such as homology-directed repair (HDR) and alternative NHEJ (alt-NHEJ), leading to different editing outcome (*20*). As its name suggests, NHEJ is imprecise and leads to undesired insertion and deletion (indel) events at the target site as well as the off-target sites throughout the genome. One strategy to mitigate the potential adverse effects of NHEJ is to prevent double-strand break (DSB) formation by using a nuclease-inactive Cas9 variant generated through mutating the HNH and/or the RuvC domains. The resulting deactivated Cas9 (dCas9) lacks endonuclease activity and does not generate DSBs at all, whereas the nickase Cas9 (nCas9) variant cleaves only a single strand of the DNA.

1.3.5 Base editors

Base editors were developed by fusing deaminases, such as cytidine deaminase APOBEC or adenine deaminase engineered TadA, with nuclease inactive Cas9 (*21-24*). The base editor ribonuclease complex is located to the target sequence with the help of the guide RNA, followed by the deaminase working to deaminate bases within the editing window. A cytidine base editor (CBE) converts C: G-to-T: A; whereas an adenine base editor (ABE) converts A: T-to-G: C. Other types of base editors capable of other types of base conversions and transversions have also been developed in recent years (*25-27*). Compared with the DSB-based editing method, the base editors provide a powerful route to efficiently install or correct point mutations with much less genotoxicity concerns. Figure 1.3 illustrates the two major types of BEs: CBE and ABE.

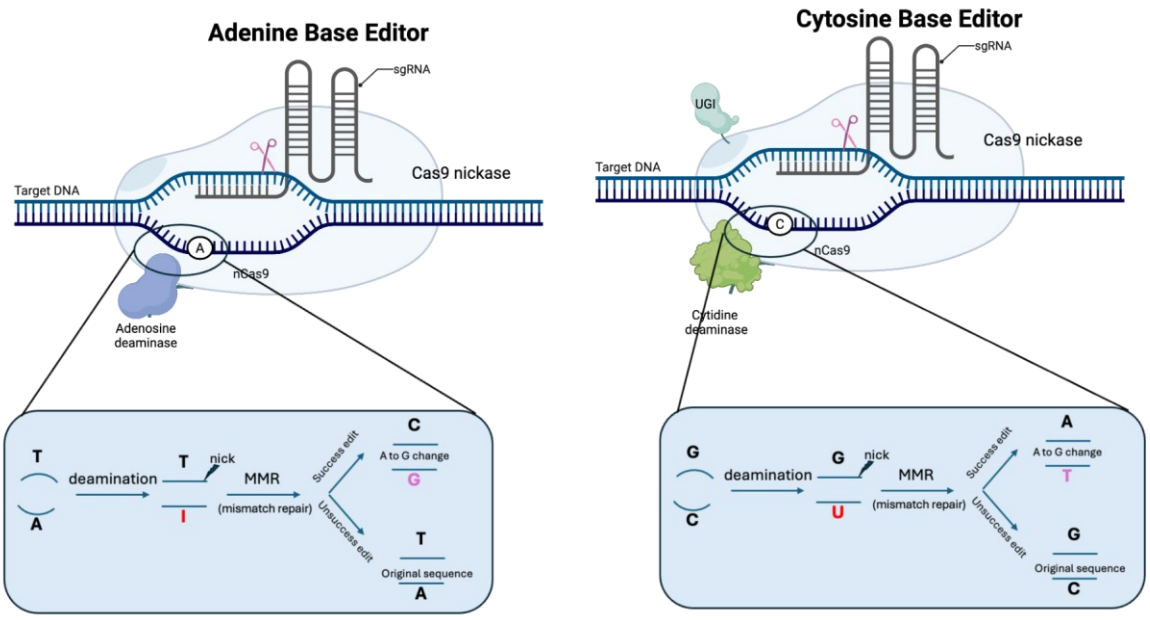


Figure 1.3: Illustration of Adenine base editor (ABE) and Cytosine base editor (CBE).

Base editors use Cas9 nickase (nCas9) to introduce single stranded breaks at the target strand, followed by the deaminase that is often fused to the N-terminus of Cas9 to edit the "A" (in ABE) or "C" (in CBE) that is within the editing window on the non-targeted strand. Base editors exploits the mismatch repair (MMR) mechanism to achieve the desired base editing outcome. UGI: Uracil Glycosylase Inhibitor. Created in BioRender. Xu, J. (2025).

1.3.6 PRIME editors

One limitation with base editors is that they can only install point mutations, but not other types of edits, for example insertions or deletions. The PRIME editors are developed to address such needs (*28, 29*). Like base editors, PRIME editors utilize nuclease defective Cas9, most cases Cas9 nickase, to avoid generating DSBs. Unlike base editors, the PRIME editor's fusion partner is a reverse transcriptase domain, and instead of using the sgRNA, as in Cas9 and Cas9 base editors, PRIME editors use a pegRNA. The pegRNA contains the guide RNA sequence to locate the complex to the target sequence; it also contains a reverse transcription (RT) template to introduce the edit, and a primer binding site (PBS) sequence where the reverse transcription initiates. PRIME editors can achieve versatile editing types, including insertion, deletion and point mutation, as long as such desirable changes are coded in the RT template. Figure 1.4 illustrates the PRIME editor working mechanism.

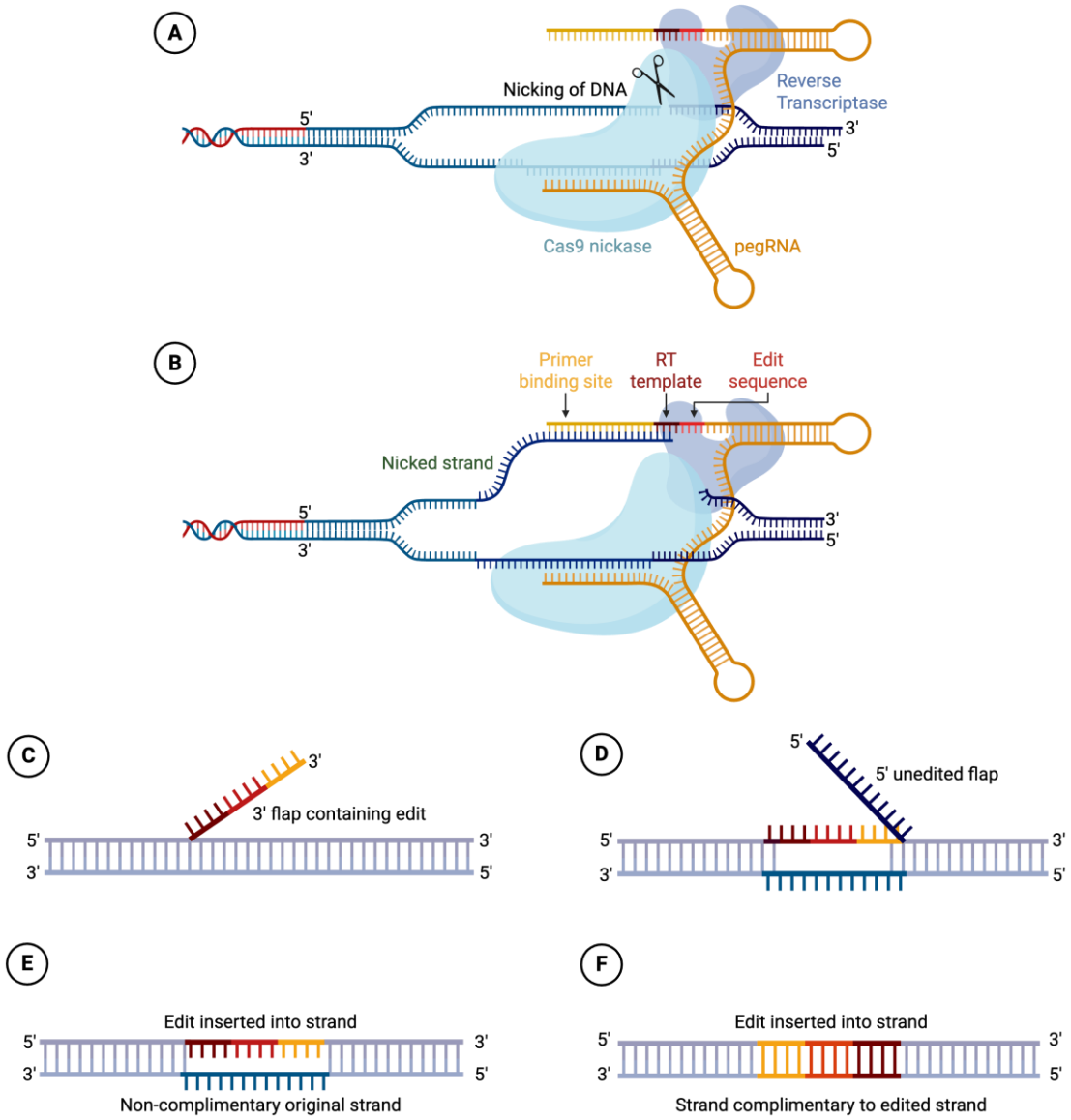


Figure 1.4: Illustration of PRIME editor.

Prime editor's protein part consists of a Cas9 nickase (nCas9) and a reverse transcriptase domain, and its pegRNA consists of the guide RNA sequence and additional sequences including the primer binding site, reverse transcription (RT) template and the edit sequence (A and B). After the nick is created, the RT is initiated by the reverse transcriptase to introduce the edit sequence into the 3' flap end at the target site (C), followed by additional steps to incorporate the edit into the genome (D to F). Modified from reference (*15, 16*) and created in BioRender. Xu, J. (2025).

1.4 GETx Strategies

The application of gene editing tools to cure or treat human diseases is referred to as GETx in this review. GETx can be broadly classified into three main categories (Figure 1.5) based on the specific editing type it exploits (*30*), each tailored to address different genetic etiologies and clinical needs: (i) loss of function editing; (ii) point mutation correction; and (iii) large size gene knock-in. In the context of LivGETx-CVD, the first two are of more relevance than the third one. This is because, as we shall see later in this review, investigators are mostly targeting genes whose loss-of-function mutation provides cardioprotective effects.

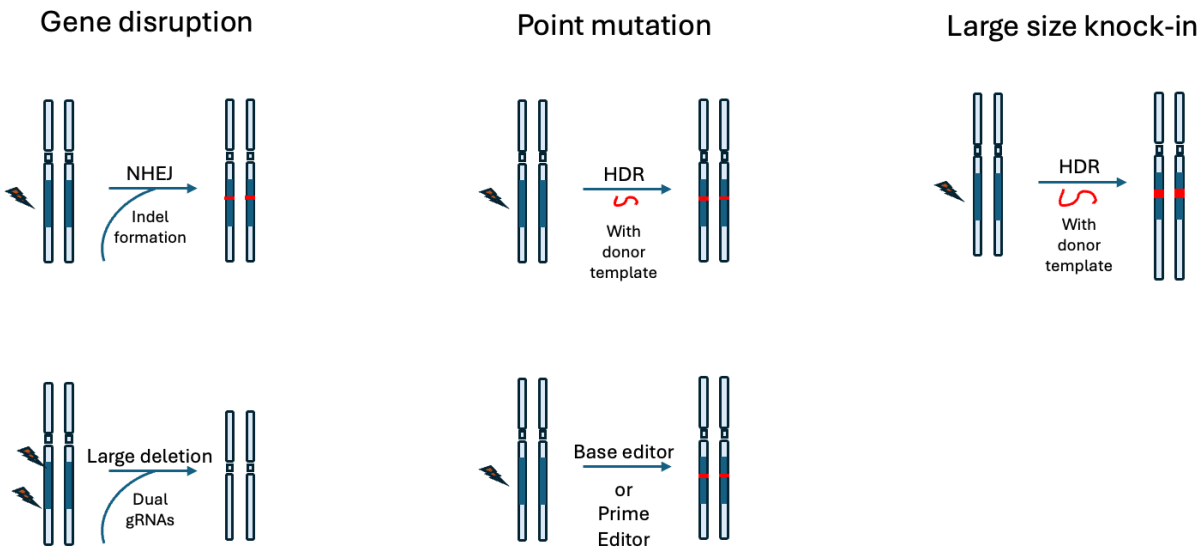


Figure 1.5: Illustration of therapeutic strategies: gene disruption, point mutation, and large size gene knock-in.

Left: gene disruption is often created by an indel mutation (top) or large deletion (bottom). Middle: point mutation is often created by HDR mediated mutation (top) or by base editor or prime editor (bottom). Right: large size gene knock-in is often created by HDR mediated knock-in.

1.4.1 Gene disruption

This approach inactivates or disrupts the function of a target gene, often to confer disease resistance or eliminate pathogenic gene activity. Clinically, for example, it has been utilized to knock out the C-C motif chemokine receptor 5 (*CCR5*) gene to provide human immunodeficiency virus (HIV) resistance or to disrupt programmed cell death 1 (*PD1*) in immune cells to enhance anti-tumor immunity (*31-33*).

Applicable editing strategies to achieve loss-of-function edits include: (i) small insertions or deletions (indels) resulting from NHEJ that leads to frameshift and consequently premature stop codons. This is often achieved by using spCas9 + sgRNA without any repair templates; (ii) large size deletions to remove one or more exons. This can be achieved by using spCas9 with two or more sgRNAs; (iii) point mutations at the splicing donor or acceptor site to disrupt normal splicing and consequently the reading frame, leading to loss of protein production or function. This can be achieved by using a Cas9 base editor + sgRNA, which we will introduce in a later session.

1.4.2 Point mutation

Precise point mutation represents a substantial percentage of clinical needs. This strategy is often used to repair pathogenic single-nucleotide variants or small mutations responsible for monogenic disorders. A classic example is the correction of the CFTR-F508del mutation in cystic fibrosis (*34, 35*), restoring normal protein function. Another example is to correct the E6V mutation in the hemoglobin subunit beta (HBB) gene to cure sickle cell disease (*36*).

Applicable editing strategies to achieve precise point mutation corrections include: (i) HDR, using canonical Cas9 + sgRNA along with double stranded or single stranded DNA donor

templates which harbors the correct/function sequence; (ii) base editor + sgRNA to install single-nucleotide substitutions (transition or transversion) for correction; (iii) prime editor + pegRNA to replace the pathogenic sequence in the genome with a repair template coded in the pegRNA.

1.4.3 Large size gene knock-In

Knock-in strategies to insert a functional gene or a super exon or other genetic element at a specific locus in the genome is another GETx strategy. It is often used to provide a "one size fits all" cure to a disease that could result from different types of mutations on the same gene. For example, knocking in a full-length, functional cystic fibrosis transmembrane conductance regulator gene (*CFTR*) can restore the channel activity and potentially cure the disease, regardless of which particular *CFTR* mutation a cystic fibrosis (CF) patient carries, which could be one of the several hundred CF causing mutations (*37*). In this way, instead of developing hundreds of mutation-specific GETx drugs, this one large size gene knock-in based GETx drug would suffice all.

Applicable editing strategies to achieve precise large-size gene knock-in include: (i) HDR, using canonical Cas9 + sgRNA along with donor templates that harbor the large-size knock-in sequence; (ii) Site-specific insertion of large-size gene fragment mediated by transposases, integrases, or recombinases or other methods, which are well reviewed in these publications (*14, 38, 39*).

1.5 Delivery considerations

How to efficiently and precisely deliver gene editing modalities to the target site *in vivo* has remained the paramount challenge in GETx. In this session, we provide an overview of current delivery options. Table 1.1 summarizes the primary features of these systems.

Table 1.1: Primary features of major potential delivery systems to achieve LivGETx-CVD.

Platform (reference)	Cargo Type	Cargo Size	Immunogenicity	Genome Integration	Tissue Tropism	Particle Size
AAV (*40*)	DNA	~4.7 kb	Low-moderate	Rare (episomal)	Broad, serotype-dependent	~20–25 nm
AdV (*41*)	DNA	~8–36 kb	High	No	Broad (liver, airway, etc.)	~70–100 nm
LV (*42*)	RNA (retroviral)	~8–10 kb	Moderate	Yes (integrates)	Broad, envelope-dependent	~80–120 nm
VLP (*43*)	Protein or peptide	Variable (<150 kDa protein typical)	Low	No	Customizable by engineering	~20–200 nm (system-dependent)
LNP (*44*)	DNA, mRNA, protein, or small molecules	Up to ~15 kb mRNA	Low-moderate	No	Liver primarily, or engineered targeting	~60–150 nm

1.5.1 Adeno-associated Virus

Adeno-associated viruses (AAVs) are non-enveloped viruses with a single-stranded DNA genome, flanked by inverted terminal repeats (ITRs) (*45*). The genome contains three main functional genes: Cap, which encodes the capsid proteins responsible for protecting the viral DNA and enabling cell attachment; AAP, which produces an assembly-activating protein supporting capsid assembly; and Rep, which is necessary for viral replication and packaging (*46, 47*).

Since the first AAV-based gene therapy drug Luxturna gained approval by FDA in 2017 (*48*), AAV has become the most widely used vector for delivering GETx components. This popularity is largely due to its good safety profile, high transduction efficiency to diverse tissues and low DNA integration into the host genome, instead typically persisting as an episome (*49*).

A major disadvantage of AAV is its limited packaging capacity of only 4.7 kb. This challenges the delivery of large gene editors such as spCas9, base editors, and prime editors that are unable to fit inside a single AAV vector. There are several methods to address the size limitation. The intein-split dual-AAV system is a prominent example, where large gene editing nucleases are split into two halves, fused to split inteins, and delivered in separate AAV vectors (*50*). After entry into the same cell, protein splicing by inteins allows reconstitution of the full-length gene editor. This technique has demonstrated robust editing efficiencies across various organs such as the liver, retina, brain, heart, and skeletal muscle (*51, 52*). In addition, advances in the discovery of smaller Cas orthologs now allow efficient single-AAV delivery. Cas9 variants such as SaCas9 (*53*), Nme2Cas9 (*54*), CjCas9 (*55*), and SauriCas9 (*56*) are further expanding the toolbox.

Another clinically relevant consideration is patients' pre-existing immunity to natural AAV serotypes, especially at high doses (*57*). To overcome these immune barriers, strategies have been developed, including engineering capsids with reduced immunogenicity, employing immune evasion strategies, and using plasmapheresis to lower neutralizing antibody levels (*58-61*).

1.5.2 Lentivirus

As single-stranded RNA viruses, lentiviruses (LVs) carry the enzymes reverse transcriptase, integrase, and protease, which facilitate the reverse transcription and integration of their RNA cargo into the host genome. Due to the large packaging capacity (up to 10 kb), long term expression and low immunogenicity, LVs are widely used for ex vivo gene delivery, most notably in hematopoietic stem cells (HSCs) and T cells.

To date, four lentiviral gene therapies have received FDA approval: Zynteglo (for severe β-thalassemia) (*62*), Skysona (for cerebral adrenoleukodystrophy) (*63*), Lenmeldy (for early metachromatic leukodystrophy) (*64*) and Lyfgenia (for sickle cell disease) (*65*). They all utilized ex vivo modification of patient-derived HSCs followed by reinfusion. Additionally, several FDA approved CAR-T therapies, including Tisagenlecleucel (*66*) for leukemia; Axicabtagene ciloleucel (*67*), Brexucabtagene autoleucel (*68*) and Lisocabtagene maraleucel (*69*) for lymphomas, use lentiviral vectors for gene delivery to T cells.

The ability of lentiviruses to integrate their genetic payload into the host genome is highly advantageous for ex vivo applications because it ensures stable and long-term gene expression. However, this same characteristic poses safety concerns for *in vivo* use, as integration may result in insertional mutagenesis or off-target effects. To address these risks,

integrase-deficient lentiviral vectors (IDLVs) have been engineered so that the delivered genetic material persists episomally rather than integrating into the host DNA (*70*). While IDLVs significantly lower integration rates, they are not entirely free from residual integration events and can still drive prolonged transgene expression (*71*), which limit the use of LVs for *in vivo* gene editing applications.

1.5.3 Adenovirus

Adenoviruses (Adv) are non-enveloped viruses with a double-stranded DNA genome. They have large cargo capacity (8-9 kb), high transduction efficiency, transient gene expression, and low integration into the host genome. Owing to these advantages, Adv vectors have been employed for *in vivo* gene delivery since the early 1990s with initial studies targeting alpha-1 antitrypsin deficiency (*72*) and cystic fibrosis (*73*).

However, the clinical development of Adv gene therapies has been significantly hampered by safety concerns. Notably, a 1993 clinical trial for ornithine transcarbamylase (OTC) deficiency resulted in fatal multisystem organ failure in one participant, and other subjects experienced serious complications, such as acute elevations in hepatic transaminase, hypophosphatemia, and thrombocytopenia (*74*). To address these risks, researchers are investigating several strategies. For example, administration of anti-inflammatory agents such as dexamethasone can ease inflammatory responses and increase tolerance to the vector (*75*). Chemical modification of the viral capsid, for instance, by attaching synthetic polymers (*76*), can help shield the virus from immune detection. Furthermore, genetic alterations of the capsid structure (*77*) can reduce immune recognition and enable more durable expression of the therapeutic gene.

1.5.4 Lipid Nanoparticles

Lipid nanoparticles (LNPs) have emerged as a widely used nonviral vector for gene editing agents. LNPs are fully synthetic and generally constructed from four components: (i) ionizable cationic lipids are critical both for encapsulating negatively charged cargos through electrostatic interactions and facilitating endosomal escape; (ii) helper phospholipids are mostly found in the outer layer and enhance structural stability, nanoparticle integrity and membrane interactions; (iii) cholesterol fills gaps between phospholipids, boosting nanoparticle stability, integrity, and membrane fusion during cell entry and intracellular trafficking; and (iv) PEG-lipids are coated on nanoparticle surface, reducing aggregation, improving particle stability and half-life and lowering immunogenicity (*78*).

LNPs can encapsulate and deliver DNA, RNA, and protein cargos, with RNA delivery being the most established. LNPs deliver their payloads by entering cells via endocytosis, after which cargo release into the cytosol relies primarily on endosomal escape (*79*).

LNPs provide several advantages over viral vectors for GETx delivery which include the transient expression duration and the flexibility in cargo size. Further, most LNP components are biodegradable and well-tolerated *in vivo*. However, a notable challenge remains: the efficiency of endosomal escape remains low, as cargos trapped in endosomes are often destined for lysosomal degradation (*79*). To overcome this, ongoing research explores optimized particle compositions, surface modifications by adding cell penetrating peptides (*80*) and external triggers (like light or ultrasound) to trigger cargo release at the desired time (*81*).

Clinically, LNPs have enabled major advances, including the FDA-approved siRNA therapy for hereditary transthyretin (ATTR) amyloidosis (*82*), and the mRNA COVID-19

vaccines from Pfizer-BioNTech and Moderna (*83, 84*). Ongoing trials using LNPs for gene editing therapies are summarized in Table 1.2.

Table 1.2: Summary of loss of function effects of targeted genes.

Gene	Key mechanism exploited in LivGETx-CVD	Hypothesized Loss of function effects in LivGETx-CVD
PCSK9	Degrade LDLR	Retention of LDLR → reduced cholesterol in the blood→ less CVD risks
ANGPTL3	Inhibit LPL	Less inhibition of LPL → increased digestion of triglycerides → reduced triglycerides levels in the blood→ less CVD risks
CETP	Convert HDL to LDL	Less conversion of HDL to LDL → increased HDL-C and decreased LDL-C levels in the blood→ less CVD risks
APOC3	Inhibit LPL	Less inhibition of LPL → increased digestion of triglycerides → reduced triglycerides levels in the blood→ less CVD risks
ASGR1	Inhibition of ASGR1 promotes bile excretion	Upregulation of reverse cholesterol transport → increased cholesterol excretion through feces → reduced cholesterol levels→ less CVD risks
LPA	Pro-inflammation	Less inflammation→ less CVD risks
IDOL	Degrade LDLR	retention of LDLR → reduced cholesterol→ less CVD risks

1.5.5 Virus Like Particles

Engineered virus-like particles (eVLPs) are constructed from retroviral capsid proteins but they do not contain the viral genome, which makes them non-replicative and incapable of integrating into the host DNA, two desirable features in GETx. Typically, the viral capsid structural framework is provided by proteins such as Gag. To highjack the system to deliver GETx components, Gag can be fused with the desired cargo (e.g., Cas9 base editor) via a linker that is cleavable by protease, ensuring cargo release once the particle matures. The tissue specificity of eVLPs is determined by envelope glycoproteins like VSV-G for broad tropism or FuG-B2 for neuron-specific targeting (*85*). Therefore, eVLPs utilize the high efficiency and precise tissue targeting advantages of viral vectors but avoid the risk of insertional mutagenesis and persistent transgene expression that can occur with conventional viral vectors (*86*).

The therapeutic promise of this technology has been demonstrated in animal studies (*87, 88*). Despite these significant advantages, the clinical translation of eVLPs still faces barriers, primarily due to that large-scale manufacturing and batch-to-batch particle stability can be difficult. Plus, their viral protein origin raises some concerns about immunogenicity. To address these issues, researchers are engineering capsid protein (*89*), optimizing purification processes (*90*) and using human-derived gag-like structural protein such as PEG10 to decrease immune responses (*91*).

1.6 Genes of interest in LivGETx-CVD

Here we focus specifically on liver genes regulating lipid metabolism, with the aim of modulating these targets to promote healthier lipid profiles, thereby decreasing atherosclerosis risk and ultimately reducing the incidence of cardiovascular disease (Figure 1.6 and Table 1.2).

We present the rationale why targeting these genes may render benefits to the patients, followed by preclinical and clinical supporting evidences, snapshots of ongoing LivGETx-CVD clinical trials targeting these genes (as of November 1, 2025, summarized in Table 1.3), as well as risk considerations.

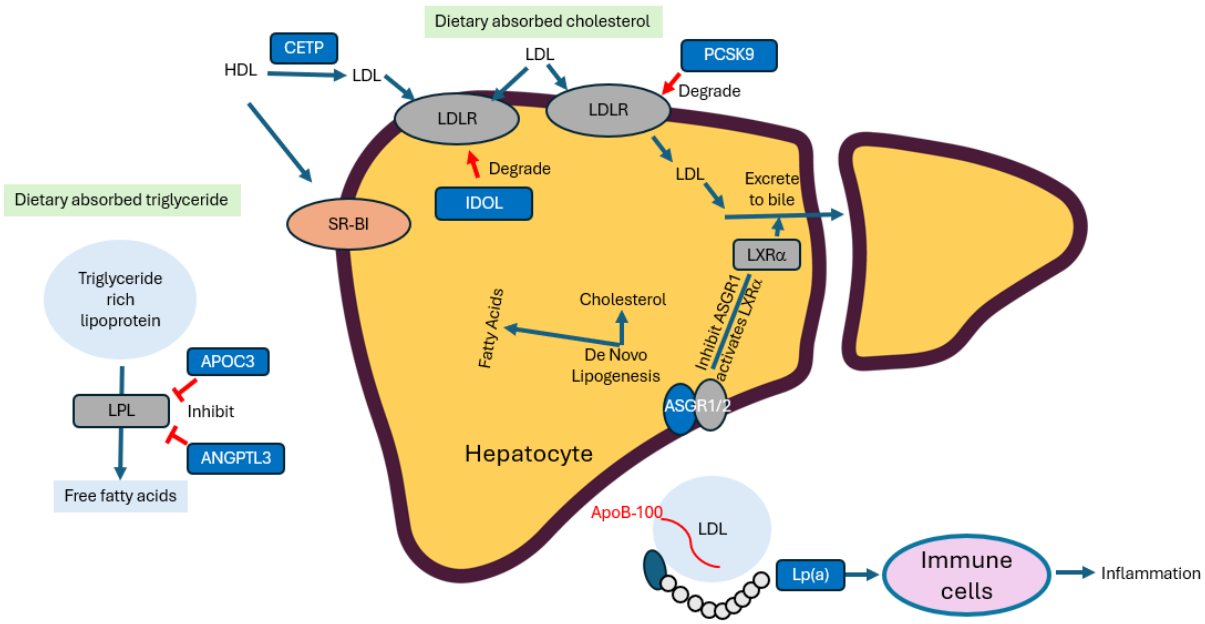


Figure 1.6: Illustration of key targets and their mechanistic pathways in LivGETx-CVD.

One focal point is LDLR, which plays a central role in cholesterol metabolism. PCSK9 and IDOL contribute to the degradation of LDLR. Therefore targeting PCSK9 or IDOL is expected to reduce the degradation of LDLR and consequently reduce LDL-C levels. CETP and ASGR1 are also involved in LDL-C metabolism: CETP moves cholesteryl esters from HDL to LDL in exchange for triglycerides, thereby regulating cholesterol levels and ASGR1 regulates hepatic cholesterol excretion and inhibition of ASGR1 is shown to promote cholesterol excretion. Therefore targeting CETP or ASGR1 are expected to increase HDL-C and reduce LDL-C levels. Another focal point is LPL, which breaks down TG to free fatty acids. APOC3 and ANGPTL3 both inhibit LPL's activity. Therefore targeting APOC3 or ANGPTL3 is expected to enhance LPL activity and reduce TG levels. Lp(a) plays a role that is not directly involved in cholesterol or TG metabolisms. Rather its existence in LDL particle is associated with enhanced inflammatory effect. Targeting LPA is expected to reduce inflammation which is another risk factor for atherosclerosis and CVD.

Table 1.3: Summary of active LivGETx-CVD trials as of November 1, 2025.

LNP (IV): Lipid nanoparticle, intravenous delivery. HeFH: Heterozygous familial hypercholesterolemia. FH: Familial hypercholesterolemia. RH: Refractory hypercholesterolemia. HoFH: Homozygous familial hypercholesterolemia. SHTG: Severe hypertriglyceridemia. TG↓: triglyceride reduction. LDL-C↓: LDL cholesterol reduction. PCSK9 KO: Knockout of PCSK9 gene. SAEs: Serious adverse events. All table data are drawn from the most recent primary updates and clinical trial listings as of November 2025.

Trial	Company	Editor Type	Editing Target	Mutation Type	Delivery Method	Indication(s)	Phase/Status	Main Results/Outcomes (reference)
VERVE-101	Verve Therapeutics	Adenine base editor	*PCSK9*	Loss-of-function	LNP (IV)	HeFH	Phase 1b	Up to 55% LDL-C ↓ ; durable PCSK9 KO; good safety (*92*)
VERVE-102	Verve Therapeutics	Adenine base editor	*PCSK9*	Loss-of-function	LNP (IV)	HeFH, premature CAD	Phase 1b	Up to 69% LDL-C ↓ , 84% PCSK9 ↓ ; no treatment SAEs (*93*)
ART002	AccurEdit Therapeutics	Canonical Cas9 nuclease	*PCSK9*	Loss-of-function	LNP (IV)	HeFH	Single-arm IIT complete	>50% LDL-C ↓ , good safety; triglyceride data not highlighted (*94*)
YOLT-101	YolTech Therapeutics	Adenine base editor	*PCSK9*	Loss-of-function	LNP (IV)	HeFH	Phase 1	50% LDL-C ↓ , >70% PCSK9 ↓ at 4 months, mild transient events (*95*)
VERVE-201	Verve Therapeutics	Adenine base editor	*ANGPTL3*	Loss-of-function	GalNAc-LNP (IV)	RH, HoFH	Phase 1b Ongoing	Preclinical: 98 – 99% ANGPTL3 ↓ ; clinical data pending (*96*)
CTX310	CRISPR Therapeutics	Canonical Cas9 nuclease	*ANGPTL3*	Loss-of-function	LNP (IV)	FH, SHTG, mixed dyslipidemia	Phase 1	Up to 82% TG ↓ , up to 86% LDL-C ↓ , well-tolerated (*97*)
CS121	Correctseq	Transformer base editor	*APOC3*	Loss-of-function	LNP (IV)	FCS, severe hypertriglyceridemia	Phase 1	Rapid TG ↓ (initial patient); no adverse events; longer safety pending (*98*)
CTX320	CRISPR Therapeutics	Canonical Cas9 nuclease	*LPA*	Loss-of-function	LNP (IV)	Elevated Lp(a), ASCVD/aortic stenosis	Phase 1 Ongoing	Preclinical: 95% Lp(a) ↓ ; clinical data awaited (*99*)

1.6.1 PCSK9

Rationale

Proprotein convertase subtilisin/kexin type 9 (PCSK9) regulates circulating cholesterol levels by modulating the number of LDL receptors (LDLR) on the hepatic cell surface. When intracellular cholesterol decreases, transcriptional activity of sterol regulatory element-binding protein 2 (SREBP2) increases, which upregulates both PCSK9 and LDLR expression. PCSK9 is secreted and subsequently binds to LDLR, leading to lysosomal degradation of the receptor. This reduces hepatic LDLR availability and consequently decreases hepatic clearance of LDL from the bloodstream (*100, 101*). Based on this knowledge, it is hypothesized that PCSK9 loss of function will lead to reduced cholesterol levels (see below).

PCSK9 loss of function → retension of LDLR → reduced cholesterol in the blood → less CVD risks

Human population genetics studies have shown that individuals carrying natural loss-of-function alleles in *PCSK9* have significantly lower LDL cholesterol levels throughout life and a reduced risk of coronary heart disease and major cardiovascular events compared to non-carriers (*102*). Large cohort studies and meta-analyses demonstrate that these variants are associated with up to a 50% reduction in coronary heart disease risk, providing strong genetic evidence that lifelong inhibition of PCSK9 lowers cardiovascular risk in humans (*103*).

Preclinical Supporting Evidences

In 2014, Ding et al., employed an all-in-one Adv vector to deliver Cas9 and sgRNA targeting *PCSK9* exon 1 in mice, achieving over 50% mutagenesis and a 40% reduction in LDLC levels after four days (*104*). Application to humanized mouse livers yielded a 52% reduction in

human PCSK9 (*105*). In 2017, Chadwick et al. utilized a base editor (BE3) delivered by Adv vector, which reduced PCSK9 expression by more than 50% and decreased cholesterol levels by approximately 30% in mice (*106*). Later AAV delivered smaller Cas9 variants, saCas9, enabling up to 95% PCSK9 knockdown and 40% reduction in total cholesterol in mice (*107*). David Liu's group further overcame AAV capacity constraints by delivering intein split base editors on dual AAVs, achieving comparable editing as all-in-one systems (*51*). As prolonged Cas9 expression can cause off-target effects, a self-cleaving AAV-CRISPR-Cas9 system was developed to minimize these risks without sacrificing gene-editing efficiency (*108*). VLPs have also been used to deliver base editors to target *PCSK9*, achieving a 78% knockdown of PCSK9 and 63% editing efficiency in the mouse liver (*87*).

In 2024, it is reported that a single injection of LNP-formulated mRNAs encoding epigenetic editors resulted in up to 75% inhibition of circulating PCSK9 for almost one year in mice (*109*). Notably, gene silencing and epigenetic repressive effects at the *PCSK9* locus persisted even after liver regeneration, supporting the heritability of this epigenetic modification (*109*). Another epigenetic editor designed to methylate the human *PCSK9* locus and delivered via LNP achieved near-complete and durable *PCSK9* silencing in humanized transgenic mice for at least one year. Remarkably, reversibility was demonstrated using an activator to demethylate previously silenced *PCSK9*, underscoring the potential of this approach for both durable and reversible gene silencing (*110*).

Translation into large animal models includes AAV-meganuclease–mediated *PCSK9* targeting in rhesus macaques, a non-human primate (NHP) model species, which produced an 84% reduction in PCSK9 and a 60% decrease in LDL, though off-target and immune responses were observed (*111*). In a subsequent study, LNP–delivered ABE mRNA resulted in near-

complete PCSK9 knockdown and a 60% reduction in LDL in another NHP species Macaca fascicularis, with minimal off-target effects (*112*). Another study demonstrated that the same strategy achieved stable reductions of PCSK9 (32%) and LDL (14%) in macaques (*113*). In yet another NHP study, a single intravenous dose of AAV injection is well tolerated and lowers PCSK9 by 83% and LDL-C by 69% for up to 476 days, with no germline tissue distribution (*114*).

In 2025, a split Prime Editor architecture (split-PE-367 with Rma intein) was developed. When packaged in AAV9, it achieved 17.5% precise editing at the *PCSK9* locus in mice (*115*). This work established new split sites to enable effective and robust prime-editing strategies in LivGETx-CVD.

Clinical Supporting Evidences (other than LivGETx-CVD)

Clinical trials have shown that PCSK9 inhibitors reliably lower plasma LDL levels. Currently there are two FDA approved PCSK9 monoclonal antibodies: alirocumab (*116*) and evolocumab (*117*); one approved siRNA: inclisiran (*118*). Other candidates progressing through clinical trials include monoclonal antibodies: ongericimab (*119*), tafolecimab (*120*), ebronucimab (*121*), recaticimab (*122*); anti-sense oligonucleotide (ASO): AZD8233 (*123*); siRNA: RBD7022 (*124*); adnectin: Lerodalcibep (*125*); oral peptide: MK-0616 (*126*), NNC0385-0434 (*127*); small molecule: AZD0780 (*128*).

Ongoing LivGETx-CVD Clinical Trials Targeting PCSK9

VERVE-101 is developed by Verve Therapeutics, designed to treat cardiovascular disease by targeting the *PCSK9* gene in the liver. The therapy uses an adenine base editor (ABE),

which makes a precise A-to-G base change at the *PCSK9*, resulting in a loss-of-function mutation that shuts down PCSK9 protein production. VERVE-101 is delivered via LNPs specifically targeted to hepatocytes. The trial is currently in Phase 1b (Heart-1), but enrollment was paused due to safety concerns, including transient liver enzyme elevations and thrombocytopenia in some participants, which were attributed to the LNP delivery system rather than the gene editor itself. Early results show dose-dependent reductions in PCSK9 protein (up to 84%) and LDL cholesterol (up to 55%) that have been durable for at least 180 days, with mean LDL-C reductions of 42–57% in higher dose cohorts. The trial remains paused while Verve investigates the safety profile and advances a successor therapy, VERVE-102 (see below), with an improved LNP formulation (*129*).

VERVE-102 is developed by Verve Therapeutics and is currently in Phase 1b clinical trials (the Heart-2 study) for patients with heterozygous familial hypercholesterolemia (HeFH) and/or premature coronary artery disease. Like its predecessor VERVE-101, VERVE-102 uses ABE to make an A-to-G transition without double-stranded breaks to inactivate the *PCSK9* gene in hepatocytes. VERVE-102 is delivered as an mRNA and guide RNA packaged in LNPs for liver targeting. As of April 2025, VERVE-102 showed promising interim results: a mean 53% reduction in LDL cholesterol across dose cohorts, with the highest cohort achieving up to 69% LDL-C reduction and up to 84% reduction in PCSK9 levels; safety profile has been favorable, with no treatment-related serious adverse events. Triglyceride effects are not prominently reported, as focus remains on LDL-C and PCSK9; the trial is ongoing, with plans to launch Phase 2 after regulatory clearance, supported by involvement from Eli Lilly as a collaborator.

ART002 is developed by AccurEdit Therapeutics for the treatment of heterozygous familial hypercholesterolemia (HeFH). The therapy uses a canonical Cas9 mRNA and a single-

guide RNA, delivered to the liver via LNPs. ART002 creates a loss-of-function mutation in the *PCSK9* gene by silencing its expression, resulting in sustained reductions in LDL cholesterol levels. The therapy is administered as a single intravenous dose, and clinical trial data from a multicenter, open-label, single-arm investigator-initiated trial in China (now completed) demonstrated that a single dose led to pharmacological saturation, significant (>50%) reductions in LDL-C, and favorable safety with no serious adverse events reported (*94*).

YOLT-101 is developed by YolTech Therapeutics, currently in a Phase 1 investigator-initiated clinical trial in China and cleared for IND-enabling trials in both China and the US for the treatment of heterozygous familial hypercholesterolemia (HeFH). The therapy uses YolTech's proprietary adenine base editor (hpABE5), composed of a Cas9 nickase (nCas9) fused to a deaminase derived from Hafnia paralvei, enabling precise A-to-G base conversion within the target gene *PCSK9*. YOLT-101 creates a loss-of-function mutation in the *PCSK9* gene, providing long-lasting reductions in LDL cholesterol. Delivery is achieved via LNPs administered by intravenous infusion targeting hepatocytes in the liver. Interim results from six subjects in the highest dose group (0.6 mg/kg) revealed a mean 50% LDL cholesterol reduction and more than 70% decrease in PCSK9 protein at 4 months post-dose, with no serious adverse events and only mild, transient infusion-related or liver enzyme elevations reported; effects on triglycerides have not been prominently reported.

Risk Considerations

One potential risk of gene editing *PCSK9* to prevent cardiovascular disease is that complete loss of PCSK9, although unlikely, could result in very low LDL cholesterol levels, which may impair the body's ability to maintain adequate cholesterol supply for hormone

synthesis and cell membrane function. Lifelong loss of PCSK9 function is generally well tolerated, but extremely low LDL levels may increase the risk of developing diabetes in some individuals due to altered lipid signaling affecting glucose metabolism (*130*). PCSK9 also has roles in immunity and modulating viral infection risk, so its absence could potentially weaken innate immune responses or increase susceptibility to certain pathogens (*131*). Since PCSK9 influences lipid homeostasis in the brain, chronic deficiency might have subtle effects on neurocognitive function, though evidence in humans is still limited (*132*).

1.6.2 ANGPTL3

Rationale

Angiopoietin-like protein 3 (ANGPTL3) is a critical regulator of plasma triglyceride and cholesterol metabolism, primarily through inhibition of lipoprotein lipase (LPL) and endothelial lipase (EL) activity (*133*). Consequently, loss of ANGPTL3 function is hypothesized – and has been proved in both human genetic studies and animal models - to reduce circulating triglyceride and LDL-C levels (see below).

ANGPTL3 loss of function → less inhibition of LPL → increased digestion of triglycerides → reduced triglycerides levels in the blood → less CVD risks

Individuals with heterozygous loss-of-function mutations in *ANGPTL3* exhibit reduced triglycerides, HDL-C, LDL-C, and a lower risk of cardiovascular disease (*134*). Moreover, individuals in the lowest tertile of circulating ANGPTL3 protein concentrations have significantly reduced risks of myocardial infarction, confirming that reduced ANGPTL3 activity confers natural protection against atherosclerotic cardiovascular disease (*135*).

Preclinical Supporting Evidences

Gene editing has demonstrated strong potential for ANGPTL3 inhibition. In a study by Chadwick et al., an adenoviral base editor (BE3) targeting *ANGPTL3* in C57BL/6J mice led to reductions in plasma ANGPTL3 (49%), triglycerides (31%), and total cholesterol (19%), with even higher efficacy in LDLR knockout mice (*136*). *ANGPTL3*-targeted therapies predominantly lower triglycerides, whereas PCSK9 inhibition is more effective for LDL lowering; combined targeting provided no additive benefit (*136*).

CRISPR/Cas9 delivery via LNP also enabled efficient, liver-specific silencing of *ANGPTL3* in mice, significantly reducing LDL-C and triglyceride levels without off-target effects or liver toxicity (*137*). Similarly, dual AAV delivered intein split CBE in mice nearly eliminated all circulating ANGPTL3 and lowered triglycerides and total cholesterol by 58% and 61%, respectively (*138*). Single-AAV delivery of a mini ABE achieved robust dual knockdown of PCSK9 and ANGPTL3 (>90%) and markedly reduced cholesterol (*139*). LNP-delivered ABE mRNA targeting an *ANGPTL3* splice site in mice achieved over 60% liver editing and sustained reductions in ANGPTL3, LDL-C, and triglycerides for at least 100 days. Lipid levels remained low after 191 days when challenged with a high cholesterol diet (*140*).

Clinical Supporting Evidences (other than LivGETx-CVD)

A variety of strategies are being explored to target ANGPTL3. Evinacumab, a monoclonal antibody, is already approved in 2021 for managing homozygous familial hypercholesterolemia. It has shown impressive reductions in both LDL cholesterol by 50% and triglycerides by 55% in clinical trials (*141-143*). In addition, Arrowhead's siRNA drug ARO-ANG3 (*144*) and Lilly's siRNA agent solbinsiran (*145*) have both reached Phase 2 studies with

significantly decreased triglycerides and LDL-C. However, the antisense oligonucleotide, vupanorsen, was discontinued for safety concern (*146*).

Ongoing LivGETx-CVD Clinical Trials Targeting ANGPTL3

VERVE-201 is developed by Verve Therapeutics, utilizing an adenine base editor (ABE) system to precisely install a loss-of-function mutation in the *ANGPTL3* gene. The therapy is delivered by Verve's proprietary ligand-targeted GalNAc-lipid nanoparticle (GalNAc-LNP) system, enabling efficient and LDLR-independent liver targeting via intravenous infusion. VERVE-201 is being tested in the ongoing open-label Phase 1b Pulse-1 clinical trial for adults with refractory hypercholesterolemia (RH) and homozygous familial hypercholesterolemia (HoFH), aiming to achieve long-term reduction of LDL cholesterol, triglyceride-rich lipoproteins, and blood ANGPTL3 protein. Detailed quantitative clinical trial results are anticipated in late 2025; safety signals remain favorable, and the trial has not been terminated.

CTX310 is developed by CRISPR Therapeutics for the treatment of dyslipidemias such as familial hypercholesterolemia and severe hypertriglyceridemia. The technology utilizes a canonical CRISPR-Cas9 nuclease, delivered as mRNA with a guide RNA, targeting the *ANGPTL3* gene for direct gene disruption. By creating double-strand breaks, CTX310 induces a loss-of-function mutation in *ANGPTL3* to reduce circulating triglycerides and LDL cholesterol. The therapy is administered via a single intravenous infusion, using LNPs to direct liver-specific editing. The recently-published (Nov 2025) Phase 1 trial results demonstrated robust, dose-dependent lipid lowering effects in adults with severe or refractory dyslipidemia (*147*). At the highest dose tested (0.8 mg/kg), the therapy produced mean reductions from baseline of 73% in circulating ANGPTL3 protein (maximum 89%), 55% in triglycerides (maximum 84%), and 49%

in LDL cholesterol (maximum 87%). Safety was favorable, with no treatment-related serious adverse events and no greater than grade 3 liver enzyme elevations.

Risk Considerations

Gene editing *ANGPTL3* to prevent cardiovascular disease may cause excessive lowering of triglycerides and cholesterol. There has been evidence showing that deficiency in ANGPTL3 is associated with familial combined hypolipidemia (*148*). In addition, ANGPTL3 is important for lipid partitioning and regulation of lipase activity in multiple tissues, so its absence could disrupt normal fat metabolism and lead to hepatic steatosis or abnormal fat accumulation in the liver (*149*).

1.6.3 CETP

Rationale

CETP plays a crucial role in lipoprotein metabolism by mediating the transfer of cholesteryl esters, triglycerides, and phospholipids between HDL, LDL, and VLDL, thereby contributing to reverse cholesterol transport from peripheral tissues to the liver (*150*). Since high levels of HDL-C are inversely associated with cardiovascular disease risk, raising HDL-C through CETP inhibition has been explored as a therapeutic strategy (*151*). It is therefore hypothesized that CETP loss of function will lead to increased HDL-C levels and decreased LDL-C levels (see below).

CETP loss of function → less conversion of HDL to LDL → increased HDL-C and decreased LDL-C levels in the blood → less CVD risks

Recent large cohort studies indicate that people with genetic CETP deficiency have lower non-HDL cholesterol, higher HDL cholesterol, and an overall antiatherogenic lipid profile. In particular, a Danish population-based study found that genetic CETP deficiency was associated with reduced risks for cardiovascular death, ischemic heart disease, myocardial infarction, and peripheral artery disease (*152*). However, some studies in other populations (such as Chinese adults) found increased HDL but little or no reduction in CVD risk unless non-HDL cholesterol was also lowered (*153*). Overall, population genetics provides evidence that CETP loss-of-function confers reduced CVD risk when it leads to lower non-HDL cholesterol as well as higher HDL cholesterol.

Preclinical Supporting Evidences

Our group generated CETP knockout (KO) rabbits using zinc finger nuclease exhibit increased HDL-C, decreased total cholesterol, and significantly reduced development of diet-induced atherosclerosis compared to wild-type controls (*154*). This study demonstrates that *in vivo* CETP gene editing offers a promising approach to cardiovascular disease prevention.

Clinical Supporting Evidences

Current treatments such as antisense oligonucleotides (*155*) and small molecule inhibitors, have shown the ability to raise plasma HDL and reduce atherosclerosis in preclinical models. However, translation CETP inhibition to human has been challenging. Early CETP inhibitors, including torcetrapib (*156*), dalcetrapib (*157*), Anacetrapib (*158*) and evacetrapib (*159*) were either discontinued in clinical trials for unsuccessful in demonstrating reduced CVD risk or severe adverse effects, or lacked commercial potential. Obicetrapib is the only candidate

in the ongoing Phase III trial and exhibited significant elevation of HDL, reduction of LDL and Lp(a) with tolerated safety profile (*160*).

Risk Considerations

Gene editing CETP to prevent cardiovascular disease may lead to marked increases in HDL cholesterol, but could also result in impaired reverse cholesterol transport. This disruption might paradoxically affect the ability to clear cholesterol from arterial walls, which could limit or even negate the expected protection against atherosclerosis in some individuals. Also, when CETP is inhibited, the resulting HDL particles tend to be more enriched in cholesteryl esters and may lose their protective effects against atherosclerosis (*161*). Additionally, CETP deficiency has been associated with an increased risk of age-related macular degeneration and retinal abnormalities, raising concerns about eye health with long-term CETP inhibition (*152*). Lastly, the failures of CETP small molecule inhibitor drugs ring a loud alarm to any new drug development targeting CETP.

1.6.4 ApoC3

Rationale

Apolipoprotein C3 (ApoC3) is a small apolipoprotein primarily produced in the liver and, to a lesser extent, in the small intestine. It plays a pivotal role in triglyceride-rich lipoprotein (TRL) metabolism. Its actions are mediated through three main mechanisms: (1) inhibition of LPL-mediated lipolysis of TRLs (*162, 163*); (2) suppression of TRL clearance by interfering with the binding of ApoB and ApoE to hepatic lipoprotein receptors (*164*); and (3) promotion of

VLDL assembly and secretion under lipid-rich conditions (*165*). It is therefore hypothesized that ApoC3 loss of function will result in substantially reduced triglyceride levels (see below).

ApoC3 loss of function → less inhibition of LPL → increased digestion of triglycerides → reduced triglycerides levels in the blood → less CVD risks

Studies in human populations have demonstrated an association between *ApoC3* and cardiovascular diseases. Individuals carrying loss-of-function mutations in *ApoC3* exhibit lower plasma triglyceride levels and a substantially reduced risk of coronary heart disease (*166*), and even heterozygous carriers tend to have reduced triglyceride compared to non-carriers (*167*).

Preclinical Supporting Evidences

CRISPR/Cas9 technology has been used to generate ApoC3 knockout animal models to advance dyslipidemia research. Although overexpression of human ApoC3 greatly accelerates atherosclerosis in mice, interestingly ApoC3 deficiency does not confer atherosclerosis protection in this species. To address this, researchers created an ApoC3 knockout hamster. Compared to mice, hamsters exhibit lipid metabolism and lipoprotein profiles more similar to human. This model revealed a direct correlation between ApoC3 and atherogenesis (*168*). Likewise, ApoC3 knockout rabbits generated via ZFN with an adenine insertion exhibited lower triglyceride and reduced atherosclerosis on both chow and western diets, as well as accelerated clearance of β-VLDL, a major atherogenic lipoprotein (*169*). These findings suggest that inhibition of ApoC3 not only holds promise for the treatment of hypertriglyceridemia, but may also be a therapeutic strategy for atherosclerosis. Expanding on these findings, Scribe Therapeutics reported that its LNP delivered CRISPR/CasX based lead molecule STX1400,

achieved more than 90% ApoC3 knockdown and produced marked reductions in triglyceride level in a humanized mouse model (*170*).

Clinical Supporting Evidences (other than LivGETx-CVD)

ApoC3 has gained attention as a promising target for reducing triglyceride levels and cardiovascular disease risk. Volanesorsen is an early generation ApoC3-inhibiting ASO drug. It exhibited triglycerides reduction up to 77% in phase 3 trials (*171*) and has been approved in Europe. However, Volanesorsen faced regulatory hurdles in the US for the risk of thrombocytopenia (*172*). Olezarsen, the GalNAc-conjugated ASO, has shown significant efficacy in lowering triglycerides by 44% (*173*). It was approved by FDA in 2025 for patients with familial chylomicronemia syndrome (FCS). In addition, GalNAc-conjugated siRNA plozasiran has demonstrated sustained reductions in triglycerides by 62% and is currently under Phase III trials (*174*). Other clinical testing siRNA drugs include RBD-5044 (*175*) and RN0361 (*176*), both in Phase II. There are no monoclonal antibody drugs targeting ApoC3 at present but several candidates are in pre-clinical stage (*177, 178*).

LivGETx-CVD Clinical Trials Targeting ApoC3

CS121 is developed by CorrectSequence Therapeutics for treating familial chylomicronemia syndrome (FCS) and severe hypertriglyceridemia. The therapy uses Correctseq's proprietary next-generation transformer Base Editor (tBE), which enables precise single-base A-to-G transitions at the *APOC3* gene without creating DNA double-strand breaks. CS121's mechanism mimics natural loss-of-function variants of APOC3, delivering a sustained reduction in plasma triglyceride levels by permanently downregulating APOC3 expression. The

therapeutic components are delivered intravenously using LNPs for liver-targeted editing. As of November 2025, CS121 is in a Phase 1, open-label, single-arm, adaptive dose-escalation clinical trial; the first treated patient saw fasting triglycerides drop significantly within three days post-treatment, was discharged without any adverse events, and longer-term follow-up for safety, PK/PD, and pancreatitis outcomes is ongoing.

Risk Considerations

Since ApoC3 inhibits lipoprotein lipase, its loss might lead to excessively rapid clearance of triglycerides, potentially disrupts energy reserve in the body and causes metabolic disorders. Loss of triglycerides could also alter the function of remnant particles involved in fat-soluble vitamin transport, with possible impacts on vitamin absorption (*179*). ApoC3 also inhibits hepatic uptake of TG-rich lipoprotein (TRL) remnants, so its deficiency may lead to hepatic steatosis or abnormal fat deposition (*180*).

1.6.5 ASGR1

Rationale

ASGR1 encodes a subunit of the asialoglycoprotein receptor, which is responsible for mediating the endocytosis and degradation of desialylated proteins in the bloodstream (*181, 182*). Blocking or mutating ASGR1 disrupts the internalization and lysosomal breakdown of asialoglycoproteins, which in turn suppresses mTORC1 signaling and activates AMPK. Activated AMPK destabilizes the BRCA1/BARD1 complex and increases LXRα, leading to the upregulation of cholesterol transporters such as ABCA1 and ABCG5/G8. With more ABCG5/G8, cholesterol is more efficiently pumped into bile and eliminated from the body

through feces (*183*). This mechanism suggests that inhibiting ASGR1 could promote cholesterol clearance and be a promising strategy for treating hyperlipidemia. It is therefore hypothesized that ASGR1 loss of function will lead to reduced cholesterol levels (see below).

ASGR1 loss of function → upregulation of reverse cholesterol transport → increased cholesterol excretion through feces → reduced cholesterol levels → less CVD risks

In 2016, a study published in the New England Journal of Medicine reported that a loss-of-function variant in *ASGR1* was associated with lower non-HDL cholesterol levels and reduced risks of atherosclerosis in human (*184*). Studies of large Icelandic cohorts identified individuals carrying the del12 deletion variants in *ASGR1*, who have a 34% lower risk of coronary artery disease compared to non-carriers (*184*).

Preclinical Supporting Evidences

Similar findings were observed in ASGR1 knockout pigs, which serves as a useful model due to their cardiovascular system similarities to humans. These pigs had lower non-HDL cholesterol and developed fewer atherosclerotic lesions after six months on a high-cholesterol diet (*185*). Targeting ASGR1 was further validated in mouse models, where ASGR1 knockout led to reduced blood cholesterol and increased cholesterol excretion into bile (*183*).

Risk Considerations

Gene editing ASGR1 to prevent cardiovascular disease may interfere with the liver's ability to clear asialoglycoproteins, which could lead to impaired liver detoxification and accumulation of glycoproteins. ASGR1 deficiency has been shown to increase susceptibility to liver injury in chronic or acute liver injury mouse models. And ASGR1 deficiency-mediated

liver injury was identified to be associated with increasing GP73-mediated hepatic endoplasmic reticulum stress (*186*). However, ASGR1 KO mice showed no liver toxicity under dietary challenge in Wang et al's Nature paper (*183*).

1.6.6 LPA

Rationale

Lipoprotein(a) is a complex molecule consisting of apolipoprotein(a), encoded by the *LPA* gene, covalently attached to apolipoprotein B100 (ApoB100). Elevated Lp(a) levels are recognized as an independent, causal, and largely genetic risk factor for atherosclerosis, primarily due to mechanisms involving enhanced atherogenesis, inflammation, and thrombosis (*187*).

It is therefore hypothesized that Lp(a) loss of function will lead to reduced inflammation levels and provide benefits to CVD (see below).

Lp(a) loss of function → less inflammation → less CVD risks

Numerous large-scale epidemiological and Mendelian randomization studies have found that individuals with genetic variants resulting in lower *LPA* gene expression or reduced Lp(a) levels have substantially lower risk of coronary heart disease, aortic valve stenosis, stroke, and other cardiovascular outcomes (*188, 189*). These clinical studies provided strong genetic evidence that *LPA* inhibition is beneficial for cardiovascular disease prevention.

Preclinical Supporting Evidences

Gene-editing strategies targeting *LPA* are under active investigation. Doerfler et al. developed *LPA* transgenic mice (as rodents don't have the LPA gene) and disrupted the gene

using AAV-delivered saCas9. This resulted in nearly complete knockdown of apo(a) protein as measured by ELISA, although total cholesterol levels remained unchanged in both genders (*190*). In 2025, another approach utilized TALEN mRNAs encapsulated in LUNAR® LNPs, administered to mice carrying a human *LPA* transgene. A single treatment reduced plasma Lp(a) levels by more than 80%, persisting for at least five weeks (*191*). Although hamsters, rabbits and pigs exhibit lipid metabolism and lipoprotein profiles more similar to human compared to mice, none of them naturally express *LPA* gene and produce Lp(a). Therefore, studies involving *LPA* will need to use transgenic approaches to introduce the human *LPA* gene when modeling Lp(a) biology as with mice. Because non-human primates (NHP) share closer genetic and physiological similarities to human, including natural expression of *LPA*, they serve as valuable models for studying Lp(a) biology and therapies targeting the *LPA* gene.

The gene-editing therapy CTX320™ involves encapsulating Cas9 mRNA and its guide RNA in LNPs for targeted delivery. In cynomolgus monkeys, a single CTX320™ infusion produced 94% reduction in plasma Lp(a) sustained through Day 224. CTX320™ has now advanced into clinical trials (*99*).

Clinical Supporting Evidences (other than LivGETx-CVD)

Several therapeutic interventions are being explored to lower Lp(a). Pelacarsen is an antisense oligonucleotide (ASO) therapy currently in Phase III trials with Lp(a) reduction by 92% (*192*); it works by reducing hepatic synthesis of apo(a) in patients with high Lp(a) level (*193*). Similarly, siRNA-based drugs have shown remarkable efficacy. Olpasiran, Lepodisiran, and Zerlasiran achieved reductions in Lp(a) of almost 100% and have all entered Phase III (*193-196*). The Lp(a) oral inhibitor LY3473329 has completed Phase II (*197, 198*).

Ongoing LivGETx-CVD Clinical Trials Targeting LPA

CTX320 is developed by CRISPR Therapeutics, currently in a Phase 1 clinical trial targeting the *LPA* gene, which encodes apolipoprotein(a), to treat patients with elevated Lp(a) and atherosclerotic cardiovascular disease or aortic valve stenosis. The therapy uses canonical Cas9 mRNA with a guide RNA, delivered to the liver via LNPs through a single intravenous infusion. By targeting and permanently disrupting the *LPA* gene, CTX320 introduces a loss-of-function mutation, leading to durable reductions in plasma Lp(a). As of November 2025, safety is reported as favorable, and the trial remains ongoing with no termination announced. Quantitative clinical results on LDL cholesterol and triglycerides are not yet published, as the main reported outcome to date is Lp(a) reduction, with further updates anticipated.

Risk Considerations

Lp(a) has a role in wound healing and tissue repair through its structural similarity to plasminogen, so reducing it to very low levels could theoretically impair fibrinolysis and healing processes (*199*). However, no convincing human data support this in practice. Since Lp(a) functions are not fully understood, complete or lifelong deficiency could have unforeseen effects on vascular biology and systemic health.

1.6.7 IDOL

Rationale

IDOL, also known as MYLIP, is a widely expressed E3 ubiquitin ligase induced transcriptionally by LXR/RXR in response to increased sterol signaling (*200, 201*). Three IDOL

targets, LDLR, VLDLR and ApoER2, are intimately related to lipid metabolism (*202*). IDOL-mediated ubiquitination promotes their lysosomal degradation. Lack or down-regulation of IDOL increases LDLR stability, LDL-C uptake and protects mice against atherosclerosis, independently of SREBP or PCSK9 (*203, 204*). Based on this knowledge, it is hypothesized that IDOL loss of function will lead to reduced CVD risk (see below).

IDOL loss of function → retention of LDLR → reduced cholesterol → less CVD risks

Findings of human genetic variants in *IDOL* support the basic research results, with loss of function carriers having very low levels of LDL-C and reduced CVD risk (*205-208*). Large-scale genetic outcome data for CVD risk reduction are still emerging, and the overall population frequency of *IDOL* loss-of-function alleles is relatively low compared to *PCSK9* or *ANGPTL3*.

Preclinical Supporting Evidences

Advancement towards clinical translation of IDOL's therapeutic potential has been hampered by critical differences between IDOL biology in humans and monkeys when compared to the extensive research in mouse models (*209*). Rabbits better approximate human lipid metabolism overall, providing superior models in pre-clinical settings for CVD research and beyond. Our lab therefore engineered IDOL KO rabbits by employing CRISPR/Cas9 genome editing, resulting in the complete loss of IDOL function and consequently elevated protein levels of its downstream targets. When challenged with high-cholesterol diet (HCD), IDOL KO rabbits had markedly reduced plasma concentrations of TC and TG compared with WT rabbits. As a result, IDOL deficiency significantly attenuated the development of atherosclerosis (*210*). These findings collectively support IDOL inhibition as a promising strategy for the simultaneous reduction of TC, TG, and CVD risk.

Risk Considerations

Gene editing *IDOL* to prevent cardiovascular disease could disrupt cholesterol homeostasis by causing excessive LDLR activity, potentially resulting in abnormal hepatic cholesterol accumulation and liver steatosis or dysfunction. Since IDOL also regulates VLDLR and ApoER2, its loss may affect lipid metabolism in peripheral tissues and interfere with neuronal signaling and brain development, given these receptors' roles in the central nervous system (*211, 212*).

1.6.8 General limitations of these trials

Existing LivGETx-CVD trials (Table 1.3) mostly focus on a rare indication, i.e., dyslipidemia. Although these trials provide proof-of-concept for durable LDL-C or triglyceride lowering after editing the listed target genes, they remain early-phase and in small scale. In contrast, CVD in general and atherosclerosis in particular is chronicle that often lasts for decades and affects millions of patients. Hence, current trials are underpowered to detect infrequent but potentially catastrophic events such as treatment-emergent malignancy, delayed hepatotoxicity, or immune-mediated reactions to editors or delivery vehicles that could arise decades later in life.

Moreover, participants are typically selected for relatively preserved hepatic function, controlled comorbidities, and intensive specialist follow-up, all of which limit the generalizability of these trials to the broader CVD population that commonly includes older adults with other disease conditions such as chronic kidney disease, and metabolic syndrome. As such, before LivGETx-CVD can be contemplated for primary prevention or moderate-risk

patients, much larger, longer, and more diverse trials will be required, that is, trials that not only track traditional cardiovascular endpoints but also rigorously characterize off-target mutational spectra, clonal hematopoiesis, neurocognitive outcomes, reproductive health, and multi-generational effects where feasible.

1.7 Conclusions

LivGETx-CVD, i.e., gene editing based therapy targeting the liver, holds promise as a 'one shot' treatment for dyslipidemia, a condition that has traditionally required lifelong management, and for cardiovascular diseases in general. Achieving this potential will require sustained investment in the development of advanced gene editing tools, the identification of novel therapeutic targets, the optimization of delivery systems, continued efforts to address current challenges related to efficacy and safety, as well as societal level consensus of ethical and regulatory issues.

Chapter 2 ASGR1 Knockdown via CRISPR/Cas9 Improves Glucose Homeostasis and Reduces Atherosclerosis in *ApoE*$^{-/-}$ Mice

2.1 Introduction

Cardiovascular disease (CVD) remains a leading cause of morbidity and mortality, with hypercholesterolemia identified as a major driver of atherogenesis (*213*). Current lipid-lowering therapies, such as statins and proprotein convertase subtilisin/kexin type 9 (PCSK9) inhibitors, lead to substantial risk reduction, yet a significant residual burden persists, highlighting the need for novel therapeutic targets and interventions (*5, 7*).

The asialoglycoprotein receptor 1 (ASGR1) is a transmembrane lectin receptor that mediates the endocytosis and lysosomal degradation of desialylated glycoproteins (*214*). ASGR1 is predominantly expressed in hepatocytes and has been implicated in diverse physiological functions, including modulation of immune responses, regulation of hepatic protein clearance, and maintenance of glycoprotein homeostasis. Human genetic studies have linked loss-of-function variants of ASGR1 to reduced non–HDL cholesterol levels and a lower risk of coronary artery disease (*184*). Preclinical investigations have revealed ASGR1's regulatory roles in hepatic lipid metabolism, where ASGR1 deficiency in mice leads to favorable changes in lipid profiles, including reductions in plasma very-low-density lipoprotein (VLDL) and low-density lipoprotein (LDL) cholesterol (*183*). These findings, along with others, present ASGR1 as a promising target in CVD drug development (*215-218*).

Gene editing technologies offer an unprecedented "one-shot, one-cure" option, in which a single administration of a gene editing therapy drug (GETx) creates a durable, therapeutically

beneficial genetic change (*8*). In the context of cardiovascular diseases, GETx (GETx-CVD) strategies typically target genes involved in hepatic lipid metabolism whose loss-of-function variants are associated with protection against CVD (*10*). Some candidate GETx-CVD targets include PCSK9, angiopoietin-like protein 3 (ANGPTL3), cholesteryl ester transfer protein (CETP), apolipoprotein C-III (APOC3), and ASGR1, among others, each supported by human genetic and preclinical evidence linking reduced gene activity to lower atherogenic lipoprotein levels and decreased cardiovascular risk (*112, 113, 135, 136, 153, 166, 188, 219*).

Here, we hypothesize that CRISPR/Cas9-mediated *Asgr1* disruption confers atheroprotective benefits. To test this, spCas9 and *Asgr1*-targeting guide RNAs were packaged into an adenoviral vector (Adv-Cas9-Asgr1) and delivered intravenously to *ApoE*$^{-/-}$ mice. Treatment with Adv-Cas9-Asgr1 significantly reduced total cholesterol levels and decreased atherosclerotic plaques. In addition, Adv-Cas9-Asgr1 enhanced insulin sensitivity, as evidenced by improved insulin and glucose tolerance tests, and elevated hepatic levels of phosphorylated AKT and insulin receptor. Notably, these effects were accompanied by reductions in body weight, as well as subcutaneous and visceral fat mass, demonstrating coordinated benefits for glucose homeostasis and adiposity.

2.2 Materials and methods

2.2.1 Animals

The *ApoE*$^{-/-}$ (B6.129P2-*Apoe*^{tm1Unc}/J, RRID:IMSR_JAX:002052) mice were purchased from the Jackson Laboratory. All the experimental procedures were approved by the Institutional Animal Care and Use Committee (IACUC) of the University of Michigan.

2.2.2 Cell culture and transfection

N2a cells (ATCC, Manassas, VA; Cat# CCL-131) were maintained in Dulbecco's Modified Eagle Medium (DMEM) (Thermo Fisher Scientific, Waltham, MA; Cat# 11-965-092) with 10% FBS and 1% 100X penicillin-streptomycin (Thermo Fisher Scientific, Cat# 15140122).

For transfection, cells were dissociated with 0.25% trypsin (Thermo Fisher Scientific, Cat# 25200-056) to single cells. Cells were resuspended in electroporation buffer (Celetrix, Manassas, VA; Cat# 13-0104) to 2×10^5 cells/20 μL. For Cas9 Ribonucleoprotein (RNP) transfection, 3 μg Cas9 protein (IDT, Coralville, IA; Cat# 1074182) was pre-mixed with 1 μg gRNA (Synthego, Redwood City, CA) at room temperature for 10 min first, and then the formed RNP complex was mixed with the cells and transferred to a 20 μL electroporation tube (Celetrix, Cat# CTXE00004). The electroporation conditions were 430 V for 30 ms using a tube electroporator machine (Celetrix, Cat# CTX-1500A). After electroporation, the cells were immediately transferred back to culture medium to continue culture.

2.2.3 Generation of Adenovirus particles and administration into mice

The adenovirus (Adv) vectors were constructed and packaged by Vectorbuilder (Chicago, IL). Titers are expressed as viral genome copies per ml (vg/ml): 7.4×10^{12} vg/ml for Adv-Cas9-Asgr1. Adv-Cas9-Asgr1 particles were systemically administered into *ApoE*$^{-/-}$ (referred interchangeably to as ApoE deficient or ApoE KO in this work) mice at 8 weeks of age through tail vein intravenous (i.v.) injection. Blood samples were collected via facial vein before and biweekly after western diet started. At the end of the experiment, all the animals were humanely euthanized and tissues were harvested for analysis.

2.2.4 PCR and primers

To evaluate gene editing efficiencies *in vitro*, cells were harvested 48 h after transfection and genomic DNAs were extracted with the Quickextract DNA extraction solution (Biosearch Technologies, Petaluma, CA; Cat# QE09050). Mouse liver DNAs were extracted with DNeasy Blood and Tissue Kit (Qiagen, Germantown, MD; Cat# 69504).

Targeted regions were amplified by polymerase chain reaction (PCR) using Q5 high-fidelity DNA polymerase (NEB, Ipswich, MA; Cat# M0491S). Cycling conditions were as follow: initial denaturation at 95 °C for 2 min, followed by 35 cycles of denaturation at 95 °C for 30 s, annealing at 56 °C for 30 s, and extension at 72 °C for 30s, with a final extension at 72 °C for 5 min. The products were purified using QIAquick PCR purification kit (Qiagen, Cat# 28104). The primers used for PCR of the *Asgr1* targeted regions in mouse N2a cells are listed in Table 2.1.

Table 2.1: PCR primer sequences.

Gene	Forward primer	Reverse primer
m*Asgr1*-F1/R1	TGAGAGTCTGATCTCCCGGG	CTCCTGCAGACGTCGTCATT
m*Asgr1*-F2/R2	ACCCACATCCTCTCTTGCTT	TCAAAGTCCTGACAACCCCA
m*Asgr1*-F3/R3	CGGCCCCTCTTAGTCTACTG	GACAACCACCAGCAACAGAA
m*Asgr1*-F4/R4	TCATCCAGCTCTGAGTCTGT	TCTCCGGAGTTGATGATGGT

2.2.5 T7EI assay

The purified PCR products were denatured and re-annealed and digested with T7 Endonuclease I (T7EI, NEB, Cat# M0302L) for 30 min at 37 °C, and then run in a 2% agarose gel. Non-perfectly matched DNA (presumably indel sites) would be recognized and cleaved by T7EI leading to two cleaved bands, whereas the perfectly matched DNA would not be recognized and cleaved by T7EI hence leading to only one band (the wild-type band).

The indel rate (%) was quantified using the formula $100 \times (1-(\mathrm{SQRT}(1-((A1+A2)/(A1+A2+A3)))))$, where A3 is the intensity of the wild-type band, A1 and A2 are the intensities of the two cleaved bands, respectively, and SQRT is the square root function.

2.2.6 Deep sequencing (deep-seq) and analysis

For deep sequencing, the purified PCR products were sent to the DNA Core Facility at Massachusetts General Hospital (Cambridge, MA), as previously described (*220*). Briefly, Illumina compatible adapters with unique barcodes were ligated onto each sample during library construction. Libraries were pooled in equimolar concentrations for multiplexed sequencing on the Illumina MiSeq platform with 2 × 150 run parameters. Indel rates were determined by the CRISPResso2 tool (http://crispresso.pinellolab.partners.org/) using fastq files.

2.2.7 Quantitative real-time PCR (qPCR) analysis

Total RNA was extracted using RNeasy Mini Kit (Qiagen, Cat# 74106). Reverse transcription was performed using SuperScript III First-Strand (Invitrogen, Carlsbad, CA; Cat# 18080-051) with random primers. SYBR green fast qPCR mix (ABclonal, Woburn, MA; Cat# RM21203) was used to perform qPCR with specific gene primers. ΔΔCt method was used to

quantitate gene expression, which was normalized to *Ppia* (mouse). The primers used for qPCR are shown in Table 2.2.

Table 2.2: qPCR primer sequences.

Gene	Forward primer	Reverse primer
m-*Asgr1* F1/R1	TCCAGCTCTGAGTCTGTTAGC	GTCATGATGGCACTGGATCC
m-*Asgr1* F2/R2	AGTGGAGTCGAAGCTGGAAA	TCGCACGTCAGACACTAACT
m-*Asgr1* F3/R3	TGTGAGACAAAGTTGGATAAGGC	CCAGTTCTAAACCTCAGCAGC
m-*Mttp*	CGTGCTGTTACTCTTTCCTACT	GTGGAGTACGTGAGCTTGTATAG
m-*Angptl3*	CAGGACTTCAACGAAACATGGG	GAGTATTCAACGTAGTGCTTGCT
m-*Srebp1a*	GCGCCATGGACGAGCTG	TTGGCACCTGGGCTGCT
m-*Ppia*	CGTTTTGGGTCCAGGAATGG	TACAGGACATTGCGAGCAGA
m-*Srebp2*	CCATCTTCCCCTCTCTTTCC	AGGGAAGATCCTGGGAGAAA
m-*Hmgcr*	CAAGGAACGTGCACCAAGAA	AACACAGCACGGAAAGAACC
m-*Pcsk9*	GGCTGCCAGGAACCTACATT	CTGGGCGAAGACAAAGGAGT
m-*Ldlr*	GAGGAGCAGCCACATGGTAT	GCTCGTCCTCTGTGGTCTTC
m-*Abca1*	GGGAGTCCCAGAAAAGGAAG	TGTGGTTGGTTCATCCAGAA
m-*Abcg5*	CGTCCAGAACAACACGCTAA	GCAGCATCTGCCACTTATGA
m-*Abcg8*	AAGACGGGCTGTACACTGCT	AGGAGGACATGTGGAAGGTG
m-*Lxrα*	TGCCATCAGCATCTTCTCTG	GGCTCACCAGCTTCATTAGC
m-*Cyp7a1*	ACACCATTCCTGCAACCTTC	GCTGTCCGGATATTCAAGGA
m-*Chop*	GCATGAAGGAGAAGGAGCAG	CTTCCGGAGAGACAGACAGG
m-*Sr-b1*	GACAAACTGGGAAGATTGAGCC	GGGTCAGCGTCGAGGAAGTGA
m-*Hmgcs2*	AGAGAGCGATGCAGGAAACTT	AAGGATGCCCACATCTTTTGG
m-*Fxr*	GCTGTGTGTTGTCTGTGGAG	TTCAGCCAACATCCCCATCT
m-*Srebp1c*	GGAGCCATGGATTGCACATT	GCTTCCAGAGAGGAGGCCAG
m-*Fasn*	GGAGGTGGTGATAGCCGGTAT	TGGGTAATCCATAGAGCCCAG
m-*Scd1*	CGCCCCTACGACAAGAACAT	CTCAGAAGCCCAAAGCTCAG

2.2.8 Droplet Digital PCR (ddPCR)

Large fragment deletion was quantified using the QX200 Droplet Digital PCR System (Bio-Rad, Hercules, CA) with an EvaGreen single-channel detection workflow. Each 20 μL ddPCR reaction contained 10 μL of 2× QX200 ddPCR EvaGreen Supermix (Bio-Rad, Cat# 1864034), 200 nM forward and reverse primers specific for the target locus or for a reference gene, and 30 ng of genomic DNA. Droplets were generated with the QX200 Droplet Generator according to the manufacturer's instructions. PCR amplification was performed on a PTC Tempo Deepwell Thermal Cycler (Bio-Rad) using the following cycling conditions: 95 °C for 5 min; 40 cycles of 95 °C for 30 s and 60 °C for 2 min (ramp rate 2 °C/s); followed by enzyme deactivation at 4 °C for 5 min and 90 °C for 5 min. After amplification, droplets were read using the QX200 Droplet Reader, and fluorescence amplitude was analyzed with QuantaSoft software (Bio-Rad) using the single-channel EvaGreen analysis mode. Copy number was calculated by normalizing the concentration of target-positive droplets to that of the reference gene.

2.2.9 Western blot analysis

Protein was lysed by Radio-Immunoprecipitation Assay buffer (RIPA) with protease inhibitor and phosphatase inhibitor. Proteins were isolated in 10% SDS-PAGE and transferred to 0.45 μm nitrocellulose membranes. After blocked in 5% non-fat dry milk (LabScientific, Danvers, MA; Cat# M0841) at room temperature for one hour, membranes were firstly incubated with the primary antibodies overnight at 4 °C and imaged after incubated with secondary antibodies. The following antibodies were used in the study: anti-ASGR1 antibody (Proteintech, Rosemont, IL; Cat# 11739-1-AP), anti-phosphorylated Insulin Receptor antibody (Cell signaling,

Danvers, MA; Cat# 3024S), anti-phosphorylated Akt antibody (Cell signaling, 4060S), anti-Insulin Receptor antibody (Cell signaling, Cat# 3025S), anti-Akt antibody (Cell signaling, Cat# 4691S). Secondary antibodies used: IRDye® 800CW Donkey anti-Rabbit IgG Secondary Antibody (LI-COR, Lincoln, NE; Cat# D40827-03) and IRDye® 680RD Donkey anti-Mouse IgG Secondary Antibody (LI-COR, Cat# D30322-25). Membranes were scanned using Odyssey Imaging System (LI-COR Biosciences) and quantified with the LI-COR Image Studio Software.

2.2.10 Serum analysis

Blood samples collected from the animals were allowed for clotting at room temperature for 30 min. Serum was isolated by centrifugation at 3,000 g for 10 min and stored at -80 °C in small aliquots. Determination of total cholesterol (TC) and triglycerides (TG) was performed using the cholesterol and triglyceride assay kit (Fujifilm, Tokyo, Japan; Cat# 999-02601 and NC2044372) according to the manufacturer's instructions. ALT and AST values were determined by the IVAC Diagnostic Laboratory at the University of Michigan.

2.2.11 Liver cholesterol and triglycerides measurement

Liver tissues were washed with cold PBS and then extracted lipids by resuspending the sample in Chloroform: Isopropanol: NP-40 (7:11:0.1) in a microhomogenizer. Transfer the lipid extract to a clean EP tube and spin the extract 5–10 min at 15,000 g. Transfer all of the liquid to a new tube, avoiding the pellet. Air-dry the extraction at 50 °C overnight. Dissolve the dried lipids with 100ul Wako TC buffer without adding enzyme and vortex completely. Liver cholesterol and triglycerides were detected using the cholesterol and triglyceride assay kit (Fujifilm, Cat# 999-02601 and NC2044372) according to the manufacturer's instructions.

2.2.12 Insulin tolerance and glucose tolerance test

For the insulin tolerance test (ITT), mice were fasted for 6 hours in the morning and were administered an i.p. injection of insulin at a dose of 0.5 IU/kg BW. Blood samples were collected via tail vein puncture, and blood glucose levels were measured at 0, 15, 30, 60, 90, and 120 min time points. For the glucose tolerance test (GTT), mice were fasted overnight. Glucose was administered by oral gavage at a dose of 1 g/kg BW. Blood glucose levels were measured at 0, 15, 30, 60, and 120 min time points. Additional blood samples were collected through tail vein puncture at 0, 15, 30, and 60 min time points and serum insulin concentrations were measured using a mouse insulin ELISA kit (Crystal Chem, Downers Grove, IL; Cat# 90080) following the manufacturer's protocol.

2.2.13 Oil Red O (ORO) staining of the aorta trees

Aorta trees were carefully isolated from postmortem animals and fixed in formalin (Thermo Fisher Scientific, Cat# 23-245685) at least overnight. Aorta trees were then stained in ORO solution, consisting of 1.6 mg/ml ORO (Sigma, St. Louis, MO; Cat# O0625) and 77.8% (v/v) methanol (Sigma, Cat# 179337) in 1N sodium hydroxide solution (Thermo Fisher Scientific, Cat# SS266-1) for 50 min, incubated in 70% ethanol for 30 min and then kept in distilled water until imaging. The images were taken by Olympus DP73 microscope (Center Valley, PA 18034), then analyzed by Image J2 (*221*). The red stained regions are considered positive for atherosclerosis plaques. The ratio of the area of red-stained regions/overall area of aorta tree for each animal is calculated and used as the quantitative extent of atherosclerosis for this animal.

2.2.14 Statistical Analysis

Data in bar graphs and scatter plots are expressed as the mean ± SEM, analyzed by using GraphPad Prism v.8.0.1 (GraphPad Software). Statistical differences were determined by two-tailed unpaired Student's *t* test for two groups. A p value < 0.05 was considered as significant.

2.3 Results

2.3.1 In vitro validation of Asgr1-targeting gRNAs

We designed a dual guide RNA (gRNA) based CRISPR/Cas9 knockout strategy to disrupt the mouse *Asgr1* gene. In this design, each gRNA targets a distinct Exon. Individual gRNA is expected to introduce insertion or deletion (indel) mutations at its own target site. In addition, the two targeted exons are separated by coding regions that encompass essential functional domains of the protein such that concurrent cleavage by both gRNAs on the same allele is anticipated to produce a large fragment deletion, thereby ensuring loss of critical coding sequences.

We first tested indel formation capacities of 4 single gRNAs (sg1 to sg4) in mouse N2a cells (Figure 2.1A). They were individually transfected in RNP complex with Cas9 protein by electroporation. As shown in Figure 1B, sg1 targeting Exon 9 (E9) and sg3 targeting E3 each led to >60% indel rates at their target sites. In contrast, other gRNAs produced significantly lower indel rates.

We examined the off-target (OT) editing indel rates by sg1 and sg3. Top 10 predicted OT sites for each gRNA were analyzed, and no indel events were detected (Table 2.3), indicating minimal off-target editing risks of these two gRNAs.

Based on these results, we selected sg1 and sg3 for the following *in vivo* experiments.

Table 2.3: Information of off-target sites by sg1 and sg3.

(A) Predicted off-target sites by sg1. (B) Predicted off-target sites by sg3.

A. Off-targets by sg1.

Locus details	Sequence	Mismatch count	Indel (%)
On target	GAGCAGCCAGATAACTGGTA CGG	n/a	48
exon: Fbxo7	GAGCAGCCAGCTGACTGGTA CAG	2	None
exon: Clec10a	CTGCAGCCAGATAACTGGTT CGG	3	None
exon: Mc2r	GAACATCCAGATAATTGTTA GGG	4	None
exon: Asic4	GCTCAGCCAGATACCTGGCA AGG	4	None
exon: Gm26937	GAGCAGGAAGCTAACTGGCA TGG	4	None
exon: Mgl2	CTGCAGCCGGATAACTGGCA TGG	4	None
exon: Asgr2	ACTCAGCCAGATAACTGGCA GGG	4	None
exon: Efnb3	GAGGAGCCAAAGAGCTGGTA GGG	4	None
exon: Mfsd2a	GCGCAGCCGGTCAACTGGTA CGG	4	None
exon: Proca1	GAGAACCGAGAGAACTGGTA AGG	4	None

B. Off-targets by sg3.

Locus details	Sequence	Mismatch count	Indel (%)
On target	CGCTGCAAGAGCCGTGGAGT GGG	n/a	48
exon: Pax2	CGCTCCAAGTGCCGGCGAGT TGG	4	None
exon: Alb	CTCAGCAAGAGCCCTGCAGT AGG	4	None
exon: Espl1	GGCTGCCAGAGCAGTGGAGA GGG	4	None
intron: Mamld1	TGCTGCAAGAGCCGTTGGGT GGG	3	None
intergenic: Gm26861-Gm23415	AGCTGCAAGAGCCATGGAGC AGG	3	None
intron: Epha2	GGCTGCAAGAGCCGGGGAAC AGG	4	None
intergenic: Gm14041-Sirpa	TGCTGCAAGAGGCTGGGAGT AGG	4	None
intergenic: Zmym2-B020004C17Rik	CTCTGCAAGAGCCCTGGACC AGG	4	None
intron: Dlc1	CCCTGCAAGAGCTGGGGAGA TGG	4	None
intergenic:6430571L13Rik-Cacna2d2	CACTGCAGGAGCAGTGGAGC TGG	4	None

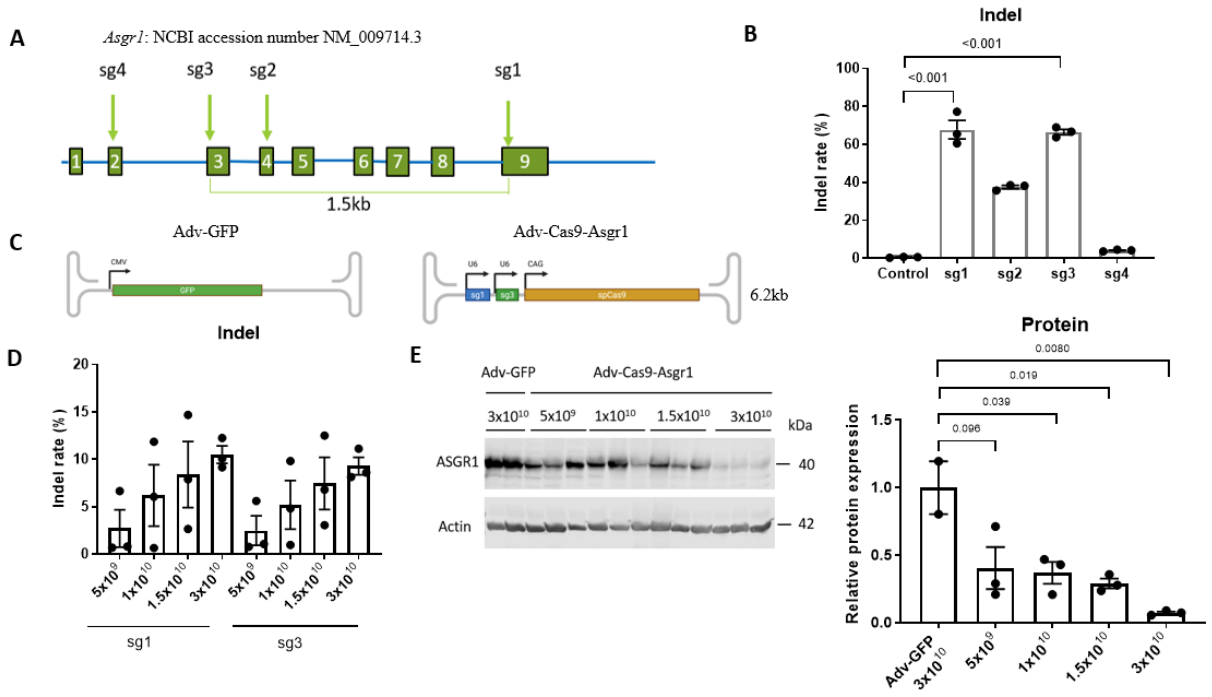


Figure 2.1: Validation of *Asgr1* targeting guide RNAs.

(A) Illustration of the mouse *Asgr1* gene layout. Numbered boxes indicate Exons. (B) Indel rates by sg1, sg2, sg3 and sg4 at the corresponding targeting sites in mouse N2a (Neuro-2a) cells. (C) Illustration of the Adenovirus vector Adv-CMV-GFP and Adv-Cas9-Asgr1 that uses U6 promoters to drive the expression of sg1 and sg3 and the CAG promoter to drive the expression of spCas9. (D) Indel rates at sg1 and sg3 targeted sites in the liver of wild-type mice treated with Adv-Cas9-Asgr1 of different doses (vg/animal). (E) Western blot of mouse ASGR1 protein in the liver of wild-type mice treated with Adv-Cas9-Asgr1 of different doses (vg/animal) and by $3x10^{10}$ vg/animal Adv-GFP.

2.3.2 Construction of Adv-Cas9-Asgr1 to disrupt Asgr1 in vivo

We constructed a single Adenovirus (Adv) vector "Adv-Cas9-Asgr1" (Figure 2.1C). In this vector, U6 promoters were used to drive the expression of sg1 and sg3, and the CAG promoter was used to drive the expression of spCas9.

To verify Adv-Cas9-Asgr1's *in vivo* editing capacity and to determine working dosages, we intravenously (i.v.) injected Adv-Cas9-Asgr1 through the tail vein at different doses ($5x10^9$, $1x10^{10}$, $1.5x10^{10}$, and $3x10^{10}$ vg/animal) to wild-type mice. 14 days post injection, the liver tissues were sampled, genomic DNA extracted, and indel rates at sg1 and sg3 targeted sites were determined. As shown in Figure 1D, both sg1 and sg3 led to indel events at targeted loci in a dose dependent manner, with the highest dose $3x10^{10}$ vg/animal led to the highest indel rates by both gRNAs. Consistently, western blot (WB) confirmed effective loss of protein signals in Adv-Cas9-Asgr1 treated animal livers at the $3x10^{10}$ vg/animal doses, with as much as >90% protein knockdown mimicking a close-to-homozygous phenotype (Figure 2.1E). Animals in the $5x10^9$ vg/animal dose group also showed ~50% protein knockdown, representing a close-to-heterozygous phenotype (Figure 2.1E).

Of note, the level of protein knockdown (~50 to 90%) appears to be much higher than the gene editing rates at the DNA level (3 -15%). Such discrepancy has been reported previously (*138*). This outcome likely stems from the fact that ASGR1 expression is exclusively to hepatocytes and the Adv-Cas9-Asgr1 vector exhibits high hepatocyte specificity, resulting in minimal editing within non-hepatocyte liver cell populations. Furthermore, standard indel evaluations may not fully capture the editing landscape, as they fail to detect the potential large fragment deletions generated by the concurrent cleavages of sg1 and sg3.

Nevertheless, these results confirmed that Adv-Cas9-Asgr1 is effective to disrupt *Asgr1 in vivo*. Based on these results, we selected $5x10^9$ (low) and $3x10^{10}$ vg/animal (high) doses for the following experiments.

2.3.3 Adv-Cas9-Asgr1 effectively knockdown ASGR1 in ApoE$^{-/-}$ mice

We proceeded to evaluate Adv-Cas9-Asgr1 in the *ApoE$^{-/-}$* mice, a classic animal model that is utilized in studies of atherosclerosis (*222*). We i.v. administered two doses: (i) $5x10^9$ (low) and (ii) $3x10^{10}$ vg/animal (high) to the animals. In the control groups, the animals received Adv-CMV-GFP at two doses (i) $5x10^9$ (low) and (ii) $3x10^{10}$ vg/animal (high), where CMV promoter is used to drive the expression of green fluorescence protein (GFP), of the same doses. Right after injection, the animals were subjected to Western diet to induce the development of atherosclerosis. Between 17 to 19 weeks post injection, the animals were humanely euthanized, and samples were collected to evaluate gene editing and atherosclerosis related parameters. Along the course of experiment, we also tested glucose tolerance, insulin tolerance and food intake of these animals. An illustration of the experiment flow is shown in Figure 2.2.

As shown in Figure 2.3A and Figure 2.4A, both adenoviral doses (5×10^9 and 3×10^{10} vg/animal) induced indel events at the sg1 and sg3 target sites in *ApoE$^{-/-}$* mice at frequencies comparable to those observed in wild-type mice (Figure 2.1D). Droplet digital PCR (ddPCR) further revealed substantial large-fragment deletions resulting from simultaneous cleavage at sg1 and sg3, occurring in 9.5% and 12% of alleles at the 5×10^9 (low) and 3×10^{10} vg/animal (high) doses, respectively (Figure 2.3A and Figure 2.4A). Consequently, Adv-Cas9-Asgr1 treatment reduced *Asgr1* expression at the mRNA (Figure 2.3B and Figure 2.4B) level in liver tissue. At the protein level, the 5×10^9 vg/animal dose of Adv-Cas9-Asgr1 decreased hepatic ASGR1

protein by approximately 50%, whereas the 3×10^{10} vg/animal dose achieved roughly 80% protein reduction (Figure 2.3C and Figure 2.4C), again mirroring the effects observed in wild-type animals (Figure 2.1E).

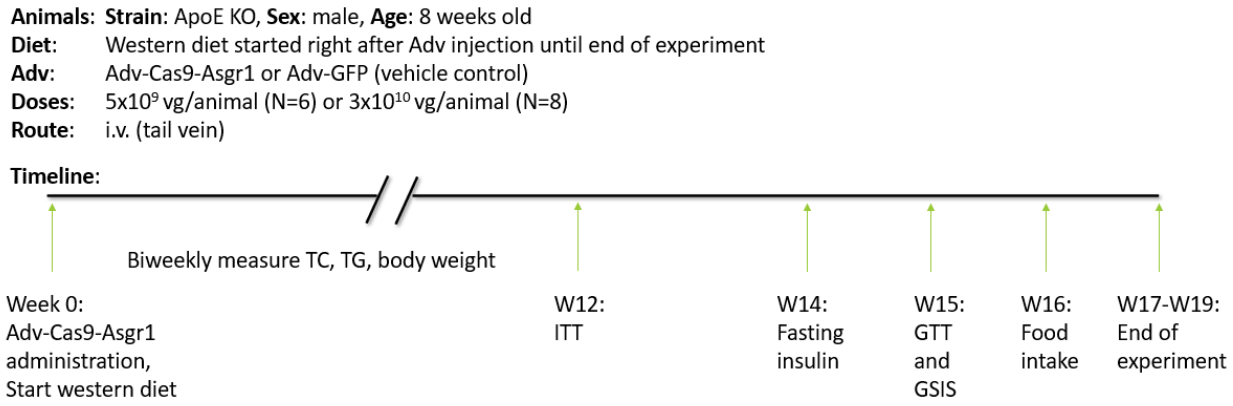


Figure 2.2: Illustration of the *in vivo* experiment.

8-week-old *ApoE*$^{-/-}$ mice were transduced with Adv-GFP or Adv-Cas9-Asgr1 at $3x10^{10}$ vg/animal or $5x10^{9}$ vg/animal through i.v injection. Western diet treatment started right after virus injection and continued for the remaining experiment. Experiments ended at W17-W19.

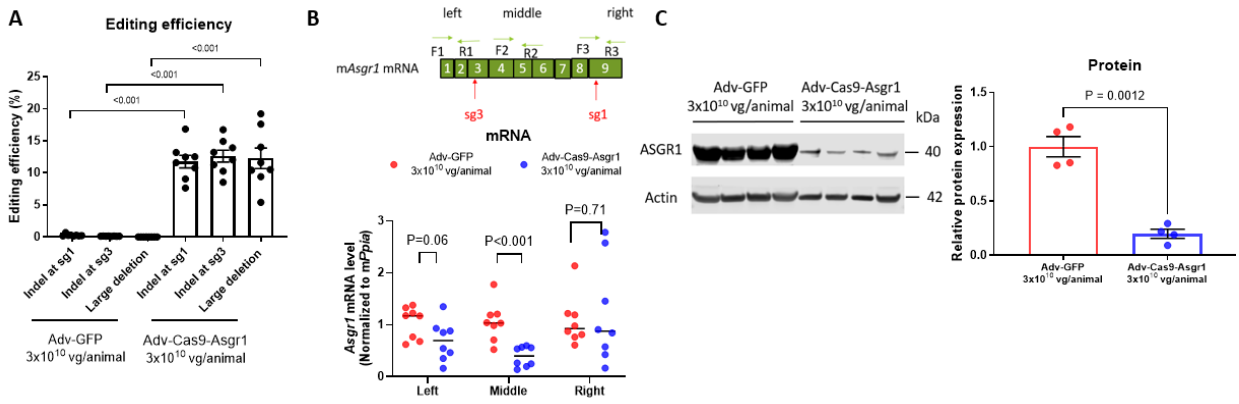


Figure 2.3: Adv-Cas9-Asgr1 mediated ASGR1 knockdown at $3x10^{10}$ vg/animal dose *in vivo*.

(A) Indel rates at individual gRNA targeting sites and the large fragment deletion rates in the liver tissues of *ApoE*$^{-/-}$ mice treated by $3x10^{10}$ vg/animal Adv-GFP or Adv-Cas9-Asgr1. (B) *Asgr1* mRNA levels in the liver of *ApoE*$^{-/-}$ mice treated by $3x10^{10}$ vg/animal Adv-GFP (red color dots) or Adv-Cas9-Asgr1 (blue color dots). Three pairs of primers (left, middle and right) were used, as illustrated in the bottom of the panel. (C) Left: WB of ASGR1 in the liver tissues of *ApoE*$^{-/-}$ mice treated by $3x10^{10}$ vg/animal Adv-Cas9-Asgr1 or Adv-GFP. Right: quantification of WB signals.

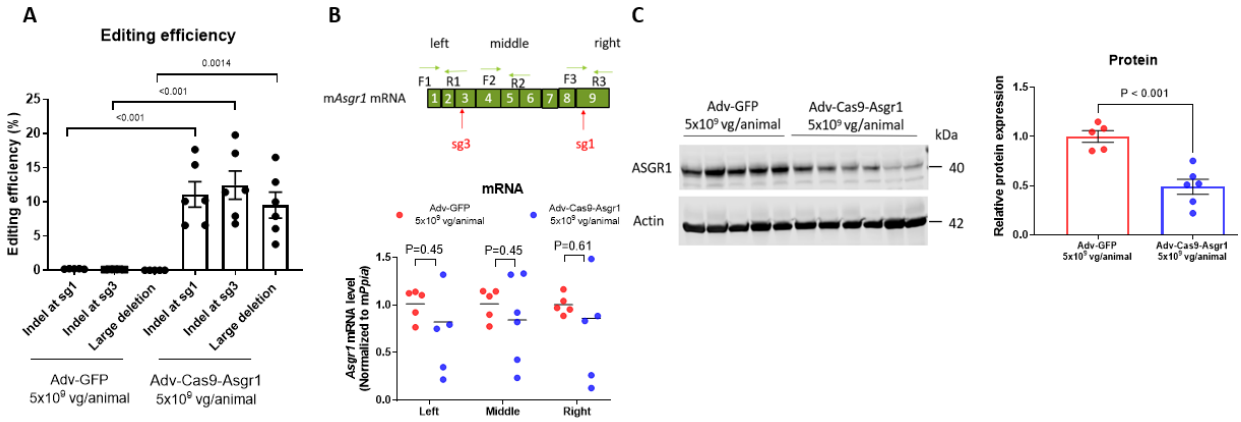


Figure 2.4: Adv-Cas9-Asgr1 mediated ASGR1 knockdown at 5x10^9 vg/animal dose *in vivo*.

(A) Indel rates at individual gRNA targeting sites and the large fragment deletion rates in the liver tissues of *ApoE*$^{-/-}$ mice treated by 5x10^9 vg/animal Adv-GFP or Adv-Cas9-Asgr1. (B) *Asgr1* mRNA levels in the liver of *ApoE*$^{-/-}$ mice treated by 5x10^9 vg/animal Adv-GFP (red color dots) or Adv-Cas9-Asgr1 (blue color dots). Three pairs of primers (left, middle and right) were used, as illustrated in panel B. (C) Left: WB of ASGR1 in the liver tissues of *ApoE*$^{-/-}$ mice treated by 5x10^9 vg/animal Adv-Cas9-Asgr1 or Adv-GFP. Right: quantification of WB signals.

2.3.4 Adv-Cas9-Asgr1 led to reduction of total cholesterol levels

We collected bi-weekly blood samples and evaluated serum TC in these animals throughout the experiment. The liver TC contents were evaluated postmortem. While serum TC levels increased in both Adv-Cas9-Asgr1 treated animals and control group animal, animals received Adv-Cas9-Asgr1 had significantly lower levels of TC in both dosing groups ($5x10^9$ and $3x10^{10}$ vg/animal, Figure 2.5A and 2.6A). Consistently, liver TC contents were also lower in Adv-Cas9-Asgr1 treated animals than those in the control groups (Figure 2.5B and 2.6B).

We also evaluated triglycerides (TG) levels in the animals received Adv-Cas9-Asgr1 versus those in the control group. Interestingly, while both serum and liver TG levels were significantly lower in the $5x10^9$ vg Adv-Cas9-Asgr1 treated animals than those in the control group (Figure 2.7C and D), the TG levels were similar in both serum and liver in the $3x10^{10}$ vg Adv-Cas9-Asgr1 treated animals (Figure 2.7A and B), suggesting inconsistent TG reducing effects by Adv-Cas9-Asgr1.

These results demonstrate that Adv-Cas9-Asgr1 mediated ASGR1 knockdown reduced TC levels in *ApoE*$^{-/-}$ mice.

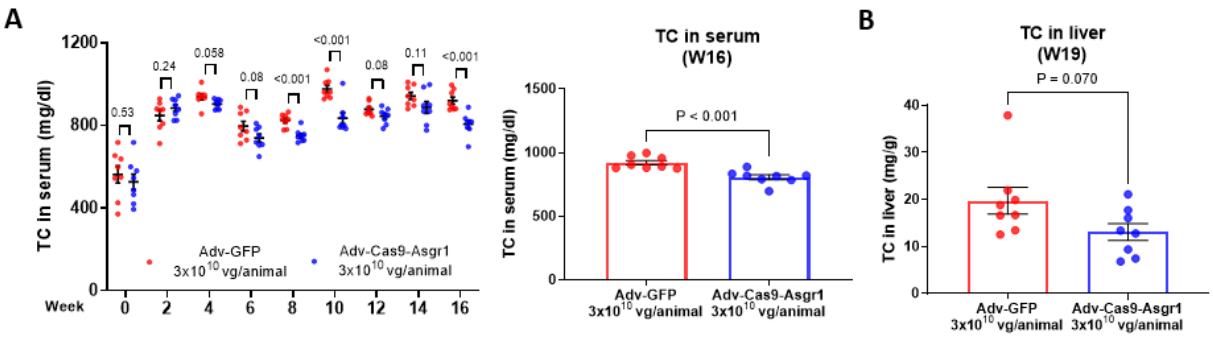


Figure 2.5: Adv-Cas9-Asgr1 treatment at $3x10^{10}$ vg/animal dose reduced total cholesterol (TC) levels in *ApoE*$^{-/-}$ mice.

(A) Left: TC levels in the serum of animals of different time points after $3x10^{10}$ vg/animal Adv-Cas9-Asgr1 (blue dots) or Adv-GFP (red dots) injection. Right: Week 16 (W16) TC levels in the serum of animals treated with $3x10^{10}$ vg/animal Adv-Cas9-Asgr1 (blue dots) or Adv-GFP (red dots). (B) Week 19 (W19) TC levels in the liver of animals treated with $3x10^{10}$ vg/animal Adv-Cas9-Asgr1 (blue dots) or Adv-GFP (red dots).

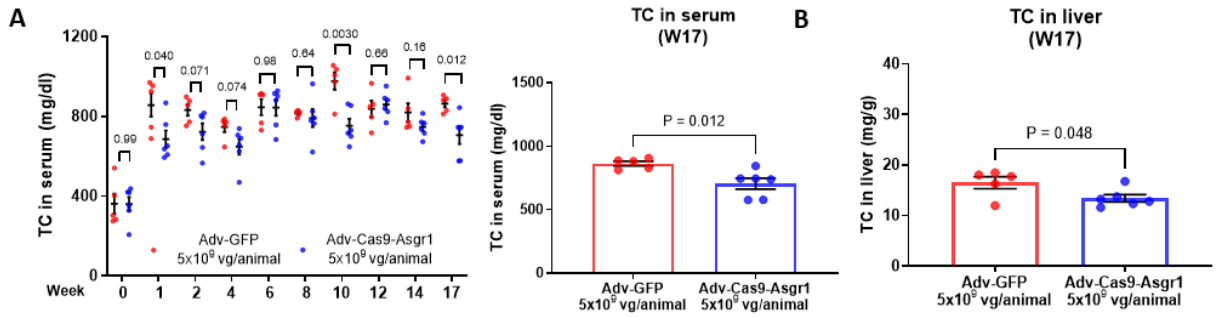


Figure 2.6: Adv-Cas9-Asgr1 treatment at $5x10^9$ vg/animal dose reduced total cholesterol (TC) levels in *ApoE*$^{-/-}$ mice.

(A) Left: TC levels in the serum of animals of different time points after $5x10^9$ vg/animal Adv-Cas9-Asgr1 (blue dots) or Adv-GFP (red dots) injection. Right: Week 17 (W17) TC levels in the serum of animals treated with $5x10^9$ vg/animal Adv-Cas9-Asgr1 (blue dots) or Adv-GFP (red dots). (B) Week 17 (W17) TC levels in the liver of animals treated with $5x10^9$ vg/animal Adv-Cas9-Asgr1 (blue dots) or Adv-GFP (red dots).

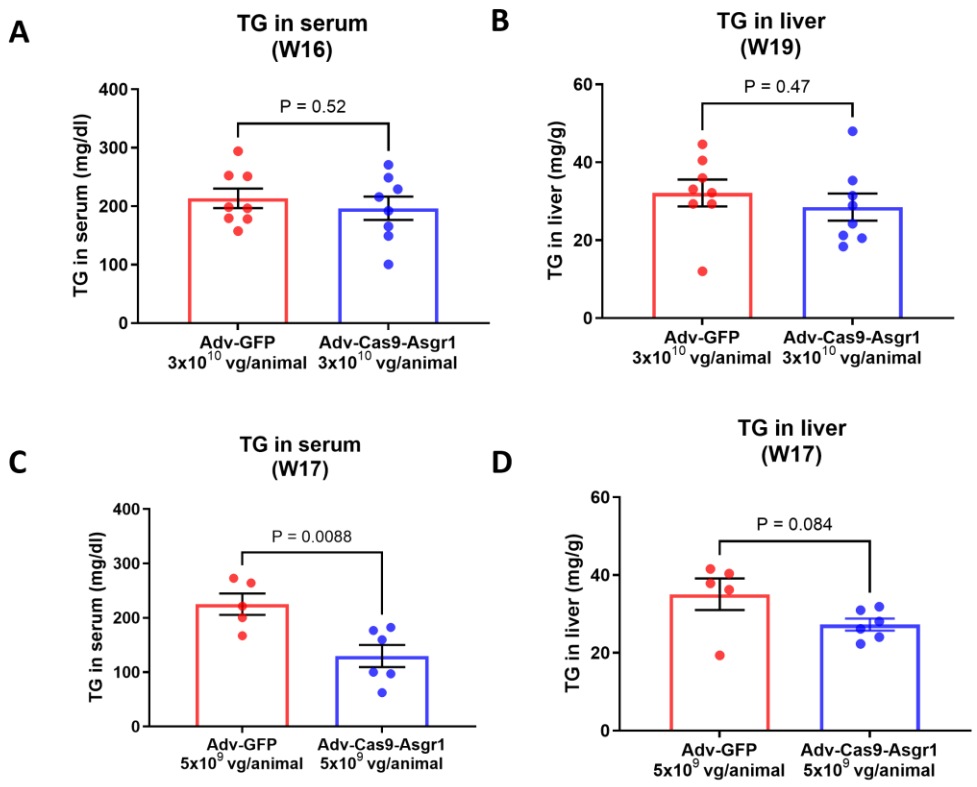


Figure 2.7: Effects of Adv-Cas9-Asgr1 on the levels of triglycerides (TG) in *ApoE*$^{-/-}$ mice.

(A) Week 16 (W16) TG levels in the serum of animals treated with $3x10^{10}$ vg/animal Adv-Cas9-Asgr1 (blue dots) or Adv-GFP (red dots). (B) Week 19 (W19) TG levels in the liver of animals treated with $3x10^{10}$ vg/animal Adv-Cas9-Asgr1 (blue dots) or Adv-GFP (red dots). (C) Week 17 (W17) TG levels in the serum of animals treated with $5x10^{9}$ vg/animal Adv-Cas9-Asgr1 (blue dots) or Adv-GFP (red dots). (D) Week 17 (W17) TG levels in the liver of animals treated with $5x10^{9}$ vg/animal Adv-Cas9-Asgr1 (blue dots) or Adv-GFP (red dots).

2.3.5 Adv-Cas9-Asgr1 mediated ASGR1 knockdown attenuated atherosclerosis in ApoE$^{-/-}$ mice

We evaluated atherosclerosis development in animals treated with Adv-Cas9-Asgr1 at a dose of $3x10^{10}$ vg/animal (n=8) and compared the results with those from Adv-GFP-treated control animals (n=8). Oil red O staining showed that the extent of atherosclerosis plaques ranged from 3 to 16 % in treatment group animals, which was on average are ~60% lower than that observed in the control group (ranging from 15% to 33%) (Figure 2.8A). At the lower dose ($5x10^9$ vg/animal), animals treated with Adv-Cas9-Asgr1 also exhibited a trend toward reduced atherosclerosis burden, albeit this difference did not reach statistical significance (Figure 2.9).

To gain mechanistic insight on how ASGR1 knockdown attenuated atherosclerosis in these animals, we evaluated the transcriptions of a panel of genes (i.e., *Angptl3*, *Srebp2*, *Srebp1a, Hmgcr, Pcsk9, Ldlr, Mttp, Abca1, Abcg5, Abcg8, Lxrα, Cyp7a1, Chop, Sr-b1, Hmgcs2, Fxr, Srebp1c, Fasn,* and *Scd1*) involved in the atherosclerosis development (Figure 2.10). RT-qPCR results revealed that the transcription of a key lipid regulator *Angptl3* was significantly downregulated in Adv-Cas9-Asgr1 treated mouse livers than in the control group (Figure 2.10).

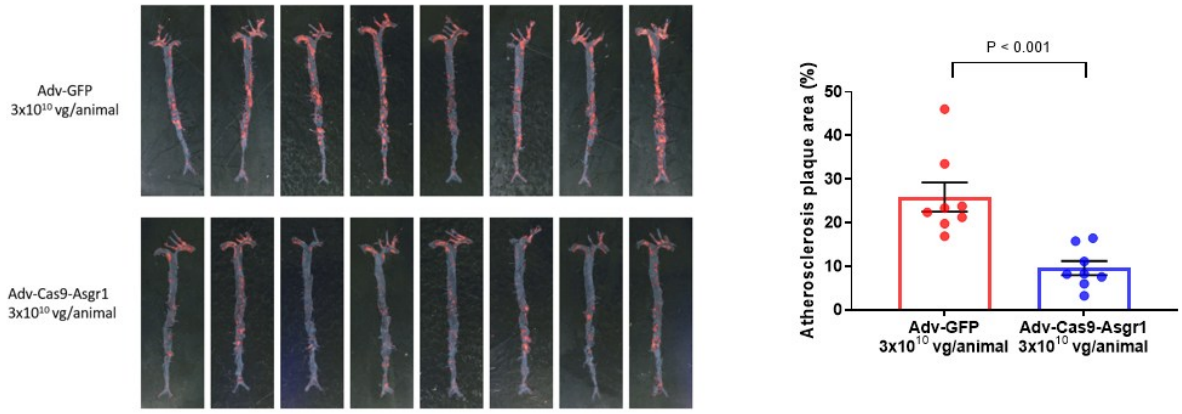


Figure 2.8: Adv-Cas9-Asgr1 at $3x10^{10}$ vg/animal dose reduced the extent of atherosclerosis in *ApoE*$^{-/-}$ mice.

(A) Left: oil-red-O staining of aorta trees of *ApoE*$^{-/-}$ mice treated with $3x10^{10}$ vg/animal Adv-Cas9-Asgr1 or Adv-GFP. Right: quantification of oil-red-O positive areas in the aorta trees of *ApoE*$^{-/-}$ mice treated with $3x10^{10}$ vg/animal Adv-Cas9-Asgr1 (blue dots) or Adv-GFP (red dots).

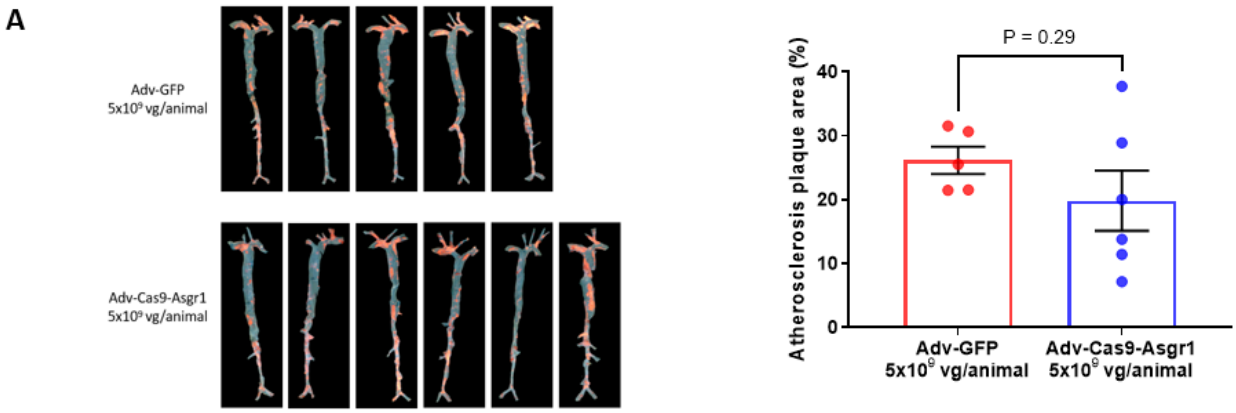


Figure 2.9: Adv-Cas9-Asgr1 treatment at $5x10^9$ vg/animal dose reduced the extent of atherosclerosis in *ApoE*$^{-/-}$ mice.

Left: oil-red-O staining of aorta trees of *ApoE*$^{-/-}$ mice treated with $5x10^9$ vg/animal Adv-Cas9-Asgr1 (bottom) or Adv-GFP (top). Right: quantification of oil-red-O positive areas in the aorta trees of *ApoE*$^{-/-}$ mice treated with $5x10^9$ vg/animal Adv-Cas9-Asgr1 (blue dots) or Adv-GFP (red dots).

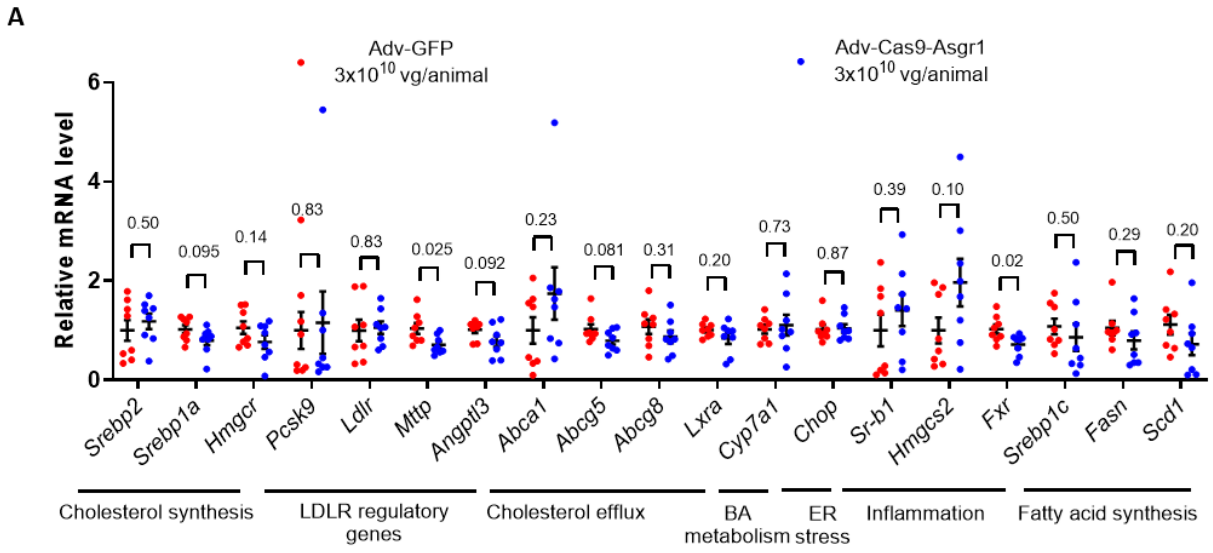


Figure 2.10: Effects of Adv-Cas9-Asgr1 on atherosclerosis related gene expressions in the liver of *ApoE*$^{-/-}$ mice.

A total of 19 genes involved in cholesterol synthesis, LDLR regulatory, cholesterol efflux, bile acid metabolism, ER stress, inflammation and fatty acid synthesis were selected.

2.3.6 Adv-Cas9-Asgr1 mediated ASGR1 knockdown improves insulin sensitivity

We conducted intraperitoneal insulin tolerance test (IPITT) at Week 12 (W12) in animals receiving a dose of $3x10^{10}$ vg/animal. Following insulin injection, blood glucose levels were measured at 0, 15, 30, 60, 90 and 120 min. The results showed that Adv-Cas9-Asgr1 treated animals exhibited a more rapid decline in plasma glucose levels, followed by faster glucose recovery, compared with vehicle control (i.e., Adv-GFP) animals (Figure 2.11A, left panel). Analysis of the area under the curve (AUC) of the IPITT profiles demonstrated a statistical significant difference between the two groups (Figure 2.11A, right panel).

At Week 15, Glucose-Stimulated Insulin Secretion (GSIS) and Oral Glucose Tolerance (OGTT) tests were conducted in these animals. After injection of the glucose, serum insulin levels were measured at 0, 15, 30, and 60 min. The Adv-Cas9-Asgr1 treated animals had a blunted insulin peak and a more rapid return to baseline compared with control animals (Figure 2.11B, left panel). AUC of the GSIS profiles also demonstrated statistical difference between these two groups (Figure 2.11B, right panel). Consistently, fasting insulin levels at week 14 (W14) were also significantly lower in the Adv-Cas9-Asgr1 treated animals than in the control group animals (Figure 2.11C). In the OGTT, blood glucose levels were measured at 0, 15, 30, 60, and 120 min after glucose administration by gavage. Adv-Cas9-Asgr1 treated animals showed reduced blood glucose levels compared with control animals, further supporting enhanced insulin sensitivity in this group (Figure 2.11D). Similar improvements in OGTT and IPITT profiles were also observed in animals treated with the lower dose ($5x10^9$ vg/animal) of Adv-Cas9-Asgr1 (Figure 2.12).

We performed western blot (WB) analysis to investigate whether insulin stimulated phosphorylation of Protein kinase B (AKT) and insulin receptor (IR) contribute to the improved

insulin sensitivity observed in the Adv-Cas9-Asgr1 treated animals. WB analysis revealed significantly increased levels of phosphorylated AKT (p-AKT) and phosphorylated IR (p-IR) in the livers of Adv-Cas9-Asgr1 treated animals compared with those in control animals (Figure 2.13).

Together, these data suggest that Adv-Cas9-Asgr1 mediated ASGR1 knockdown enhances insulin signaling and improves insulin sensitivity in the *ApoE*$^{-/-}$ mice.

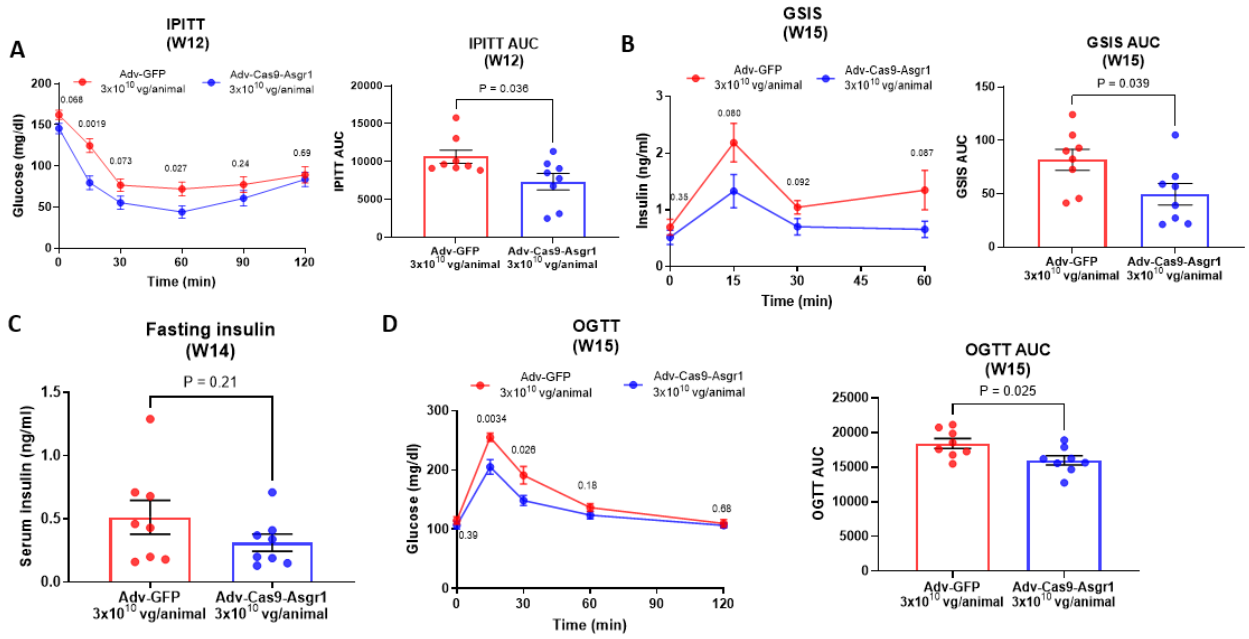


Figure 2.11: Adv-Cas9-Asgr1 treatment at $3x10^{10}$ vg/animal dose improved insulin sensitivity in *ApoE*$^{-/-}$ mice.

(A) Left: IPITT results in *ApoE*$^{-/-}$ mice treated with $3x10^{10}$ vg/animal Adv-Cas9-Asgr1 (blue line) or Adv-GFP (red line). Right: areas under curve (AUCs) of the IPITT curves of the left panel. (B) Left: GSIS results in *ApoE*$^{-/-}$ mice treated with $3x10^{10}$ vg/animal Adv-Cas9-Asgr1 (blue line) or Adv-GFP (red line). Right: areas under curve (AUCs) of the GSIS curves of the left panel. (C) Fasting insulin levels in *ApoE*$^{-/-}$ mice treated with $3x10^{10}$ vg/animal Adv-Cas9-Asgr1 (blue line) or Adv-GFP (red line). (D) Left: OGTT results in *ApoE*$^{-/-}$ mice treated with $3x10^{10}$ vg/animal Adv-Cas9-Asgr1 (blue line) or Adv-GFP (red line). Right: areas under curve (AUCs) of the OGTT curves of the left panel.

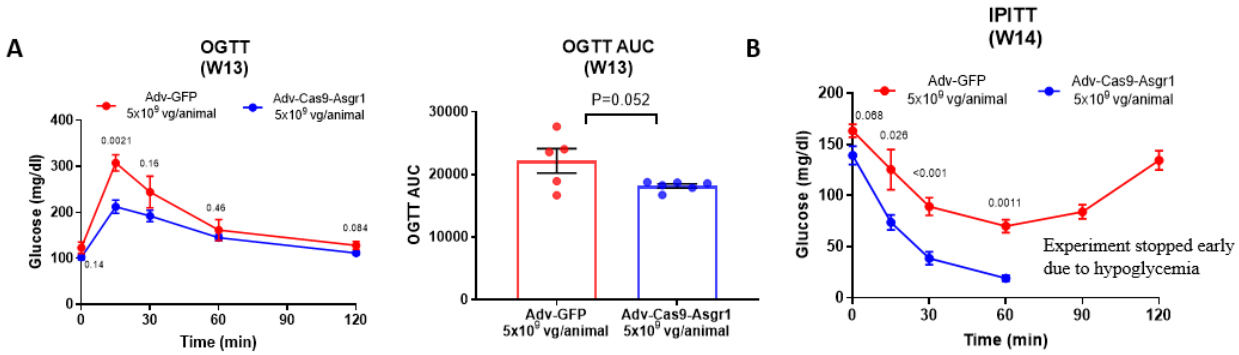


Figure 2.12: Adv-Cas9-Asgr1 treatment at $5x10^9$ vg/animal dose improved insulin sensitivity in *ApoE*$^{-/-}$ mice.

(A) Left: OGTT results in *ApoE*$^{-/-}$ mice treated with $5x10^9$ vg/animal Adv-Cas9-Asgr1 (blue line) or Adv-GFP (red line). Right: areas under curve (AUCs) of the OGTT curves of the left panel. (B) IPITT results in *ApoE*$^{-/-}$ mice treated with $5x10^9$ vg/animal Adv-Cas9-Asgr1 (blue line) or Adv-GFP (red line).

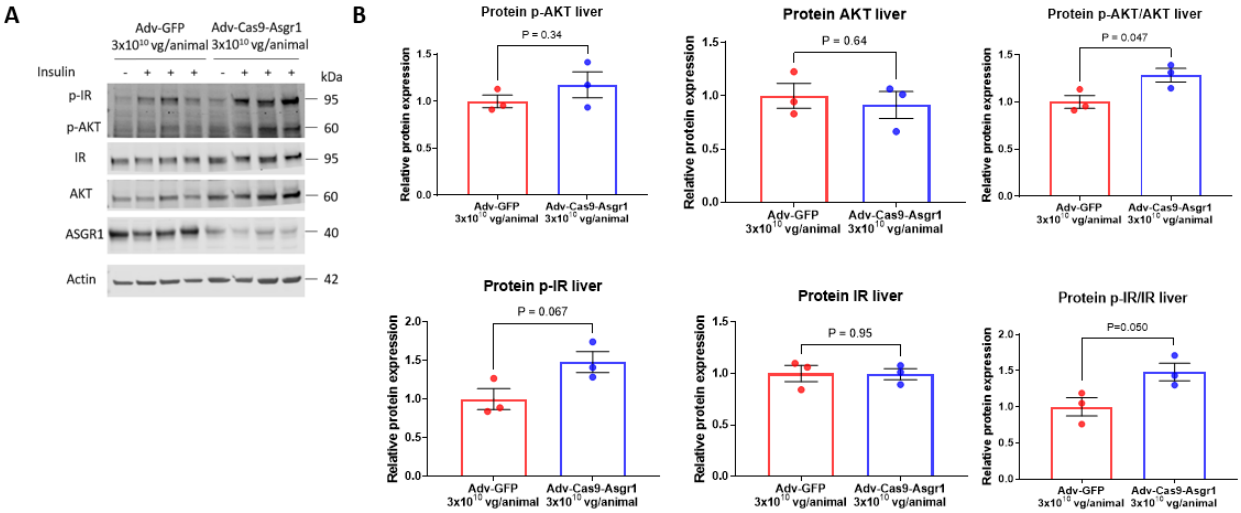


Figure 2.13: Effects of Adv-Cas9-Asgr1 on insulin sensitivity related protein expressions.

(A) WB of phosphorylated IR (p-IR), phosphorylated AKT (p-AKT), IR and AKT in the liver of *ApoE*$^{-/-}$ mice treated with 3x10^{10} vg/animal Adv-Cas9-Asgr1 or Adv-GFP. (B) Quantification of WB results in panel A.

2.3.7 Adv-Cas9-Asgr1 mediated ASGR1 knockdown reduces body weight and adipose tissue mass

Animal body weights were monitored throughout the study. Adv-Cas9-Asgr1 treated animals exhibited significantly lower body weights in both dosing groups, i.e., $3x10^{10}$ vg/animal (Figure 2.14A and B) and $5x10^{9}$ vg/animal (Figure 2.15A), compared with control animals. The reduction in body weight is likely attributable to the decreased adipose tissue mass, as evidenced by lower subcutaneous adipose tissue (SCAT) mass, reduced SCAT-to-body weight ratio, lower visceral adipose tissue (VAT) mass, and reduced the VAT-to-body weight ratio in Adv-Cas9-Asgr1-treated animals relative to controls (Figure 2.14C-F). A similar trend was observed in the $5x10^{9}$ vg/animal dosing group, in which fat mass tended to be lower and lean mass tended to be higher in Adv-Cas9-Asgr1 treated animals, although these differences did not reach statistical significance (Figure 2.15B).

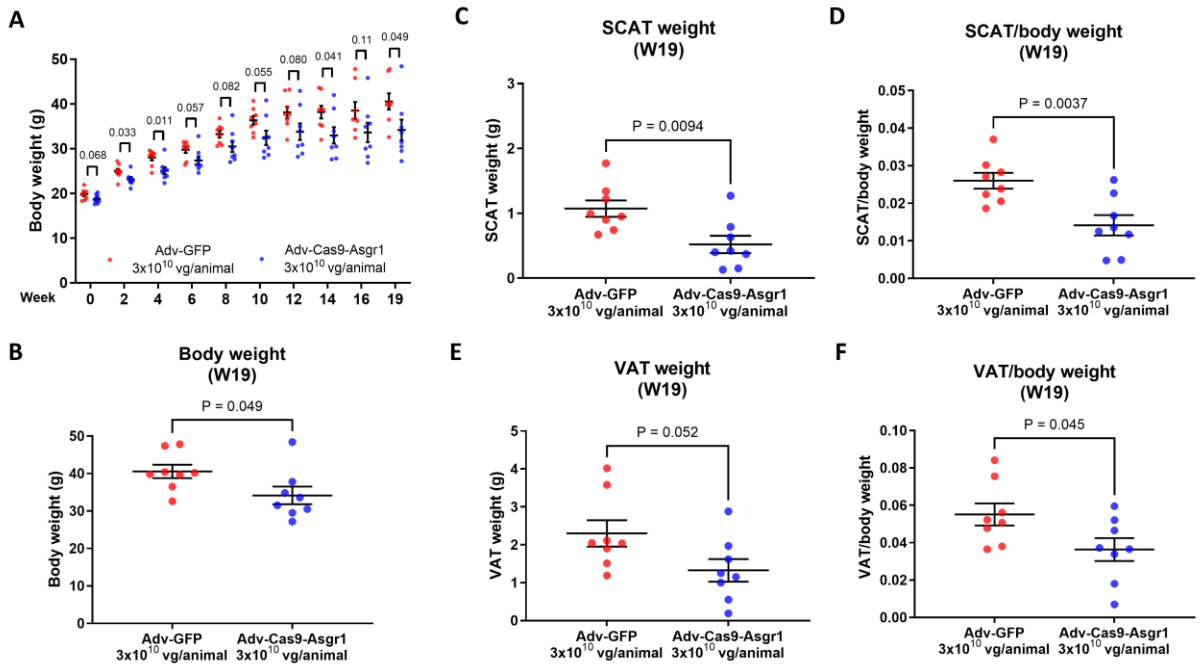


Figure 2.14: Adv-Cas9-Asgr1 treatment at $3x10^{10}$ vg/animal dose reduced body weight and adipose tissue mass in *ApoE*$^{-/-}$ mice.

(A) Body weight throughout the experiment of *ApoE*$^{-/-}$ mice treated with $3x10^{10}$ vg/animal Adv-Cas9-Asgr1 (blue dots) or Adv-GFP (red dots). (B) Week 19 (W19) of the body weights of *ApoE*$^{-/-}$ mice treated with $3x10^{10}$ vg/animal Adv-Cas9-Asgr1 (blue dots) or Adv-GFP (red dots). (C) SCAT weights of *ApoE*$^{-/-}$ mice treated with $3x10^{10}$ vg/animal Adv-Cas9-Asgr1 (blue dots) or Adv-GFP (red dots). (D) SCAT-to-body weight ratios of *ApoE*$^{-/-}$ mice treated with $3x10^{10}$ vg/animal Adv-Cas9-Asgr1 (blue dots) or Adv-GFP (red dots). (E) VAT of *ApoE*$^{-/-}$ mice treated with $3x10^{10}$ vg/animal Adv-Cas9-Asgr1 (blue dots) or Adv-GFP (red dots). (F) VAT-to-body weight ratios of *ApoE*$^{-/-}$ mice treated with $3x10^{10}$ vg/animal Adv-Cas9-Asgr1 (blue dots) or Adv-GFP (red dots).

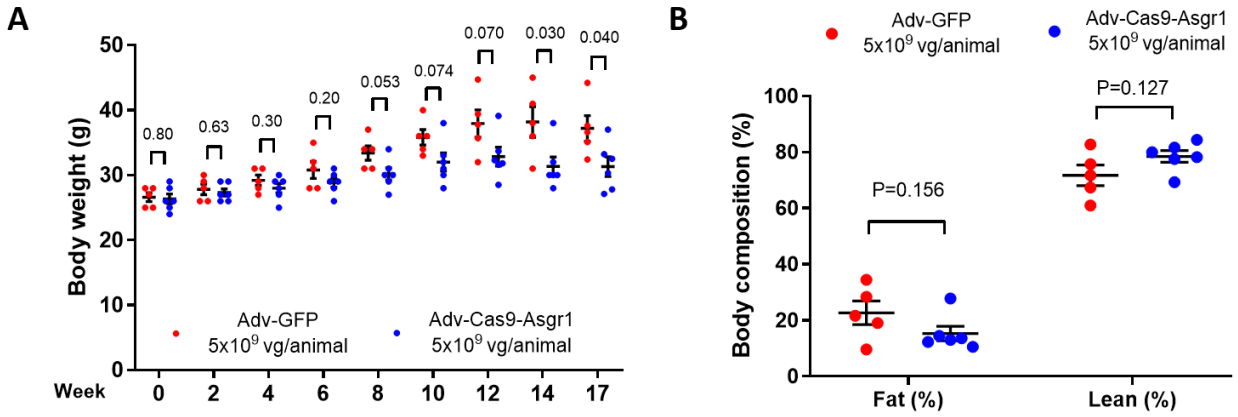


Figure 2.15: Adv-Cas9-Asgr1 treatment at $5x10^9$ vg/animal dose reduced body weights of *ApoE*$^{-/-}$ mice.

(A) Body weights of *ApoE*$^{-/-}$ mice treated with $5x10^9$ vg/animal Adv-Cas9-Asgr1 (blue dots) or Adv-GFP (red dots). (B) Fat and lean mass percentage of *ApoE*$^{-/-}$ mice treated with $5x10^9$ vg/animal Adv-Cas9-Asgr1 (blue dots) or Adv-GFP (red dots).

2.3.8 Minimal liver toxicity by Adv-Cas9-Asgr1 treated animals

We looked at potential liver toxicity. In the $3x10^{10}$ vg/animal dosing group, the liver weight and liver-to-body weight ratios are indistinguishable between treatment group animals and the control group animals (Figure 2.16A and B). We also measured the serum levels of aspartate aminotransferase (AST) and alanine aminotransferase (ALT). There were no significant differences in AST and ALT levels between treated and control animals (Figure 2.16C and D). We did not observe any differences between the treatment group animals and the control group animals in food intake either (Figure 2.16E). Similarly, in the $5x10^{9}$ vg/animal dosing group, no obvious indicators of liver toxicity were noticed as well (Figure 2.17).

These data suggest that Adv-Cas9-Asgr1 had minimal liver toxicity to the *ApoE*$^{-/-}$ mice.

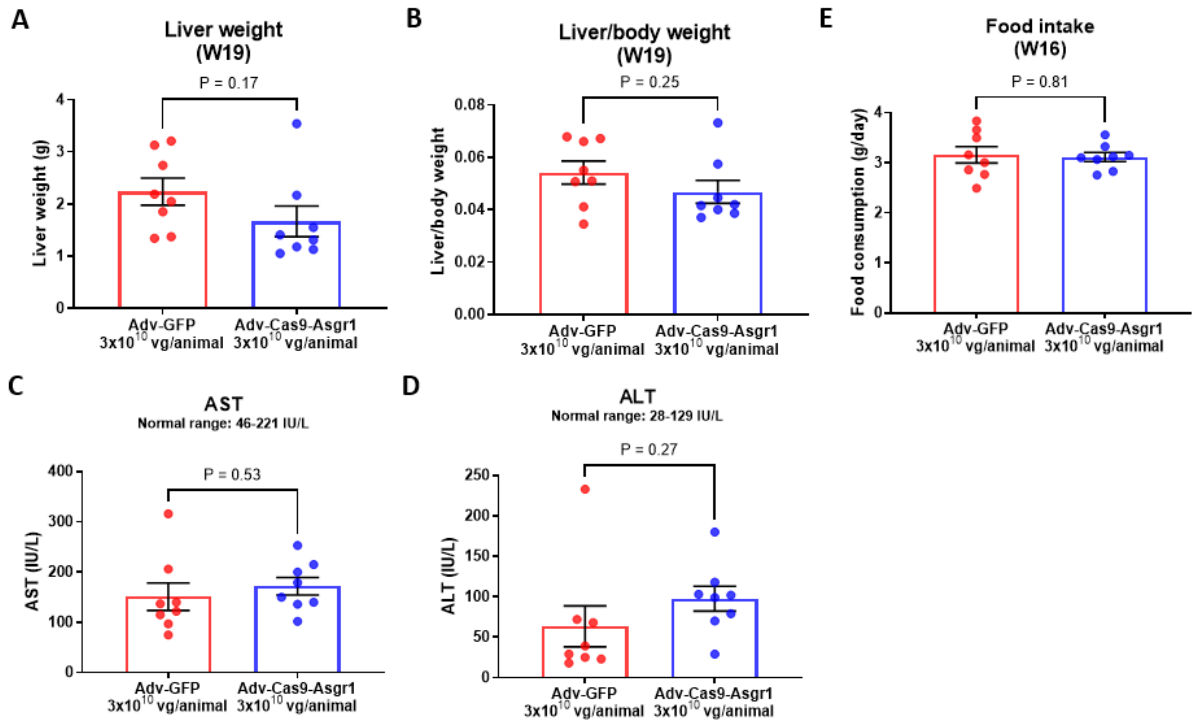


Figure 2.16: Minimal liver toxicity by Adv-Cas9-Asgr1 at $3x10^{10}$ vg/animal dose in *ApoE*$^{-/-}$ mice.

(A) Liver weights of *ApoE*$^{-/-}$ mice treated with $3x10^{10}$ vg/animal Adv-Cas9-Asgr1 (blue dots) or Adv-GFP (red dots). (B) Liver-to-body weight ratios of *ApoE*$^{-/-}$ mice treated with $3x10^{10}$ vg/animal Adv-Cas9-Asgr1 (blue dots) or Adv-GFP (red dots). (C) AST levels in the serum of *ApoE*$^{-/-}$ mice treated with $3x10^{10}$ vg/animal Adv-Cas9-Asgr1 (blue dots) or Adv-GFP (red dots) at Week 19. (D) ALT levels in the serum of *ApoE*$^{-/-}$ mice treated with $3x10^{10}$ vg/animal Adv-Cas9-Asgr1 (blue dots) or Adv-GFP (red dots) at Week 19. (E) Food intake of *ApoE*$^{-/-}$ mice treated with $3x10^{10}$ vg/animal Adv-Cas9-Asgr1 (blue dots) or Adv-GFP (red dots) at Week 16.

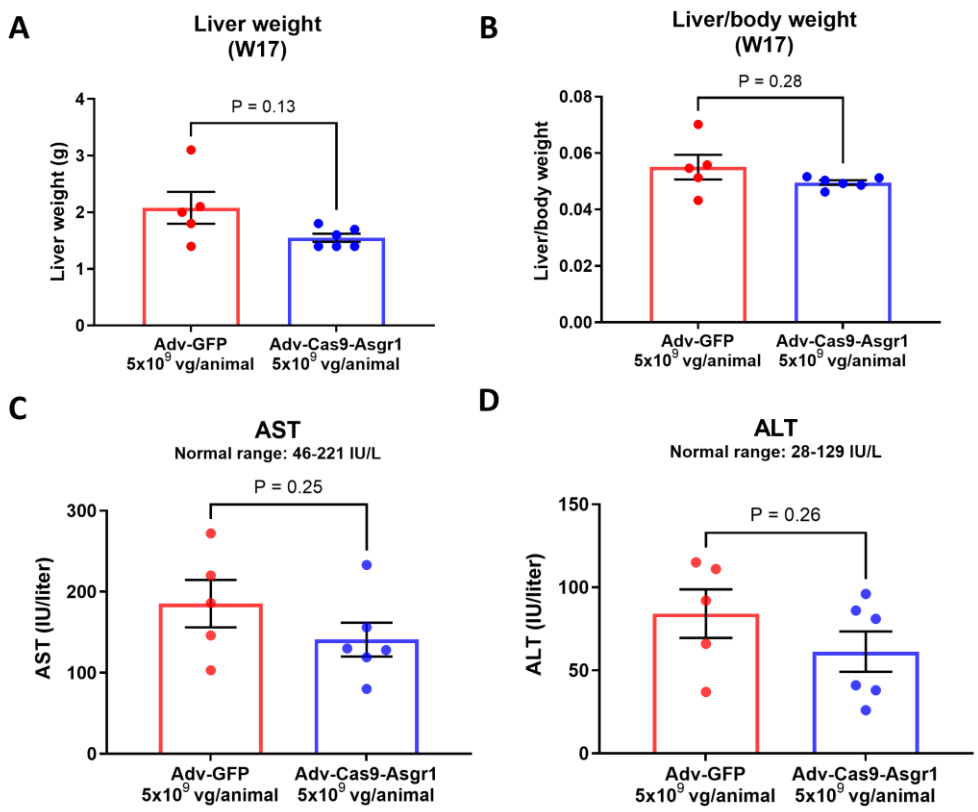


Figure 2.17: Minimal liver toxicity by Adv-Cas9-Asgr1 treatment at $5x10^9$ vg/animal dose to *ApoE*$^{-/-}$ mice.

(A) Liver weights of *ApoE*$^{-/-}$ mice treated with $5x10^9$ vg/animal Adv-Cas9-Asgr1 (blue dots) or Adv-GFP (red dots). (B) Liver-to-body weight ratios of *ApoE*$^{-/-}$ mice treated with $5x10^9$ vg/animal Adv-Cas9-Asgr1 (blue dots) or Adv-GFP (red dots). (C) AST levels in the serum of *ApoE*$^{-/-}$ mice treated with $5x10^9$ vg/animal Adv-Cas9-Asgr1 (blue dots) or Adv-GFP (red dots) at Week 17. (D) ALT levels in the serum of *ApoE*$^{-/-}$ mice treated with $5x10^9$ vg/animal Adv-Cas9-Asgr1 (blue dots) or Adv-GFP (red dots) at Week 17.

2.4 Discussion

Human genetic and preclinical data have established that ASGR1 loss-of-function renders TC reduction and atheroprotective effects. Human populations carrying heterozygous del12 mutation was associated with lowering of non-HDL cholesterol by 15.3 mg per deciliter (95% CI, 11.7 to 18.9; $P = 1.0\times10^{-16}$), which leads to 34% reduction in coronary disease risks (*184*). ASGR1 knockout pigs exhibited 18% TC reduction and 74% plaque alleviation under high cholesterol high fat (HCHF) diet (*185*). However, the effect of ASGR1 knockout on TC is more controversial in mice. In *ApoE*$^{-/-}$ mouse model, Svecla et al identified that ASGR1 knockout contributed to 22% TC reduction and 26% reduction in atherosclerosis plaque area at heart sinus after 16 weeks of western diet (*216*); while Zhang et al found no change of TC but approximately 50% atherosclerosis plaque burden decrease likely due to VLDL reduction after 12 weeks western diet (*183, 218*). In LDLR deficient mouse model, AAV-shAsgr1 mediated ASGR1 knockdown *in vivo* caused 20% reduction in serum TC and over 60% decrease in atherosclerosis plaque areas (*183*). In C57 mouse models, Wang et al demonstrated around 10% TC reduction in heterozygous ASGR1 knockout mice and 20% TC reduction in homozygous ASGR1 knockout mice under 4 weeks high fat high cholesterol diet (*183*); Xu et al showed 14% TC reduction in heterozygous ASGR1 knockout mice and 19% TC reduction in homozygous ASGR1 knockout mice under chow diet (*217*); Svecla et al's paper found 10% TC reduction in homozygous ASGR1 knockout mice after 20 weeks high fat diet (*215*).

Current study adds a gene-editing–based mouse model to this body of evidence. In *ApoE*$^{-/-}$ mice, Adv-Cas9-Asgr1 lowered serum and hepatic cholesterol levels downregulated key lipid regulating genes such as *Angptl3* and reduced aortic plaque burden. Together with ongoing clinical evaluation of anti-ASGR1 antibodies (clinicaltrials.gov # NCT03170193), these results

strengthen the rationale for *Asgr1* as a therapeutic target in lipid metabolism and atherosclerosis prevention.

Beyond lipid lowering and plaque attenuation, Adv-Cas9-Asgr1 treated mice exhibited improved insulin sensitivity on insulin and glucose tolerance testing, accompanied by increased hepatic phosphorylation of AKT and insulin receptor, indicating favorable remodeling of hepatic insulin signaling. Concomitant reductions in body weight and fat mass, including both subcutaneous and visceral fat, occurred without changes in food intake or overt liver toxicity, suggesting enhanced metabolic efficiency or altered nutrient partitioning rather than simple caloric restriction. These integrated effects on glycemic control and adiposity position ASGR1 inhibition as a potential strategy for treating type 2 diabetes and obesity, conceptually paralleling the pleiotropic benefits observed with GLP-1 based therapies (*223*).

Adenovirus was selected in the present work to enable a single vector, hepatocyte-preferential delivery of spCas9 and dual gRNAs *in vivo*. Although our data suggest robust ASGR1 protein depletion with minimal liver enzyme elevation, demonstrating feasibility in this preclinical setting, it should be cautioned that adenoviral vectors are generally unsuitable for chronic or systemic gene-editing therapy in humans due to their strong innate and adaptive immunogenicity, and limited clinical precedent compared with AAV and LNP platforms (*224*). Future work should evaluate *Asgr1* editing using clinically favored delivery systems, such as AAV or LNP, to improve safety, durability, and clinical translatability.

The current study employed conventional spCas9 with dual gRNAs targeting distinct exons to induce indels and large-fragment deletions, an efficient knockout strategy but one that relies on generating DNA double stranded breaks (DSBs) and thus carries potential genotoxicity concerns (*225*). Although on-target efficacy and short-term safety were acceptable in this mouse

model, future translational efforts should prioritize next-generation editors, such as base editors and prime editors, that minimize DSB risks while still silencing *Asgr1*. Incorporating high-depth off-target profiling, long-read sequencing for structural variants, and long-term tumorigenicity monitoring will be essential before ASGR1 or any other gene editing therapy enters clinical applications.

The efficacy of Adv-Cas9-Asgr1 mediated knockdown in the present work, together with human genetic data and the hepatic cell-surface localization of ASGR1, supports exploration of additional drug formats beyond CRISPR-based knockout. Antagonistic modalities, including monoclonal antibodies, siRNA, antisense oligonucleotides, and small-molecule inhibitors, could provide reversible, titratable suppression of ASGR1 with established delivery technologies, and early clinical experience with an anti-ASGR1 antibody (e.g., AMG529) already suggests acceptable tolerability and lipid-lowering potential in humans (clinicaltrials.gov # NCT03170193). Such approaches may be combined with or positioned as alternatives to one-time gene editing, enabling personalized selection of permanent versus adjustable ASGR1 inhibition strategies for cardiovascular and metabolic disease management.

Collectively, the present work demonstrates that *in vivo Asgr1* gene editing is technically feasible, biologically effective, and well tolerated in *ApoE*$^{-/-}$ mice, leading to coordinated improvements in lipid levels, plaque burden, insulin sensitivity, and adiposity. By validating *Asgr1* in a gene-editing therapy experiment and revealing broader metabolic benefits, the present work provides a strong foundation for advancing *Asgr1* targeted therapies, both editor-based and non–editor-based, towards clinical translation for atherosclerotic cardiovascular disease, and potentially other diseases such as diabetes and obesity.

Chapter 3 AAV-Mediated *Idol* Gene Disruption Does Not Confer Atheroprotection in *ApoE*$^{-/-}$ Mice

3.1 Introduction

Cardiovascular diseases (CVD) represent the leading cause of mortality worldwide, accounting for approximately one in three global deaths in recent years (*213*). Atherosclerosis, characterized by lipid and inflammatory cell accumulation within arterial walls, is a major cause of cardiovascular disease, and many studies aim to reduce its progression to ultimately lower cardiovascular risk (*226*). At the molecular level, elevated concentrations of low-density lipoprotein cholesterol (LDL-C) and very-low-density lipoprotein cholesterol (VLDL-C) are major risk factors to atherosclerosis (*227, 228*). Pharmacologic inhibition of 3-hydroxy-3-methylglutaryl coenzyme A (HMG-CoA) reductase by Statins greatly ameliorates atherosclerosis and reduces CVD risks (*229, 230*). Combination therapy with statins and non-statin agents, such as proprotein convertase subtilisin/kexin type 9 inhibitors (PCSK9i), provides additional benefit for individuals at moderate to high CVD risk (*5-7, 231, 232*). Nevertheless, a subset of patients exhibits limited or absent functional LDL receptor (LDLR) activity, fails to achieve target LDL-C concentrations (≤70 mg/dl in non-familial hypercholesterolemia), presents with drug intolerance, or does not meet the criteria outlined by the U.S. Food and Drug Administration (FDA) and the American College of Cardiology Expert Consensus Guidelines (*227*). For these individuals, the development of novel therapeutic modalities remains an unmet clinical need.

Gene editing technology, represented by CRISPR/Cas9, has become a major tool nowadays utilized in research and medicine (*1*). Gene editing therapeutics, hereafter also referred

to as GETx, offer new possibilities for the treatment, and potentially cure, of a broad spectrum of diseases, including monogenic diseases, infectious diseases, and others. The concept of employing GETx for cardiovascular diseases (GETx-CVD) was first articulated by Gupta in 2014, one year after the introduction of Cas9 gene editing technology (*8*). The rationale is that genetic predisposition plays a central role in CVD etiology; thus, precise modification of relevant gene(s) could theoretically confer durable therapeutic benefit (*9*).

Most GETx-CVD attempts focus on liver genes because current *in vivo* delivery means, such as adeno-associated virus (AAV), lipid nanoparticles (LNP), and others, target liver primarily (*40, 44*). Population genetics and preclinical animal model studies have suggested several liver-specific genes, which include *PCSK9*, *ANGPTL3*, *APOC3*, *LPA*, and *CETP*, as promising candidates for GETx-CVD (*112, 113, 135, 136, 153, 166, 169, 188, 219, 233*). Progressing from proof-of-concept to clinical translation, a number of ongoing GETx-CVD clinical trials targeting these genes in patients with severe or refractory dyslipidemia, familial hypercholesterolemia, or elevated lipoprotein(a), have indicated marked reductions in LDL-C, triglycerides, and/or other cardiovascular risk markers (*92-96, 98, 147, 234*).

Recently, IDOL (inducible degrader of LDL receptor, also known as MYLIP) stands out as a potential candidate gene for GETx-CVD, given its central regulatory role in hepatic cholesterol homeostasis and atherosclerotic risk. Functionally, *IDOL* encodes an E3 ubiquitin ligase that mediates the ubiquitination and lysosomal degradation of LDLR, VLDLR, and ApoER2, thereby directly limiting hepatic LDL uptake and influencing plasma lipoprotein concentrations (*235*). Human population genetic studies show that loss-of-function mutations in *IDOL* are associated with lower plasma LDL-C and reduced cardiovascular disease risk (*208, 236*). Experimental models also established that loss or down-regulation of IDOL leads to

increased LDLR stability, enhanced LDL clearance, and robust protection against diet-induced atherosclerosis (*237, 238*).

In the present work, we used spCas9 and developed dual guide RNA (dgRNA) based strategies (Cas9-dgRNA-IDOL) to disrupt the *IDOL* genes in human, rabbit and mouse cells. We then packaged the dual gRNAs that target the mouse *Idol* gene into AAV particles (AAV-dgRNA-mIdol), and tested AAV-dgRNA-mIdol effects in a mouse model of atherosclerosis.

3.2 Materials and methods

3.2.1 Animals

The *ApoE*$^{-/-}$ (B6.129P2-*Apoe*^{tm1Unc}/J, RRID:IMSR_JAX:002052) and Cas9 KI mice (B6J.129(Cg)-*Gt(ROSA)26Sor*$^{tm1.1(CAG-cas9*,-EGFP)Fezh}$/J, RRID:IMSR_JAX:026179) were purchased from the Jackson Laboratory. All the experimental procedures were approved by the Institutional Animal Care and Use Committee of the University of Michigan.

3.2.2 Plasmid construction

The plasmids including AAV-CMVc-Cas9 (Addgene, Cat# 106431) and PX458 (Addgene, Cat# 48138) were obtained from Addgene (Watertown, MA). gRNA sequences were synthesized by IDT and cloned into AAV-U6-gRNA-CMV-GFP plasmid (Addgene, Cat# 308180).

3.2.3 Generation of AAV particles and administration into mice

The AAV8 vectors were produced and purified by University of Michigan Vector Core. Titers are expressed as DNase resistant particles in genome copy ml (vg/ml): 1.7×10^{13} gc/ml for AAV-dgRNA-mIdol. AAV-dgRNA-mIdol particles were systemically administered into *ApoE*$^{-/-}$ mice at 8 weeks of age through tail vein injection. Blood samples were collected via facial vein before and biweekly after western diet start. 12 weeks after western diet, all the animals were humanely euthanized and tissues were harvested for analyses.

3.2.4 Cell culture and transfection

HEK293T (Cat# CRL3216), RK13 (Cat# CCL37), Human iPSCs (Cat# ACS-1030), mouse ESCs (Cat# CRL1934) were acquired from American Type Culture Collection (ATCC, Manassas, VA). Rabbit fibroblast cells were isolated and cultured from rabbit ears.

HEK293T, RK13 and rabbit fibroblast cells were maintained in Dulbecco's Modified Eagle Medium (DMEM) (Thermo Fisher Scientific, Cat# 11-965-092) with 10% FBS and 1%100X penicillin-streptomycin (Thermo Fisher Scientific, Cat# 15140122).

Human iPSC cells were cultured in feeder-free condition in mTeSR1 (StemCell Technologies, Vancouver, BC; Cat# 85850) on Matrigel (Corning Inc, Corning, NY; Cat# 354277)-coated cultureware surface.

The mouse ES cells were maintained in knockout DMEM (Gibco, Cat# 10829018) supplemented with 15% KSR (Thermo Fisher Scientific, Cat# 10828028), glutamax (Gibco, Grand Island, NY; Cat# 35050061), nonessential amino acids (Gibco, Cat# 11140050), penicillin-streptomycin, β-mercaptoethanol (Sigma, Cat# M7522), Leukemia Inhibitory Factor (LIF) (Thermo Fisher Scientific, Cat# PHC9464), PD0325901 (SC7, Greenville, SC; Cat#

391210-10-9) and CHIR99021 (Stem Cell Technologies, Cat# 72054) on coating plates with gelatin solution (Sigma, Cat# ES-006-B).

3.2.5 PCR and primers

Cells were harvested 48 h after transfection and genomic DNAs were extracted with the Quickextract DNA extraction solution (Biosearch Technologies, Cat# QE09050). Mouse liver DNAs were extracted with DNeasy Blood and Tissue Kit (Qiagen, Cat# 69504).

Targeted regions were PCR amplified using Q5 high-fidelity DNA polymerase (NEB, Cat# M0491S). Cycling conditions were as follow: initial denaturation at 95 °C for 2 min, followed by 35 cycles of denaturation at 95 °C for 30 s, annealing at 56 °C for 30 s, and extension at 72 °C for 30s, with a final extension at 72 °C for 5 min. The products were purified using QIAquick PCR purification kit (Qiagen, Cat# 28104). The primers used for PCR of the *Idol* targeted regions are listed in Table 3.1.

Table 3.1: PCR primer sequences.

Gene	Forward primer	Reverse primer
h*IDOL*-F1/R1	GTGCAGAGTATGCTGGTGGAG	CTGAGGCAGAGGTTACTATCGG
h*IDOL*-F2/R2	CTAGACATGCATGTGCGCAC	GTGCAGCTCACACACATGCA
rIdol-F1/R1	CAAAATGCGCCCAGGTCAACTATGTG	ACTGCTCTTTCTGGGCTGCTGTGG
rIdol-F2/R2	AAGACCCACGGACACAGCGG	GCGTTGCAATGAGTCACCCCTTCT
mIdol-F1/R1	ATCAGCTGTGCAGATGGTGC	CACTGCTGAGGCGGGGTTAC
mIdol-F2/R2	TACCTGTGTCGGCTTCTGCC	GTGCCACAGCTCCGGGAAAG

3.2.6 T7EI assay

The purified PCR products were denatured and re-annealed and digested with T7EI (NEB, Cat# M0302L) for 30 min at 37 °C, and then run in a 2% agarose gel. Non-perfectly matched DNA (presumably indel sites) would be recognized and cleaved by T7EI leading to two cleaved bands, whereas the perfectly matched DNA would not be recognized and cleaved by T7EI hence leading to only one band (the wild-type band).

The indel rate (%) was quantified using the formula $100 \times (1-(\mathrm{SQRT}(1-((A1+A2)/(A1+A2+A3)))))$, where A3 is the intensity of the wild-type band, A1 and A2 are the intensities of the two cleaved bands, respectively, and SQRT is the square root function.

3.2.7 Deep sequencing (deep-seq) and analysis

For deep sequencing, the purified PCR products were sent to the CCIB DNA Core Facility at Massachusetts General Hospital (Cambridge, MA), as previously described (*220*). Briefly, Illumina compatible adapters with unique barcodes were ligated onto each sample during library construction. Libraries were pooled in equimolar concentrations for multiplexed sequencing on the Illumina MiSeq platform with 2 × 150 run parameters. Indel rates were determined by the CRISPResso2 tool (http://crispresso.pinellolab.partners.org/) using fastq files.

3.2.8 TA cloning

To confirm the presence of the large-fragment deletion, PCR amplicons of the targeted region were generated using Taq polymerase and were ligated into the pCR™4-TOPO® TA vector (Thermo Fisher Scientific, Cat# 450030) following the manufacturer's instructions.

Briefly, 4 µL of purified PCR product was mixed with 1 µL of TA cloning vector and incubated at room temperature for 5 min. The ligation mixture was then transformed into chemically competent E. coli DH5α cells. Transformed cells were plated on LB agar plates and colonies were picked and expanded overnight in LB broth, plasmids were extracted using a RNeasy mini kit (Qiagen, Cat# 74106). Insert-containing plasmid sequences were verified by Sanger sequencing.

3.2.9 Quantitative real-time PCR (qPCR) analysis

Total RNA was extracted using RNeasy Mini Kit (Qiagen, Cat# 74106). Reverse transcription was performed using SuperScript III First-Strand (Invitrogen, Cat# 18080-051) with random primers. SYBR green fast qPCR mix (ABclonal, Cat# RM21203) was used to perform qPCR with specific gene primers. ΔΔCt method was used to quantitate gene expression, which was normalized to *Ppia* (mouse or human). The primers used for qPCR are shown in Table 3.2.

Table 3.2: qPCR primer sequences.

Gene	Forward primer	Reverse primer
h-*IDOL*-F/R	AGGAGAAGCTACGCAAGCTG	GCAGATAGACGTGCTGGACA
m-Idol-F1/R1	GCTGATGGAGGTAGAGGTGG	CGTGAACTGCAGCCCAAAAT
m-Idol-F2/R2	CAGAACACCGCCCAATACAG	AGTTCTCCATCGCTGACACA
m-Idol-F3/R3	ATCAACTCCACCTTCTGCCC	CAGGTAGACGTGCTGGACAT

3.2.10 Western blot analysis

Protein was lysed by Radio-Immunoprecipitation Assay buffer (RIPA) with proteinase inhibitors. Proteins were isolated in 10% SDS-PAGE and transferred to 0.45 μm nitrocellulose membranes. After blocked in 5% non-fat dry milk (LabScientific, Cat# M0841) at room temperature for one hour, membranes were firstly incubated with the primary antibodies overnight at 4 °C and imaged after incubated with secondary antibodies. The following antibodies were used in the study: anti-LDLR antibody (Abclonal, Cat# A14996), anti-VLDLR antibody (Abcam, Waltham, MA; Cat# ab203271), anti-ApoER2 antibody (Abcam, Cat# ab204112). Secondary antibodies used: IRDye® 800CW Donkey anti-Rabbit IgG Secondary Antibody (LI-COR, Cat# D40827-03) and IRDye® 680RD Donkey anti-Mouse IgG Secondary Antibody (LI-COR, Cat# D30322-25). Membranes were scanned using Odyssey Imaging System (LI-COR Biosciences) and quantified with the LI-COR Image Studio Software.

3.2.11 Serum analysis

Blood samples collected from the animals were allowed for clotting at room temperature for 30 min. Serum was isolated by centrifugation at 5000 rpm for 10 min and stored at -80 °C in small aliquots. Determination of TC and TG were performed using the cholesterol and triglyceride assay kit (Fujifilm, Cat# 999-02601 and NC2044372) according to the manufacture's instruction. Serum LDL and HDL were measured by Michigan Diabetes Research Center (MDRC) at the University of Michigan (Ann Arbor, Michigan, USA). ALT and AST values were determined by the IVAC Diagnostic Laboratory at the University of Michigan.

3.2.12 Oil Red O (ORO) staining of the aorta trees

Aorta trees were carefully isolated from postmortem animals and fixed in formalin (Fisher Scientific, Cat# 23-245685) at least overnight. Aorta trees were then stained in ORO solution, consisting of 1.6 mg/ml ORO (Sigma, Cat# O0625) and 77.8% (v/v) methanol (Sigma, 179337) in 1N sodium hydroxide solution (Thermo Fisher Scientific, Cat# SS266-1) for 50 min, incubated in 70% ethanol for 30 min and then kept in distilled water until imaging. The images were taken by Olympus DP73 microscope, then analyzed by Image J. The red stained regions are considered atherosclerosis plaque positive. The ratio of the area of red-stained regions/overall area of aorta tree for each animal is calculated and used as the quantitative extent of atherosclerosis for this animal.

3.2.13 Fluorescence microscopy

Mice were humanely euthanized and then perfused with 10 ml normal saline followed by 10 ml formalin via the left ventricle. Livers were collected and fixed in formalin overnight and then embedded in optimal cutting temperature (OCT, Thermo Fisher Scientific, Cat# 14-373-65) compound and snap-frozen in liquid nitrogen. Frozen liver tissues were sectioned at 7 μm thick. The slides were then washed 3 times with PBS and sealed with Antifade Mounting Medium with DAPI (Thermo Fisher Scientific, Cat# P36935). The slides were imaged using Olympus DP73 microscope equipped with a GFP filter set (excitation 488 nm).

3.2.14 Statistical Analysis

The data in bar graphs and scatter plots are expressed as the mean ± SEM, analyzed by using GraphPad Prism v.8.0.1 (GraphPad Software). Statistical differences were determined by

two-tailed unpaired Student's *t* test for two groups. A p value < 0.05 was considered as significant.

3.3 Results

3.3.1 In vitro validation of Idol-targeting gRNAs

We designed dual guide RNA (gRNA)–mediated CRISPR-Cas9 knockout strategies to disrupt the *Idol* genes in human iPSC, human HEK293T cells (Figure 3.1A), rabbit RK13 cells (Figure 3.2A) and mouse embryonic stem cells (mESCs, Figure 3.3A). For each cell type, two gRNAs specific to that species were designed to target distinct Exons. Individual gRNA is expected to introduce insertion or deletion (indel) mutations at its own target site. In addition, the two targeted exons are separated by coding regions that encompass essential functional domains of the protein such that concurrent cleavage by both gRNAs on the same allele is anticipated to produce a large fragment deletion, thereby ensuring loss of critical coding sequences. To evaluate editing efficiency, indel formation at each gRNA target site were quantified, and the presence of large fragment deletions were verified.

In hiPSC, hsgL3 targets Exon 2 (E2) and hsgR1 targets Exon 5 (E5) of human *IDOL*. Individually, hsgL3 led to 25% indel rates on E2 and hsgR1 led to 31% indel rates at E5, as quantified by T7E1 assay (Figure 3.1B). PCR amplification was able to capture large fragment deletion evidenced by a band of the anticipated 682-bp size (Figure 3.1C). TA cloning experiment revealed that the large fragment deletion events are heterogenous (Figure 3.1D). Of the eight TA clones that were sequenced, three (Clone #1, 5, and 7) contained the same deletion sequences; whereas the other five each had additional small deletions. Nevertheless, all had >13 kb deletions which included entire Exon 3 and Exon 4 of the human *IDOL* gene. Quantitative

RT-PCR confirmed that in single-cell derived clones (#18 and #30) that contained successful large fragment deletions h*IDOL* in HEK293T cells mRNA transcription was reduced to close to zero (Figure 3.1E). Together, these data demonstrate an efficient dual gRNAs mediated gene disruption strategy targeting human *IDOL* in human cells.

In rabbit RK13 cells, rsg1 targets E2 and rsgR2 targets E5 of rabbit *Idol*. Individually, rsg1 led to 38% indel rates on E2 and rsgr2 led to 36% indel rates at E5, as quantified by T7E1 assay (Figure 3.2B). PCR amplification was able to capture large fragment deletion evidenced by a band of the anticipated 513-bp size (Figure 3.2C). TA cloning experiment revealed that the large fragment deletion events are heterogenous (Figure 3.2D). Of the five TA clones established from edited RK13, all had the >14 kb deletions which included entire Exon 3 and Exon 4 of the rabbit *Idol* gene, but also all had different indels at the cutting ends. Similarly in TA clones established from rabbit fibroblast cells that were subjected to the same rsg1 and rsgR2 mediated gene disruption strategy, successful >14 kb deletions were observed, alone with small indels at each cutting ends (Figure 3.2D). Together, these data demonstrate an efficient dual gRNAs mediated gene disruption strategy targeting rabbit *Idol* in RK13 and fibroblast cells.

In mouse ESCs, msgL3 targets E2 and msgR3 targets E5 of mouse *Idol*. Individually, msgL3 led to 30% indel rates on E2 and msgR3 led to 40% indel rates at E5, as quantified by the T7E1 assay (Figure 3.3B). PCR amplification was able to capture large fragment deletion evidenced by a band of the anticipated 824-bp size (Figure 3.3C). TA cloning experiment revealed that the large fragment deletion events are heterogenous (Figure 3.3D). Of the 7 TA clones established from edited mESCs, all had the >15 kb deletions which included entire Exon 3 and Exon 4 of the mouse *Idol* gene, and all had different indels at the cutting ends (Figure 3.3D).

Together, these data demonstrate an efficient dual gRNAs mediated gene disruption strategy targeting mouse *Idol* in mESCs.

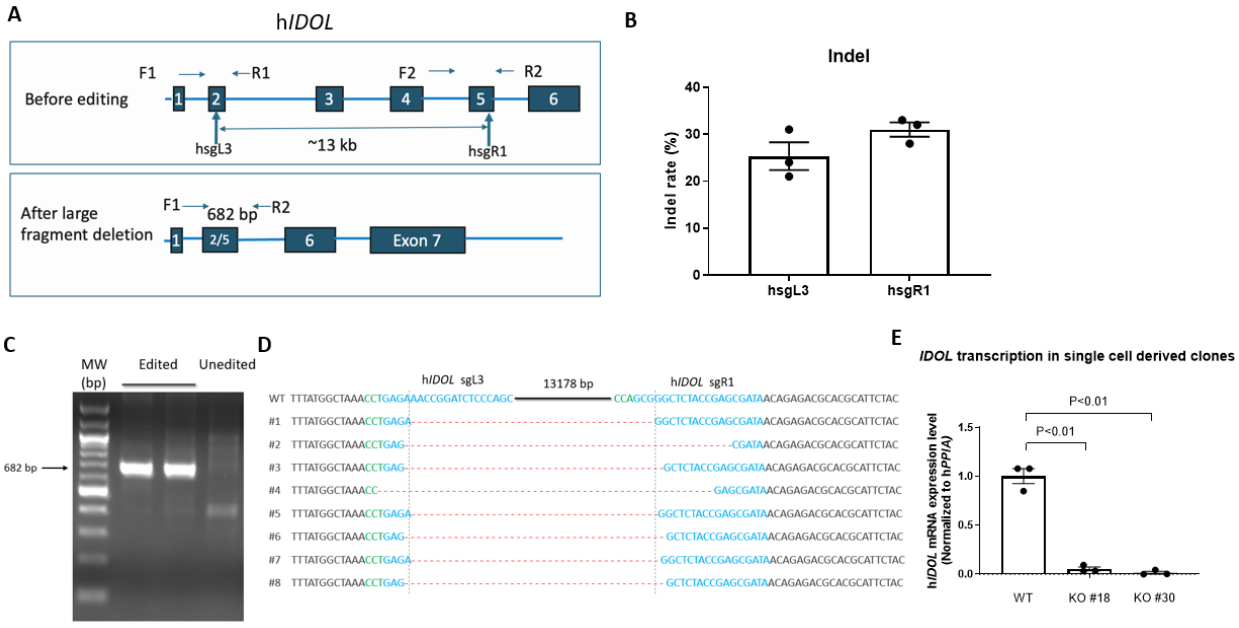


Figure 3.1: *In vitro* validation of *IDOL*-targeting gRNAs in human cells.

(A) Schematic representation of dual guide RNA (gRNA)–mediated CRISPR-Cas9 disruption strategies to disrupt the *IDOL* gene, top, and h*IDOL* exon illustration after large fragment deletion, bottom. (B) Measurement of editing efficiency of hsgL3 and hsgR1 in hiPSC. (C) Evidence of large fragment deletion by PCR amplification. (D) Evidence of large fragment deletion by TA cloning. (E) qRT-PCR analysis of *IDOL* expression in single cell derived clones that contained successful large fragment deletions. Two-tailed unpaired *t* test.

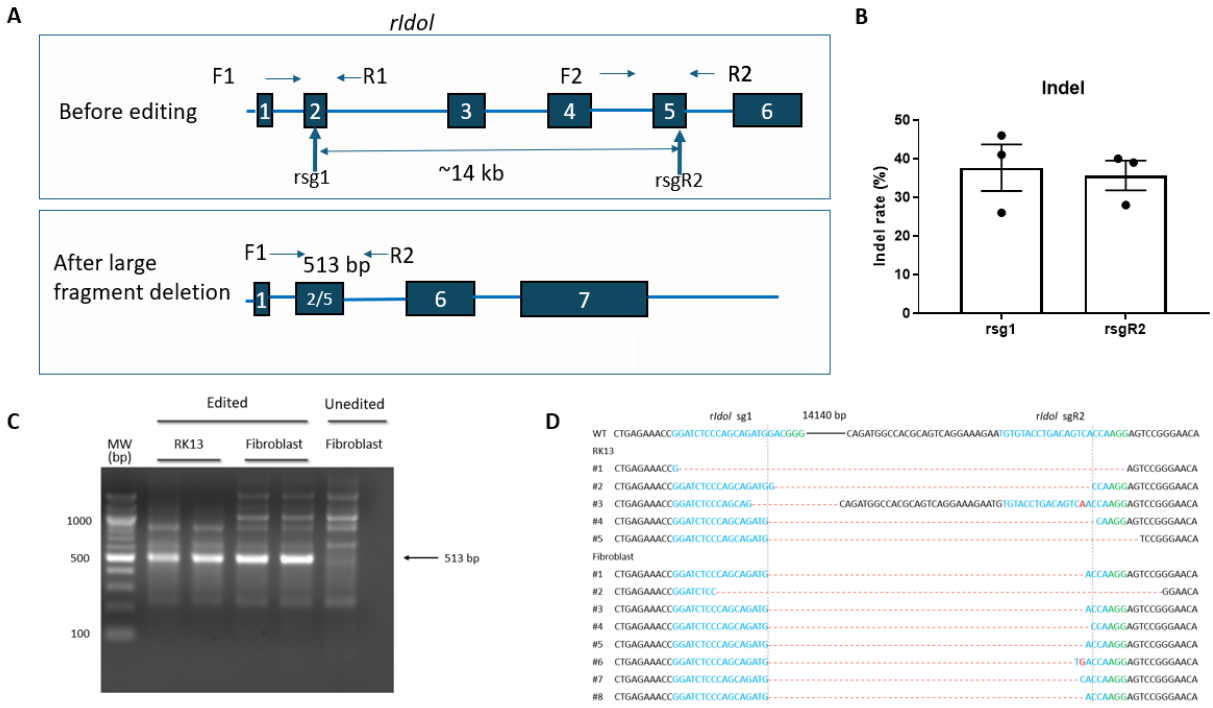


Figure 3.2: *In vitro* validation of *Idol*-targeting gRNAs in rabbit cells.

(A) Schematic representation of dual guide RNA (gRNA)–mediated CRISPR-Cas9 disruption strategies to disrupt the *Idol* gene, top, and r*Idol* exon illustration after large fragment deletion, bottom. (B) Measurement of editing efficiency of rsg1 and rsgR2 in RK13. (C) Evidence of large fragment deletion by PCR amplification. (D) Evidence of large fragment deletion by TA cloning.

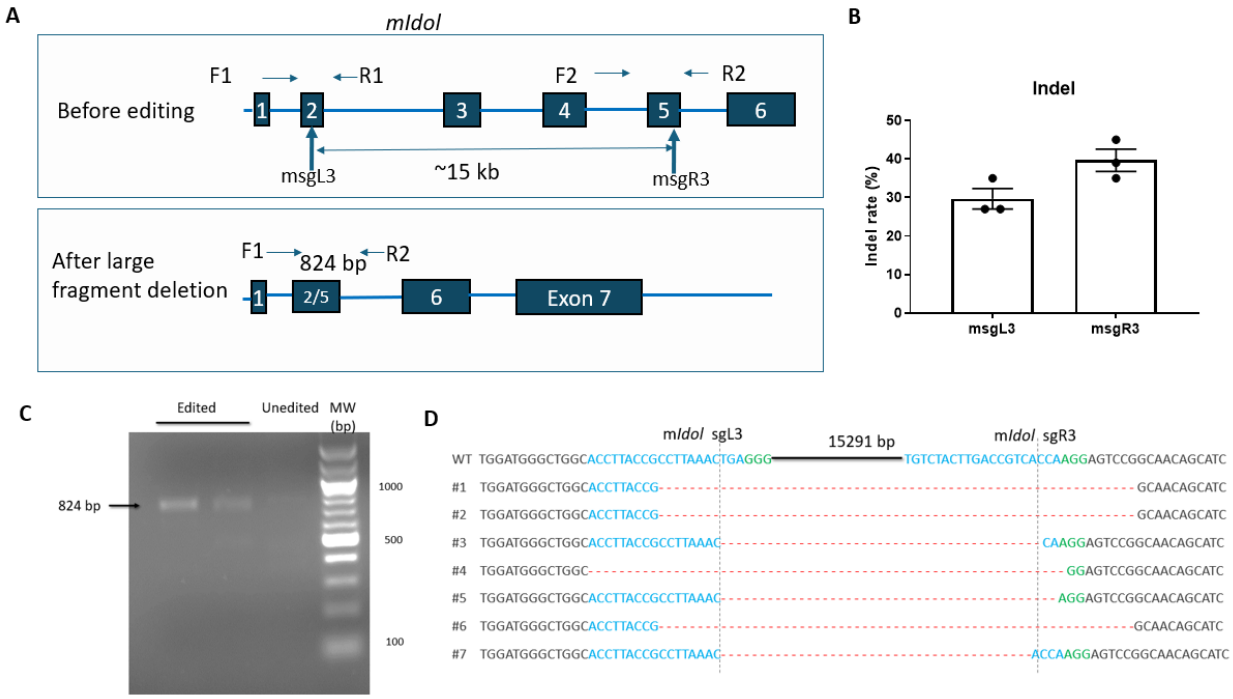


Figure 3.3: *In vitro* validation of *Idol*-targeting gRNAs in mouse cells.

(A) Schematic representation of dual guide RNA (gRNA)–mediated CRISPR-Cas9 disruption strategies to disrupt the *Idol* gene, top, and m*Idol* exon illustration after large fragment deletion, bottom. (B) Measurement of editing efficiency of msgL3 and msgR3 in mESC. (C) Evidence of large fragment deletion by PCR amplification. (D) Evidence of large fragment deletion by TA cloning.

3.3.2 Effects of dual AAV vectors mediated Idol disruption in C57 mice

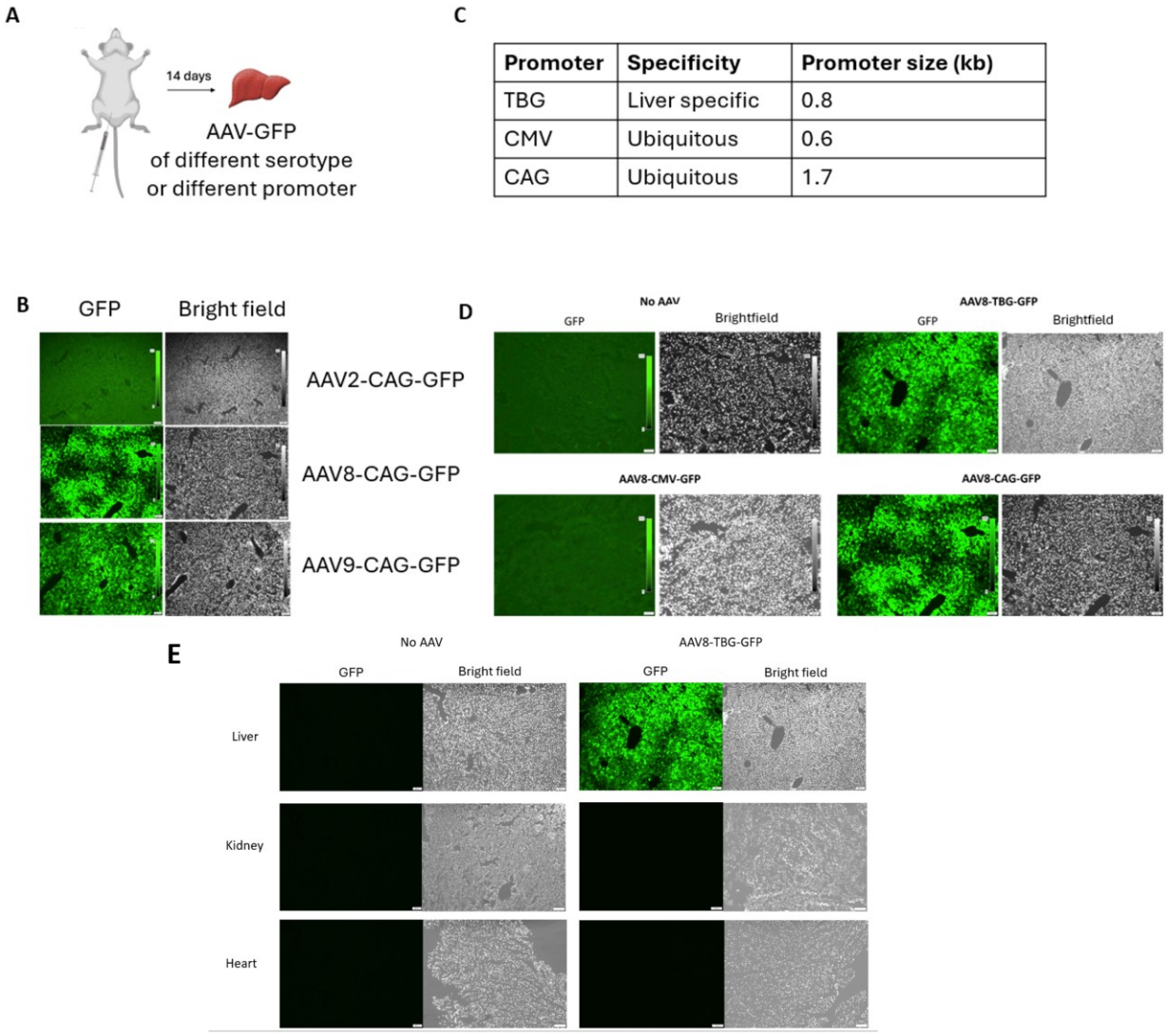
We next worked to develop AAV mediated *Idol* disruption strategies in mice. Considering the central roles that liver plays in lipid metabolism (*239*), we hypothesized that hepatic *Idol* gene disruption may provide atheroprotective effects. We first compared three different AAV serotypes, namely AAV2, AAV8 and AAV9, packaging a CAG promoter driven green fluorescence protein (GFP) coding sequence, in their capacity to transduce C57 mouse liver. We intravenously (i.v.) injected AAV vectors (AAV2-CAG-GFP, AAV8-CAG-GFP, or AAV9-CAG-GFP) at $6x10^{11}$ genome copy (gc) per mouse (gc/mouse) through the tail vein. Two weeks later, the animals were humanely euthanized, and liver sections were examined under fluorescence microscopy (Figure 3.4A). It is revealed that strong GFP signals were similarly observed in the livers of AAV8-CAG-GFP and AAV9-CAG-GFP treated animals, but were undetectable in the livers of AAV2-CAG-GFP treated animals (Figure 3.4B). Based on these observations, we selected AAV8 in the subsequent experiments.

Next, we compared the effects of promoters: (i) liver specific TBG promoter of 0.8 kb size; (ii) ubiquitous CMV promoter of 0.6 kb size; and (iii) ubiquitous CAG promoter of 1.7 kb size (Figure 3.4C). We i.v. injected AAV-TBG-GFP, AAV-CMV-GFP, or AAV-CAG-GFP at $6x10^{11}$ gc/mouse through the tail veins into the C57 mice, and examined the GFP expressions in the liver 14 days post injection. Interestingly, while AAV8-TBG-GFP and AAV8-CAG-GFP vectors robustly induced GFP expressions in the mouse livers, AAV8-CMV-GFP led to almost no GFP signals in the transduced animals' livers. Examination of AAV-TBG-GFP treated animals confirmed that this promoter is liver-specific, as GFP signals were only observed in the liver, but not in other organs (Figure 3.4E). Based on these findings, and that the TBG promoter

is of smaller than the CAG promoter, which is a favorable feature for AAV packaging, we selected TBG promoter in the next experiment.

We next tested the dual AAV strategy to edit mouse *Idol in vivo*. We had to employ a dual AAV vector approach due to AAV's packaging limit. In Vector 1 "AAV8-TBG-spCas9", the spCas9 expression is driven by the TBG promoter. In Vector 2 "AAV8-U6-msgL3", the single gRNA, msgL3, was driven by the U6 promoter (Figure 3.5A). We i.v. injected mixed AAV8-TBG-spCas9 ($6x10^{11}$ gc/mouse) and AAV8-U6-msgL3 ($6x10^{11}$ gc/mouse) vectors through the tail veins into C57 mice (n=3) and examined the *Idol* gene editing events in the mouse livers 14 days post injection. Unfortunately, only 1-2% indel rates were detected in the msgL3 targeted locus (Figure 3.5B).

Such minimal editing observed with dual AAV vectors (i.e., AAV8-TBG-spCas9 and AAV8-U6-msgL3), evidenced by low indel frequencies, suggests the limited efficiency of this strategy for disrupting IDOL protein expression *in vivo*. This outcome may result from poor co-transduction efficiency or suboptimal delivery of both Cas9 and gRNA to the same hepatocyte, and underscores a critical challenge for dual-vector AAV genome editing approaches constrained by vector packaging limits.



Promoter	Specificity	Promoter size (kb)
TBG	Liver specific	0.8
CMV	Ubiquitous	0.6
CAG	Ubiquitous	1.7

Figure 3.4: Optimization of *in vivo* AAV delivery strategy by comparing different AAV serotypes and promoters.

(A) Schematic of transduced with AAV-GFP vectors at $6x10^{11}$ genome copy (gc) per mouse (gc/mouse) through the tail vein. Two weeks later, the animals were humanely euthanized, and liver sections were examined under fluorescence microscopy. (B) Liver GFP signals of animals transduced by AAV-CAG-GFP vectors of different serotypes. (C) Summary of specificity and size of the promoters tested. (D) Liver GFP signals of animals transduced by AAV8-GFP vectors driven by different promoters. (E) GFP signals in different tissues of animals transduced by a TBG promoter driven AAV8-GFP**.**

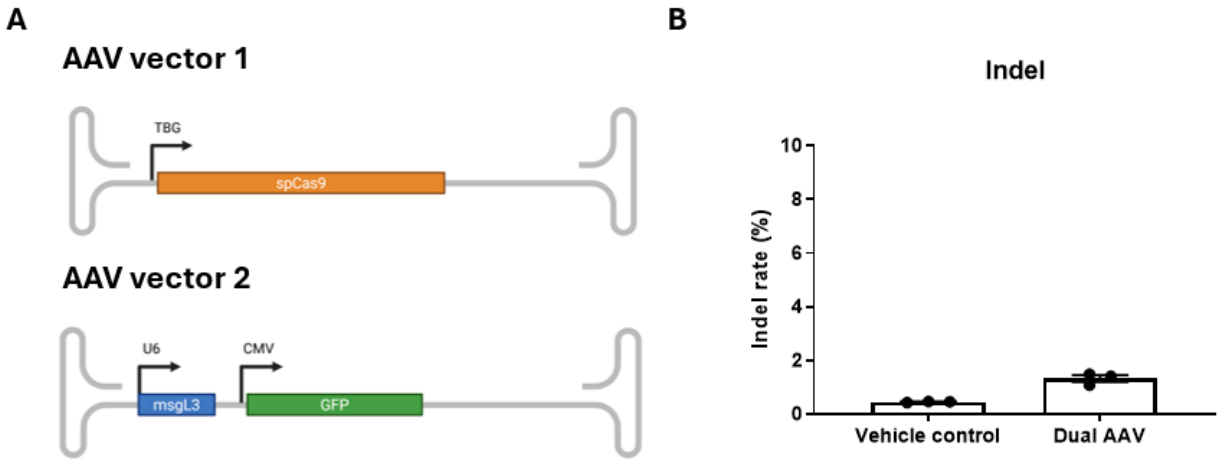


Figure 3.5: Effects of dual AAV vectors mediated *Idol* disruption in C57 mice.

(A) Schematic showing dual AAV design. (B) Liver gene editing efficiency at sgL3 locus by dual AAV delivery. Injection of mixed AAV8-TBG-spCas9 ($6x10^{11}$ gc/mouse) and AAV8-U6-msgL3 ($6x10^{11}$ gc/mouse) vectors was through the tail veins.

3.3.3 Effects of single AAV vector mediated Idol disruption in Rosa26-spCas9 KI mice

In order to overcome the limitations using dual AAV, we employed Cas9 KI mice delivering single AAV8-U6-msgL3-msgR3 vector (Figure 3.6A).

We first compared the *in vivo* editing efficiency of different administration routes Intraperitoneal (ip) VS intravenous (iv) injection. We injected AAV8-U6-msgL3-msgR3 ($6x10^{11}$ gc/mouse) vectors into Cas9 KI mice (n=3) and examined the *Idol* gene editing events in the mouse livers 14 days post injection. It reveals that the editing efficiency was almost the same at both msgL3 and msgR3 sites (Figure 3.6B). Therefore, we selected iv injection route in the subsequent experiments.

Next, we also compared the effects of doses: $6x10^{11}$ gc/mouse, $1.2x10^{12}$ gc/mouse and $1.8x10^{12}$ gc/mouse. We i.v. injected AAV8-U6-msgL3-msgR3 at doses (n=3) through the tail veins into the Cas9 KI mice, and examined the liver editing efficiency 14 days post injection. We did not observe increase in editing efficiency with increased AAV dose (Figure 3.6C). For safety consideration, we selected the lowest dose $6x10^{11}$ gc/mouse for the future experiments.

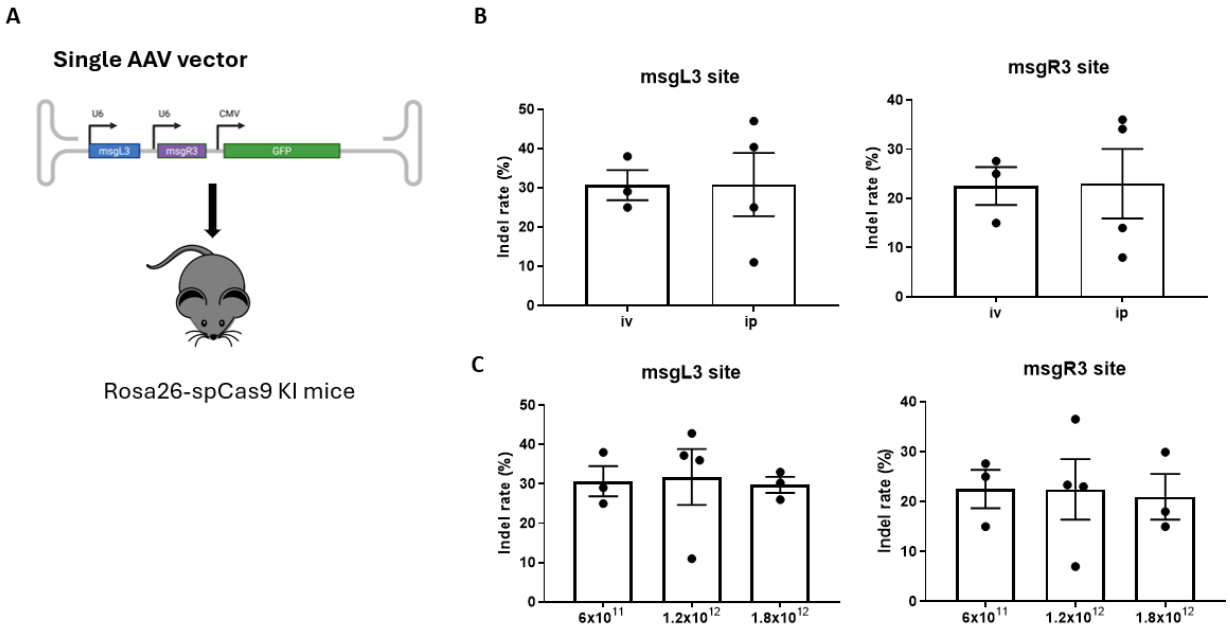


Figure 3.6: Editing outcomes of single AAV vector mediated *Idol* disruption in *ApoE*$^{-/-}$/Cas9-KI mice.

(A) Schematic of AAV vector (AAV8-U6-msgL3-msgR3) carrying dual gRNAs (gRNAs) transducing *ApoE*$^{-/-}$/Cas9 KI mice (shown as Rosa26-spCas9 KI). (B) Comparison of liver gene editing efficiency at sgL3 and sgR3 sites by using different injection routes (i.p VS i.v) at $6x10^{11}$ (gc/mouse). (C) Comparison of liver gene editing efficiency at sgL3 and sgR3 sites by using different doses ($6x10^{11}$ gc/mouse, $1.2x10^{12}$ gc/mouse and $1.8x10^{12}$ gc/mouse) through i.v injection.

3.3.4 Efficacy evaluations of AAV8-U6-msgL3-msgR3 to target Idol in ApoE$^{-/-}$/Cas9-KI mice

To continue with this proof-of-concept study to evaluate GETx-CVD-Idol *in vivo*, we first worked to establish an *ApoE*$^{-/-}$/Cas9-KI mouse line. Both lines of ApoE knockout (*ApoE*$^{-/-}$) and Cas9 knock-in (Cas9-KI) were obtained from the Jackson Laboratory (Bar Harbor, ME). The *ApoE*$^{-/-}$ mice are a classic model to study atherosclerosis (*222*), whereas the Cas9-KI mice consecutively express spCas9 through a spCas9 expression cassette knocked into the safe harbor locus Rosa 26 (*240*). We cross bred these two lines and produced *ApoE*$^{-/-}$/Cas9-KI animals for our experiments (Figure 3.7), based on the following rationale: (i) we can use a single AAV vector to deliver gRNAs only, without the need of the additional AAV vector to express spCas9; (ii) the *ApoE*$^{-/-}$ background allows evaluation of the gene editing effects on the development of atherosclerosis.

ApoE$^{-/-}$/Cas9-KI mice at 8-10 weeks old, both female (n=5) and male (n=6), were given AAV8-U6-msgL3-msgR3 through i.v. tail vein injections. We tested dose of $6x10^{11}$ gc/mouse in both male and female animals. In the control group, the animals received AAV-GFP ($6x10^{11}$ gc/mouse). One week post AAV injections, the animals were subjected to Western diet to induced the development of atherosclerosis. Blood samples were collected before AAV injection and biweekly post injection. 12-16 weeks post western diet, the animals were humanely euthanized and subjected to evaluations of editing efficiencies, atherosclerosis extent, as well as potential adverse effects (Figure 3.8A).

Deep-seq analysis of postmortem liver samples revealed substantial indel events by both msgL3 (ranging from 0.37% to 47.37%) and msgR3 (ranging from 0.32% to 40.2%) in AAV8-U6-msgL3-msgR3 treated animals (Figure 3.8B, C). No difference of indel rates were observed between sexes. In contrast, there are undetectable indel events in the AAV8-GFP treated control

group animals. Consistently, large fragment deletion, characterized by an 824-bp size band, is detected only in AAV8-U6-msgL3-msgR3 treated animals, but not in AAV8-GFP treated animals (Figure 3.8D).

To test if gene editing at the DNA level will cause any changes at the transcription level, we designed three pairs of qRT-PCR primers, illustrated in (Figure 3.8E). The left pair amplifies the region upstream of the left (i.e., 5' side) cut site and the right pair amplifies the region downstream of the right (i.e., 3' side) cut side, whereas the middle pair amplifies a region between msgL3 and msgR3. Interestingly, we were able to detect statistically significant reduction of qRT-PCR products by all three primer pairs (i.e., left, right and middle) in AAV8-U6-msgL3-msgR3 treated mouse livers than in those treated with AAV8-GFP, albeit the effect size is below our expectation at only approximately 30% (Figure 3.8E).

We next determined the protein expression levels in AAV8-U6-msgL3-msgR3 treated animal livers in comparison with those in AAV8-GFP treated animal livers. We first compared several different commercially available IDOL antibodies (Lifespan Biosciences LS-C119933-100, Novus NBP2-46069, Abcam Ab136859, Ab74562) as well as an in-house developed rabbit polyclonal anti-mIDOL antibody. The Western blot (WB) results suggested that none of these IDOL antibodies are specific. We then proceeded in conducting WB for IDOL's target proteins including LDLR, ApoER2 and VLDLR only. Contrary to our expectation however, LDLR, ApoER2 both appeared to be moderately downregulated, instead of upregulation based on the IDOL biology knowledge, in AAV8-U6-msgL3-msgR3 treated than in AAV8-GFP treated mouse livers (Figure 3.9). Such findings suggest there may be alternative pathways compensating loss-of-IDOL functions in mouse livers.

Total cholesterol (TC) levels in both treatment and control group animals significantly elevated after Western diet challenges (Figure 3.10A). A subtle reduction in TC values was noticed in AAV8-U6-msgL3-msgR3 treated animals comparing to AAV8-GFP treated animals, more obvious in the female than in the male animals (Figure 3.10A). The triglycerides (TG) levels, however, remain at similar levels between the treatment group and control group animals (Figure 3.10B). Similarly, HDL and LDL levels remain unchanged between the treatment group and control group animals (Figure 3.11A, B)

We evaluated the extent of atherosclerosis development in the female animals treated with AAV8-U6-msgL3-msgR3 (n=5) in comparison to female animals treated with AAV8-GFP (n=5). Oil red O staining revealed that the extent of atherosclerosis plaques ranged from 10 to 17% in treatment group animals, which are not different from those in control group animals (ranging from 16% to 23%) (Figure 3.12A, B).

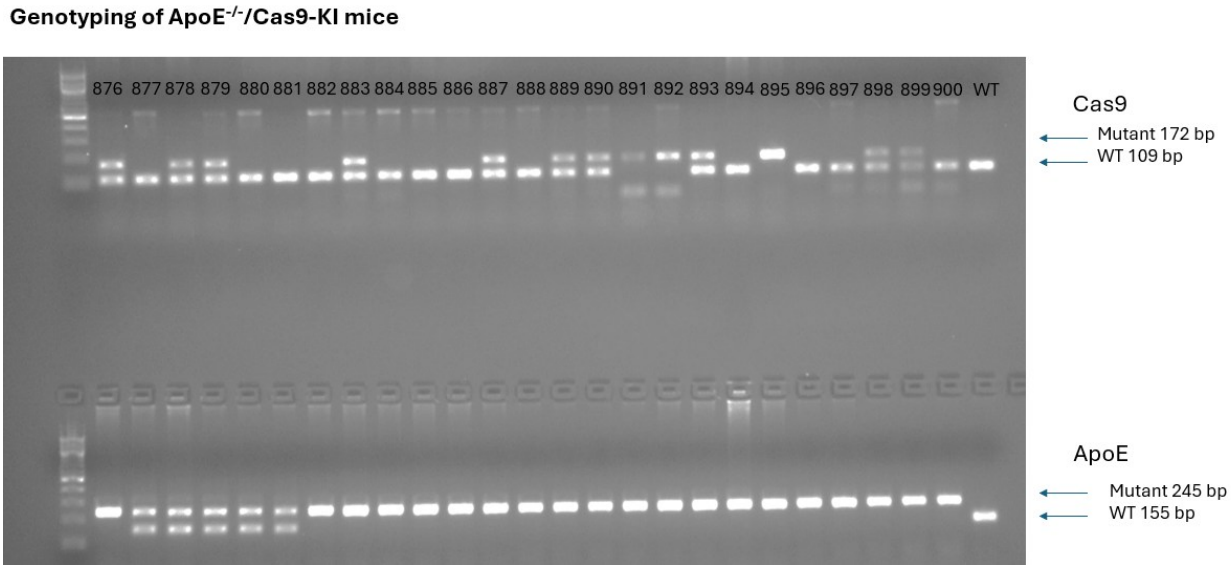


Figure 3.7: Genotyping of *ApoE*$^{-/-}$/Cas9-KI mice.

Representative genotyping results confirming successful generation of *ApoE*$^{-/-}$/Cas9-KI mice. The Cas9 KI panel shows distinct bands of the WT Rosa26 allele (109 bp) and the spCas9 knock-in cassette (172 bp). The ApoE panel displays disrupted ApoE allele (245 bp) and the WT allele (155 bp).

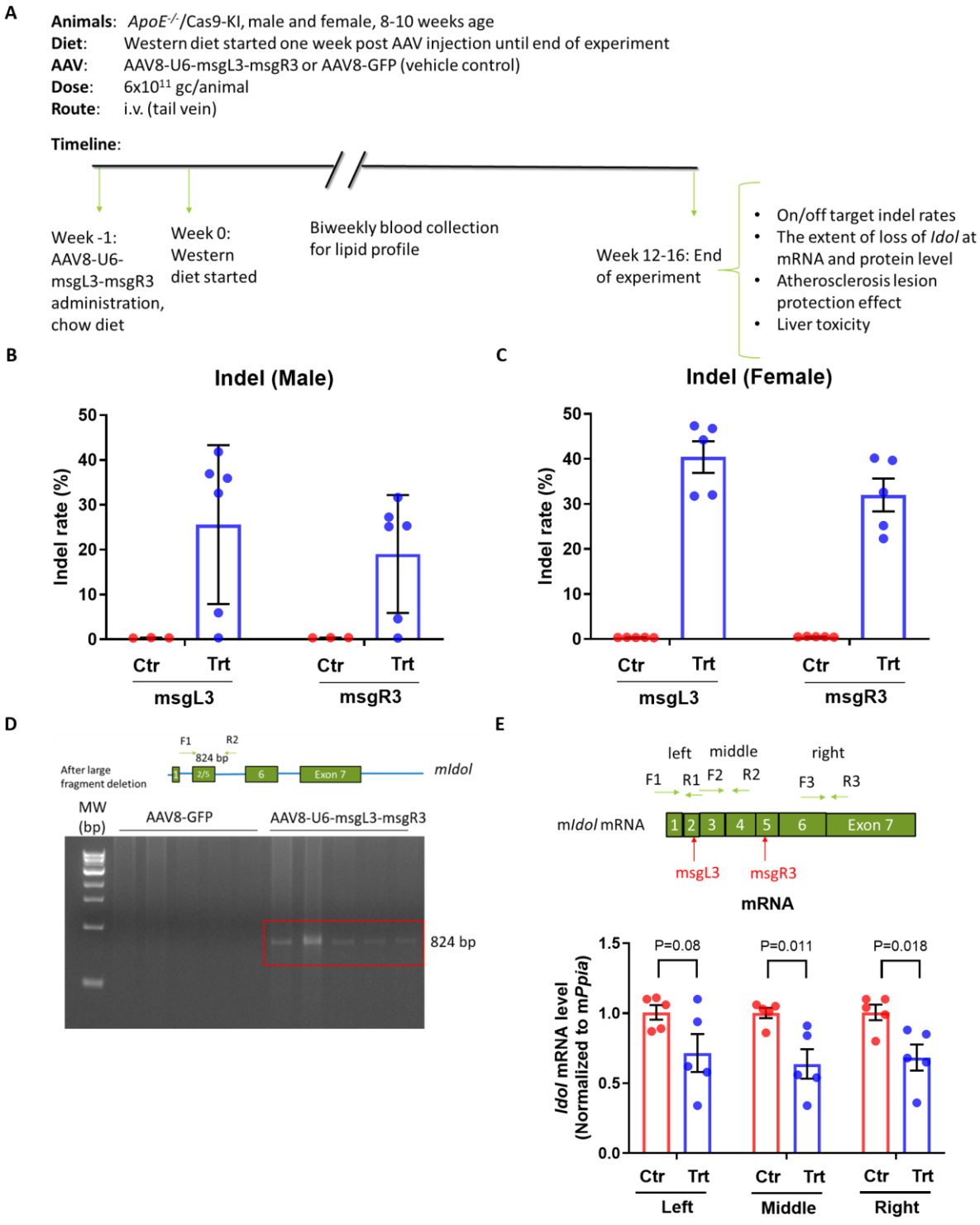


Figure 3.8: Evaluations of AAV8-U6-msgL3-msgR3 mediated *Idol* gene disruption in *ApoE*$^{-/-}$ /Cas9-KI mice.

(A) Schematic of experimental flow. 8-10 weeks old *ApoE*$^{-/-}$/Cas9 KI mice were transduced with AAV8-GFP or AAV8-U6-msgL3-msgR3 at 6x10^{11} gc/mouse through i.v injection. Western diet

treatment started one week after virus injection and continued for the remaining experiment. At the terminal point, liver editing efficiency was evaluated for (B) male and (C) female mice. (D) Evidence of large fragment deletion by PCR. (E) Top: schematic representation of the three qRT-PCR primers. The left pair amplifies the region upstream of sgL3 and the right pair amplifies the region downstream of sgR3, whereas the middle pair amplifies a region between sgL3 and sgR3. Bottom: qRT-PCR results of *Idol* expression in control and treatment group animals.

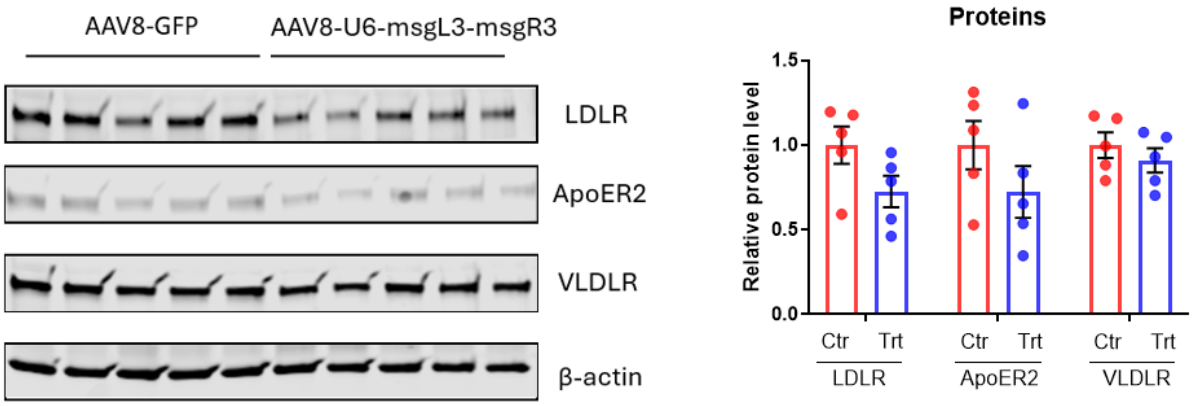


Figure 3.9: IDOL target proteins expression levels.

Verification of IDOL KO using liver tissues of AAV8-U6-msgL3-msgR3 treated and AAV8-GFP treated animals and western blot for the known IDOL targets (LDLR, ApoER2 and VLDLR). Relative abundance of each protein was normalized by β-actin. The WT average was set to 1.

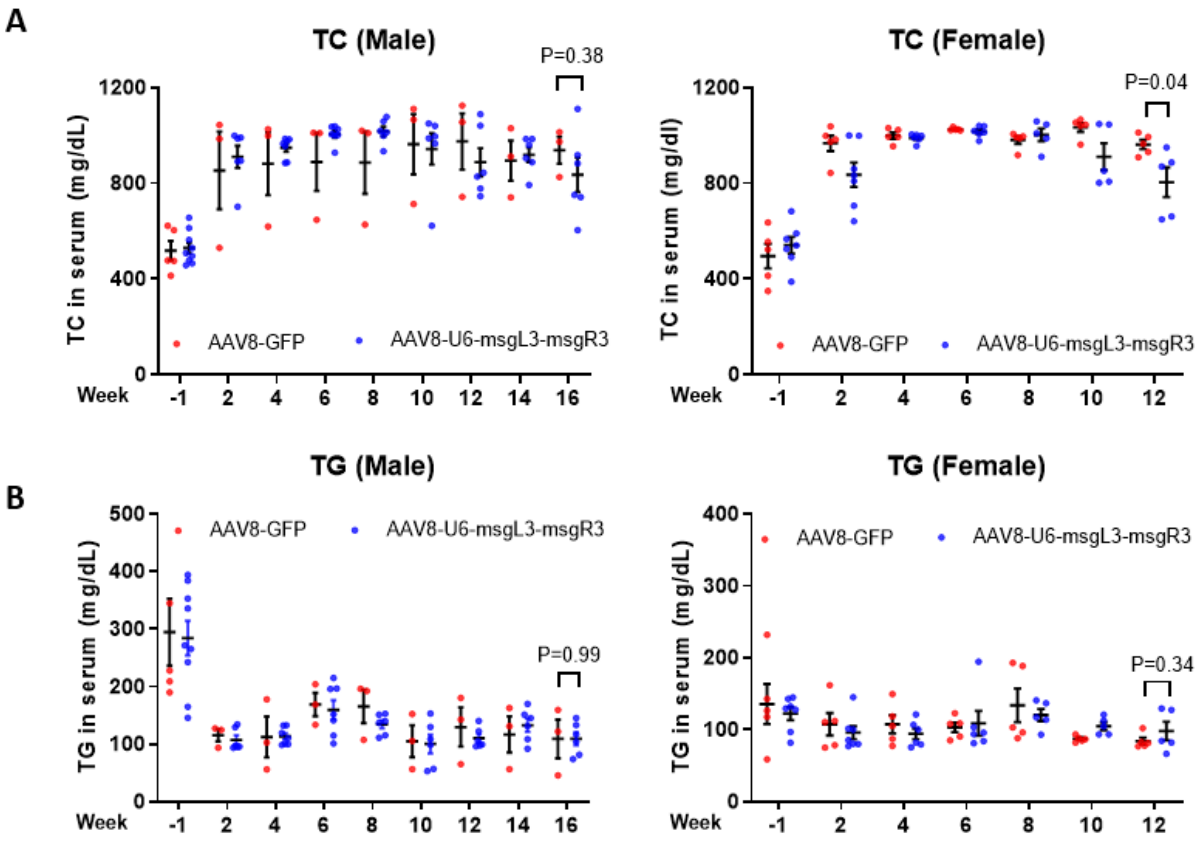


Figure 3.10: Total cholesterol (TC) and triglyceride (TG) levels of AAV8-U6-msgL3-msgR3 mediated *Idol* disruption in *ApoE*$^{-/-}$/Cas9-KI mice.

Measurements of serum (A) TC and (B) TG in male and female mice over the course of western diet.

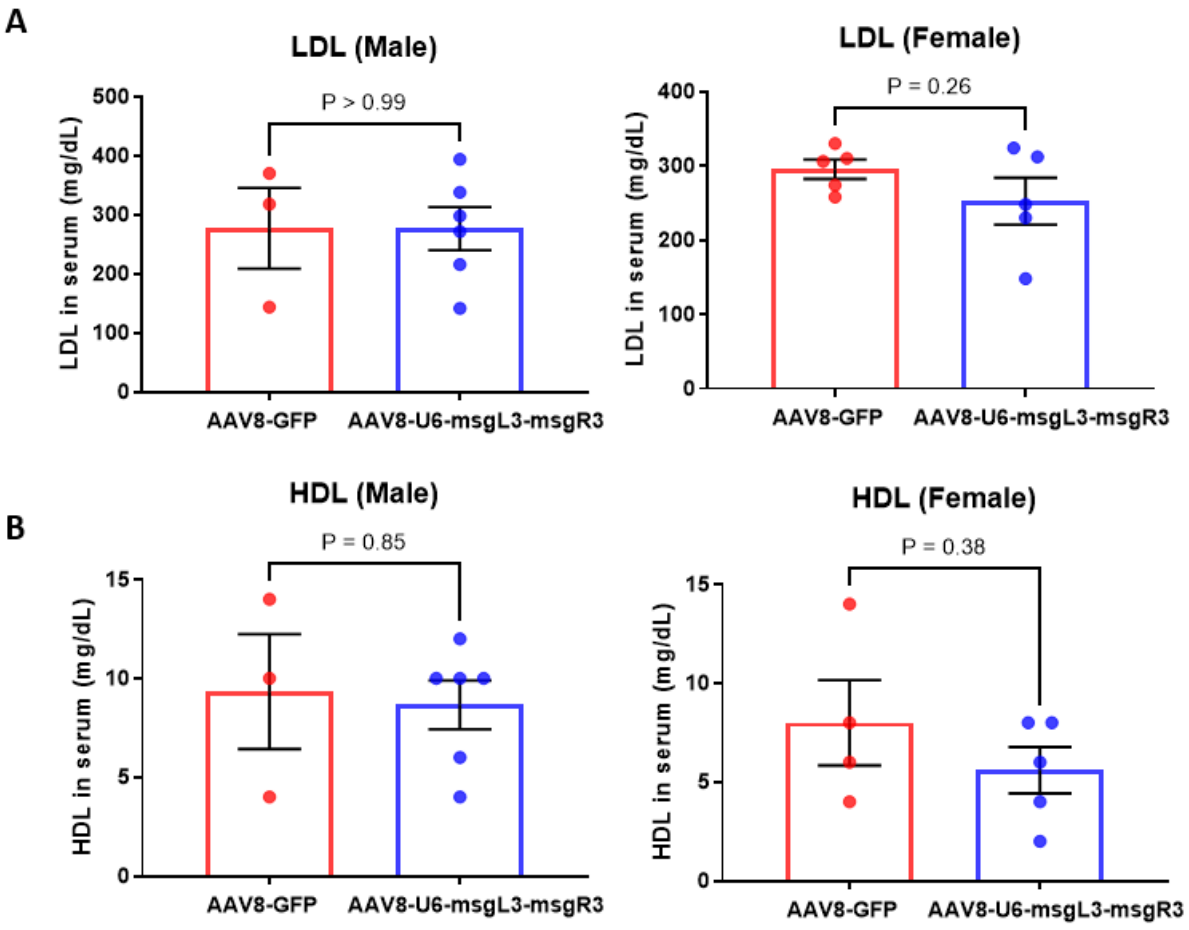


Figure 3.11: LDL and HDL levels of AAV8-U6-msgL3-msgR3 mediated *Idol* disruption in *ApoE*$^{-/-}$/Cas9-KI mice.

Measurements of serum (A) LDL and (B) HDL in male and female mice after 12 weeks of western diet. Data are mean ± SEM.

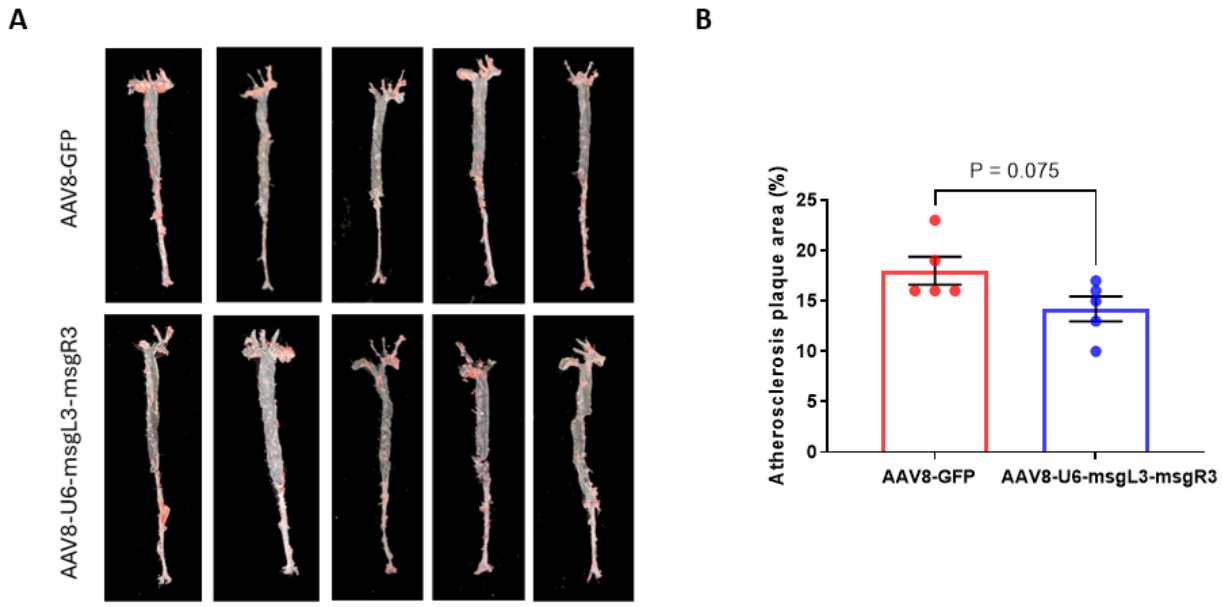


Figure 3.12: Evaluation of the extent of atherosclerosis development in the female animals treated with AAV8-U6-msgL3-msgR3.

(A) Representative pictures of aortic atherosclerosis in the female animals treated with AAV8-U6-msgL3-msgR3 (n=5) in comparison to female animals treated with AAV8-GFP (n=5) after 12 weeks on western diet. Lipids in the arterial wall were stained with Oil red O to evidence the atherosclerotic lesions. (B) Atherosclerotic lesions in the whole aorta were measured and expressed as the percentage (%) of red-stained area in the total area of aorta.

3.3.5 Safety evaluations of AAV8-U6-msgL3-msgR3 to target Idol in ApoE$^{-/-}$/Cas9-KI mice

We examined potential off-target (OT) effects of msgL3 and msgR3 in AAV8-U6-msgL3-msgR3 treated mouse livers. Off-target loci were predicted by CRISPOR and top 10 OT sites for each gRNA were selected and subjected to T7E1 assay. The results indicated that there are minimal editing events at these OT sites (Table 3.3).

Next, we looked at potential liver toxicity by measuring the serum levels of aspartate aminotransferase (AST) and alanine aminotransferase (ALT). There were no significant changes in either AST or ALT levels in the treated animals vs control animals (Figure 3.13A, B). We also evaluated potential renal toxicity by measuring Blood Urea Nitrogen (BUN) and creatinine (CREA) levels. The BUN and CREA levels of treatment and control group animals are all within normal range (Figure 3.13C, D). Consistently, the body weights as well as the liver/body weight ratios are also indistinguishable between treatment group animals and the control group animals (Figure 3.14A, B).

These data suggest that AAV8-U6-msgL3-msgR3 had minimal safety concerns at the genotoxicity level, the organ level and the overall animal body level.

Table 3.3: *In vivo* off-target activity analysis.

T7E1 assay on potential off-target loci of msgL3 (A) and msgR3 (B). No predicted indels were detected in all loci.

A Off-targets by msgL3.

Locus	Sequence	Mismatch count	Indel (%)
On target	ACCTTACCGCCTTAAACTGA GGG	n/a	30
intron: Nrg3	ACCTGATCACCATAAACTGA AGG	4	None
intron: U6	ATCTTACGGCCTTAAACATA AGG	4	None
intron: Abca15	GCCCTAACGCCTTGAACTGA AGG	4	None
intron: Lrp1b	ACTTTACTGCCTCACACTGA TGG	4	None
intron: Cux2	ACCTTACCCATTTAAACTGG TGG	4	None
intron: Nek4	ACCTTACAAACTTACACTGA AGG	4	None
intron: Kdsr	AGCTTACCACCTCACACTGA AGG	4	None
intron: Pou6f1	GCCTTCCTGCCTTAAGCTGA GGG	4	None
intron: Ulk4	ACCTTACCACATGAAACTGT GGG	4	None
intron: Fam81a	ACCTGACCCCCTGAAACTGG AGG	4	None

B. Off-targets by msgR3.

Locus	Sequence	Mismatch count	Indel (%)
On target	TGTCTACTTGACCGTCACCA AGG	n/a	38
exon: Dnahc10	TGACTATGTGACCCTCACCA TGG	4	None
exon: Zc3h6/Gm14027	TGTCTACTGGCCCATCAACA GGG	4	None
exon: Neb	TGTGTACTTGAGCTTCACCA CGG	3	None
exon: Tsga14	TTTCTACTTGCCCATCACCC AGG	4	None
exon: Dync1h1	TGTCTACCTGAACTTCACCC GGG	4	None
exon: Chi3l3	TGACTCCTTGTCCTTCACCA AGG	4	None
intron: Ablim1	TGTCTACCAGACAGACACCA TGG	4	None
intron: Itfg1	GGTCTACTTGTCTGTCACCA TGG	3	None
intron: Vti1a	TTTCTACTTAACCTTCACCA GGG	3	None
intron: Sorcs1	CTTCTAATTGACAGTCACCA GGG	4	None

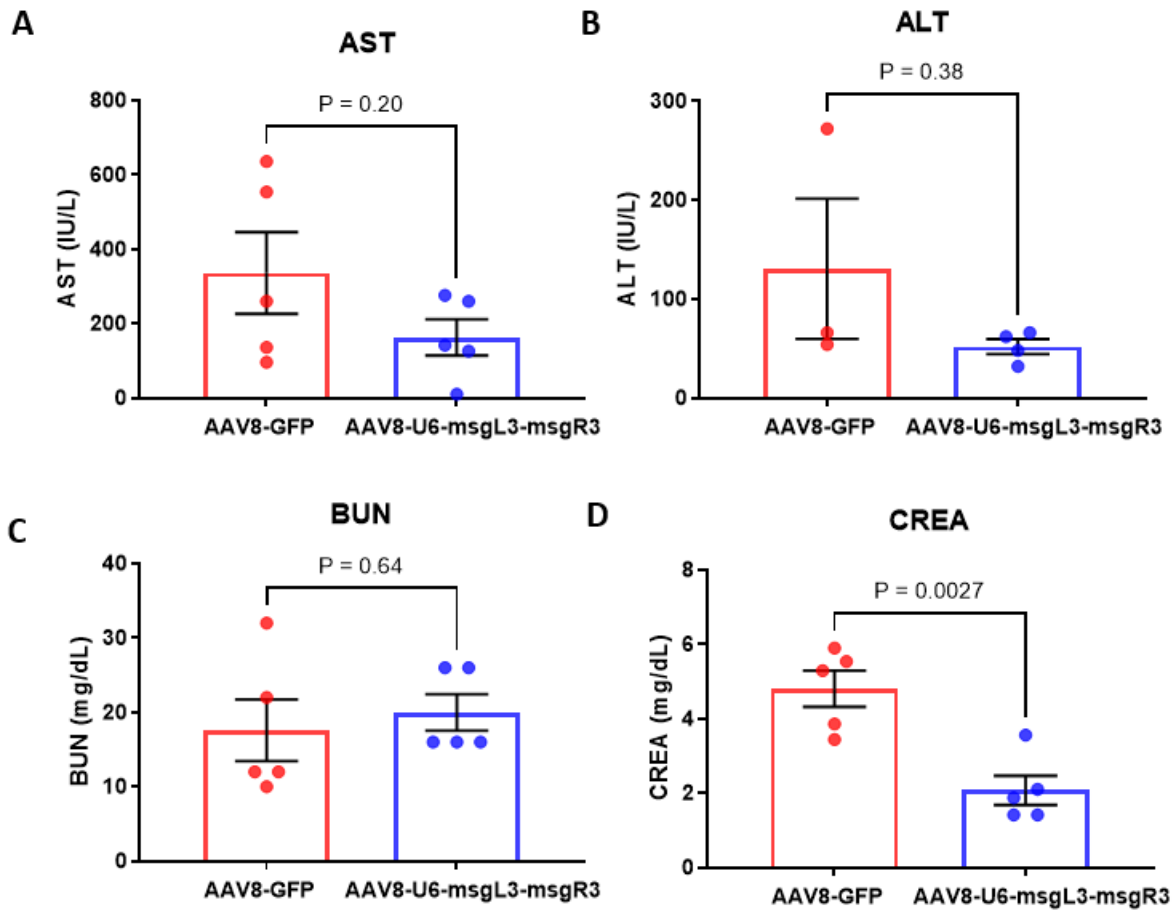


Figure 3.13: Liver and renal toxicity analysis.

(A) Aspartate aminotransferase, AST, (B) Alanine aminotransferase, ALT, (C) Blood Urea Nitrogen, BUN, and (D) Creatinine, CREA, as determined in the serum of mouse after 12 weeks on western diet. Data are shown as mean ± SEM.

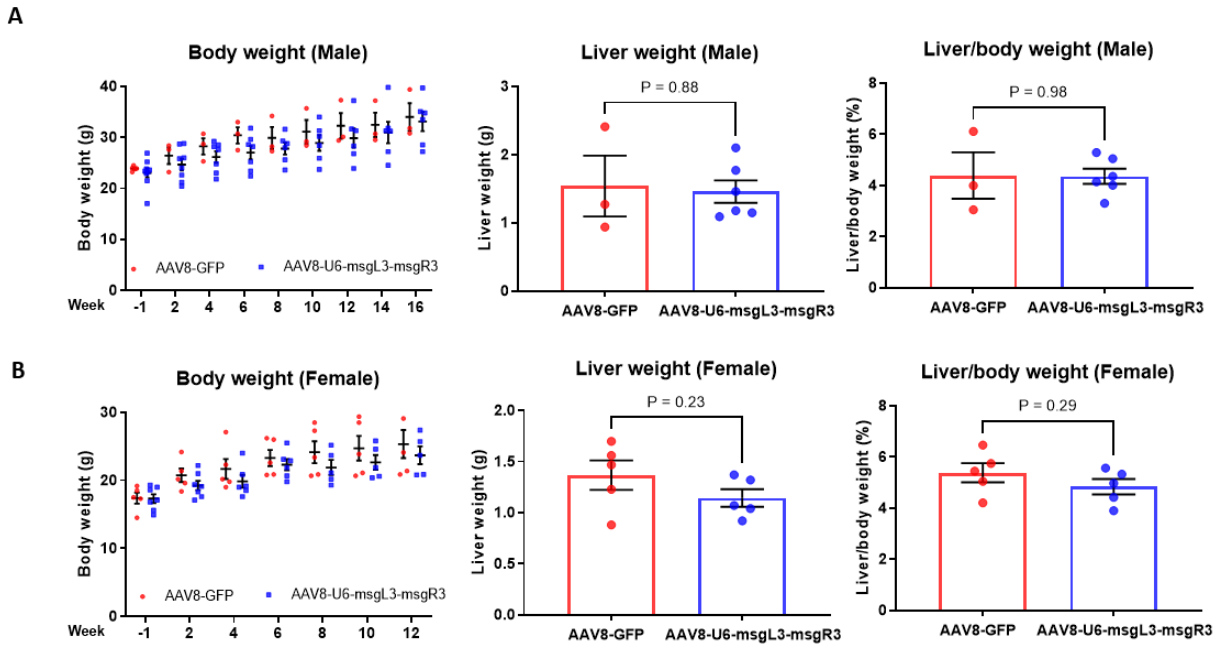


Figure 3.14: Safety evaluations of AAV8-U6-msgL3-msgR3 to target *Idol* in *ApoE*$^{-/-}$/Cas9-KI mice.

Livers were harvested from mice after 12 weeks of western diet. Body weight, liver weight and liver weight normalized by total body weight in male (A) and female (B) mice.

3.4 Discussion

In this study, we investigated the effects of an *Idol* targeting GETx-CVD strategy, in which dual guide RNAs were packaged into adeno-associated viruses (AAV8-U6-msgL3-msgR3) and delivered to *ApoE*$^{-/-}$ mice constitutively expressing Cas9 (*ApoE*$^{-/-}$/Cas9-KI). The experimental strategy leveraged the AAV8 vector's favorable tissue tropism and safety profile to deliver paired gRNAs specifically targeting the mouse *Idol* locus. Mice with hepatic delivery of AAV8-U6-msgL3-msgR3 demonstrated efficient editing at the DNA level, providing a proof-of-concept evidence to *in vivo* targeting within the context of constitutive Cas9 expression.

Despite molecular evidence of successful editing, there was no significant difference observed in the extent of atherosclerotic plaque formation between AAV8-U6-msgL3-msgR3 treated animals and controls. This lack of atheroprotection suggests that hepatic *Idol* disruption alone may be insufficient for disease modification in this preclinical setting. One likely explanation involves the global expression pattern of IDOL, as extrahepatic cells, for example immune cells, might also contribute to atherogenic processes, limiting the therapeutic impact of liver-restricted editing.

The limitations of the mouse model further contextualize these findings. It has been reported that murine IDOL regulation and function differ from those in humans and non-human primates, with species-specific differences in hepatic expression, regulatory response, and phenotypic consequences of gene inactivation. As such, the observed "no efficacy" by AAV-dgRNA-mIdol in mice does not conclusively reject the hypothesis that loss-of-function of IDOL provides atheroprotective effects. If budget allows, testing *Idol* targeting GETx-CVD in non-human primates will provide more clinically relevant information.

In our effort towards a clinically relevant yet economically affordable animal model for the study of IDOL, our lab developed IDOL knockout rabbits by employing CRISPR/Cas9 genome editing, which resulted in the complete loss of IDOL function in the animals. When challenged with high-cholesterol diet (HCD), IDOL KO rabbits had markedly reduced plasma concentrations of TC and TG compared with WT rabbits, suggesting that IDOL deficiency effectively attenuates the development of atherosclerosis in rabbits (*238*), which is in line with the human genetics observations (*208, 236*). These findings thus support future testing of *Idol* targeting GETx-CVD strategies in the rabbit model.

A further consideration for AAV-based editing is the technical limitation imposed by AAV's packaging capacity, generally under 4.7 kb; as such, we cannot include both spCas9 and the dual guide RNAs in a single vector. We circumvent this challenge by using genetically engineered Cas9 knock-in mice, requiring only the delivery of gRNA cassettes via AAV. Although this approach enabled mechanistic investigation, it does not directly translate to clinical scenarios which will require Cas9 co-delivery. Recent innovations, such as intein-based dual AAV systems where the Cas9 enzyme is split and separately packaged into two AAV vectors, or the use of non-viral modalities like lipid nanoparticles, may overcome these size constraints.

In summary, our findings highlight the technical and biological complexities associated with translating hepatic *Idol* gene editing into disease modification for atherosclerosis. The use of AAV for dual gRNA delivery in Cas9-expressing mice provides proof-of-concept for genome targeting, while also revealing key challenges related to tissue specificity, species selection, and vector engineering for clinical application. Future therapeutic development will benefit from multi-faceted approaches, including but not limited to broadening tissue targeting, optimizing

delivery systems, and recapitulating human IDOL biology in advanced models, to more accurately evaluate GETx-CVD targeting *Idol*.

Chapter 4 Summary and Perspectives

4.1 A summary of ASGR1 and IDOL projects

In this dissertation, I have used *in vivo* gene editing to interrogate two liver-related targets, ASGR1 and IDOL, in the context of dyslipidemia and atherosclerotic cardiovascular disease. Together, these projects form a coherent experimental journey from target identification based on human genetics and basic biology, through mouse model testing, to critical reflection on translational potential and limitations. ASGR1 and IDOL share a common link to hepatic lipoprotein metabolism, yet they differ markedly in tissue distribution, subcellular localization, and mechanistic roles. These differences are reflected clearly in the phenotypic outcomes observed in my studies.

The ASGR1 project focused on a hepatocyte-surface receptor that recognizes terminal galactose and N-acetylgalactosamine residues and mediates endocytosis of desialylated glycoproteins (*241*). Human genetic data and animal models have suggested that lifelong partial loss of ASGR1 function is associated with lower non-HDL cholesterol, reduced atherosclerotic risk, and a generally favorable safety profile (*184*). In *ApoE*$^{-/-}$ mice, adenoviral delivery of spCas9 and dual guide RNAs targeting *Asgr1* achieved efficient hepatic gene disruption. This intervention lowered serum and hepatic cholesterol, reduced atherosclerotic plaque burden, and improved systemic metabolic parameters such as insulin sensitivity and adiposity, without causing detectable liver toxicity over the study period. These findings support the concept that

ASGR1 is not only a lipid-modulating target but also a promising entry point for broad metabolic benefit.

In contrast, the IDOL project targeted an intracellular E3 ubiquitin ligase that can promote LDLR degradation and thereby influence circulating LDL-cholesterol. In humans and some preclinical studies, altering IDOL activity has been linked to changes in LDLR abundance and lipid levels (*208, 237, 238, 242*). In my work, dual-guide CRISPR/Cas9 editing of the *Idol* locus was achieved using an AAV8 vector delivering dgRNAs into Cas9 knock-in, *ApoE*$^{-/-}$ mice. Molecular analyses confirmed robust on-target editing in the liver. However, despite this technical success, hepatic *Idol* disruption did not increase LDLR protein levels *in vivo*, nor did it significantly change plasma cholesterol or triglyceride levels, or atherosclerotic plaque burden. Safety assessments showed minimal off-target and no obvious liver injury, but the expected lipid and cardiovascular benefits were not observed. This discrepancy between mechanistic expectation and *in vivo* outcome underscores the importance of these preclinical studies when translating from human genetics to mouse models and vice versa.

From a methodological standpoint, the two projects used different delivery and editing strategies. The ASGR1 study used an adenoviral vector to deliver both spCas9 and dual gRNAs, resulting in strong but transient expression. This design allowed for efficient editing in adult hepatocytes but raised classic concerns related to vector immunogenicity and double-strand break–mediated genotoxicity. The IDOL study separated the Cas9 nuclease and gRNA components, taking advantage of a Cas9 knock-in mouse model and used the AAV8-mediated dgRNA delivery. This strategy reduced the vector payload and simplified the AAV design, but it also constrained flexibility when considering future translation, because a germline Cas9

configuration is not appropriate for human therapy. A comparison of targeting strategies of ASGR1 and IDOL are summarized in Table 4.1.

Table 4.1: Comparison of targeting strategies of ASGR1 and IDOL

	ASGR1	**IDOL**
Mouse model	*ApoE*$^{-/-}$	*ApoE*$^{-/-}$/Cas9-KI
Delivery system	Adenovirus	AAV
Experiment time	17-19 weeks	12-16 weeks
Protein knockdown	80%	Not determined
Atherosclerosis readout	60% reduction	Minor reduction
Toxicity (Genotoxicity, organ toxicity)	Not observed	Not observed

Comparing the findings from ASGR1 and IDOL projects, a clear contrast emerges. ASGR1 knockdown in the liver produced robust lipid-lowering and atheroprotective effects, together with favorable metabolic phenotypes and an acceptable short-term safety profile in the mouse model. *Idol* disruption, despite high editing efficiency, did not provide similar biochemical or cardiovascular benefit. This suggests that ASGR1 is a higher-priority therapeutic target for liver-directed gene editing, at least in the *ApoE*$^{-/-}$ mouse context.

There are several limitations common to both projects. First, both studies used mouse models with strong genetic dyslipidemia and atherogenesis, which may only partially recapitulate human atherosclerotic disease. Second, my work relied on conventional Cas9-mediated double-strand breaks, which, although effective for knockout, are associated with risks of insertions, deletions, large-scale rearrangements, and rare on-target or off-target genotoxic events that may only become evident in the long term. Third, follow-up time was limited to months, not years, so the durability of benefit, potential late toxicities, and interactions with aging or environmental stress remain unknown. Fourth, although I assessed off-target editing and liver toxicity with standard methods, unbiased and deep profiling of structural variants and very rare off-target events was not fully achieved. These limitations define important directions for future research and also remind us to keep cautions when moving from mouse success to human therapy.

To make our studies more translational, we should work on overcoming these limitations in future studies. First, utilizing larger animal models such as rabbits or monkeys whose lipid metabolism biology is more similar to that of human can help capture the complexity of human atherosclerosis beyond the scope of genetically engineered mice. Second, adopting or developing alternative gene-editing tools without generating DSBs, like base editors or prime editors, may

reduce unintended genomic alterations, and enhance the safety assessment. Third, extending monitoring periods will provide critical insight into the long-term efficacy, toxicity, and effects of aging or environmental factors. Finally, implementing deep, unbiased screening methods for rare off-target and structural variants will ensure a more comprehensive safety evaluation.

Overall, the ASGR1 and IDOL projects jointly demonstrate that liver-directed *in vivo* gene editing is technically feasible and can produce clear therapeutic-like effects when the target biology is favorable. At the same time, they show that not every plausible target will yield benefit in the mouse model, and that careful integration of human genetics, comparative biology, and mechanistic understanding is essential when designing next-generation gene editing therapies for cardiovascular disease.

4.2 Promises of GETx-CVD informed by the ASGR1, IDOL projects, and the literature

Building on the ASGR1 and IDOL studies, this dissertation connects to a broader and rapidly evolving field that I refer to as gene editing therapy for cardiovascular diseases (GETx-CVD). In the liver-focused context, GETx-CVD strategies can be broadly divided into three categories: loss-of-function editing to inactivate pro-atherogenic genes, precise point mutation correction for monogenic lipid disorders, and large-fragment knock-in to install protective or corrective coding sequences. In practice, the first two categories—gene disruption and point mutation—are most relevant to the current stage of LivGETx-CVD, because many of the powerful cardioprotective alleles in humans arise from loss-of-function.

The ASGR1 work in this thesis is a typical example of loss-of-function editing, designed to mimic the protective effect of natural ASGR1 variants in humans. Similar logic has driven gene editing efforts targeting *Pcsk9*, *Angptl3*, *Apoc3*, and other lipid-related genes. In non-human primates and early human data, durable inactivation of *Pcsk9* using base editors has achieved

long-lasting LDL-cholesterol reduction with a single intervention (*111-113*). For *Angptl3*, both Cas9-based editing and base editing have shown strong triglyceride-lowering and cholesterol-lowering effects in preclinical models (*136-138*). These examples, together with my ASGR1 study, suggest that a "one-shot, long-term benefit" paradigm for dyslipidemia and atherosclerosis is no longer purely theoretical; it is gradually becoming a realistic therapeutic option.

Considering the broader literature, the promise of GETx-CVD can be summarized along several dimensions. First, durability: a single liver-directed editing procedure has the potential to control LDL-cholesterol, triglycerides, and possibly other risk factors for years or even decades, reducing the necessity for lifelong daily medications. Second, precision: by targeting a specific gene or locus, GETx-CVD can reproduce the protective effect of naturally occurring variants that have already been "tested" in human populations over decades. Third, combinability: edited targets can be combined with statins, GLP-1 receptor agonists, or emerging metabolic drugs to achieve additive or synergistic benefits. Fourth, scalability: one well-designed editing construct may serve many patients regardless of their underlying mutation pattern if the mechanism is based on gain of function or loss of function of a common pathway component.

At the same time, my IDOL study provides an important counterbalance to overly optimistic views. The lack of efficacy in the mouse model reminds us that not every target that looks promising *in vitro* or from human genetic association will respond to editing in a predictable way *in vivo*. In this sense, the real promise of GETx-CVD is not that it will solve every problem easily, but that it gives us a new capability to edit the human genome directly and durably, adding a fundamentally new layer to cardiovascular therapeutics. This additional capability must be used with caution, but if guided properly, it may allow us to reshape the

natural history of atherosclerotic disease in ways that were not achievable with small molecules or monoclonal antibodies alone.

4.3 Technical challenges for GETx-CVD

Despite the encouraging data, many high-level technical challenges must be addressed before GETx-CVD can be broadly implemented in clinical practice. The first and perhaps most central challenge is delivery. Liver-targeted delivery using AAV and lipid nanoparticles has shown considerable success, but each platform comes with trade-offs in terms of immunogenicity, cargo capacity, manufacturing, and long-term safety. AAV-based approaches are limited by pre-existing neutralizing antibodies, potential integration at low frequency, and difficulties with repeat dosing (*40*). Lipid nanoparticle systems are flexible and non-integrating, but they can trigger innate immune responses and may have limited targeting precision beyond the liver (*44*). For extrahepatic cardiovascular targets, such as vascular cells or cardiomyocytes, delivery remains even more difficult, and current technologies are still in early development.

The second challenge is genotoxicity and genome integrity. Conventional Cas9 nucleases create double-strand breaks, which are repaired by endogenous pathways that generate potential genotoxic events such as insertions, deletions, and occasionally larger rearrangements (*243*). Although these events may be rare at the single-cell level, the scale of liver cell editing in a clinical context means that very rare events can still translate into meaningful risks over time. Next-generation editors such as base editors and prime editors can, in principle, reduce the dependence on double-strand breaks and thereby lower genotoxicity risk. However, these enzymes introduce their own off-target profiles at both DNA and RNA levels, and they often have narrower editing windows or sequence constraints. Comprehensive off-target

characterization, structural variant analysis, and long-term tumorigenicity monitoring are therefore indispensable for any GETx-CVD program.

A third major challenge is immunogenicity. Both the editing nuclease (such as Cas9) and the delivery vehicle can stimulate innate and adaptive immune responses. Many humans already have pre-existing immunity against bacterial nucleases and common viral capsids. A strong immune response can limit editing efficiency, cause systemic inflammation, and complicate repeat administration. Strategies to mitigate immune responses include transient immunosuppression (*244*), engineering of less immunogenic nucleases or capsids (*245*), and the development of non-viral protein or mRNA delivery systems (*246*). However, each of these approaches introduces added complexity and potential side effects.

Fourth, there is the problem of species differences and model predictivity, as highlighted by the IDOL project. Mouse models of dyslipidemia and atherosclerosis are convenient and informative, but hepatic lipoprotein metabolism and immune responses differ substantially between mice and humans (*247*). Some targets, such as ASGR1 or PCSK9, may show relatively consistent phenotypes across species, whereas others may not. This gap underscores the importance of large-animal models, including non-human primates and, in some cases, pigs, rabbits, as well as human organoid and ex vivo liver models. However, large-animal studies are expensive, time-consuming, and limited in number, which slows the pace of translation.

Finally, manufacturing, quality control, and regulatory science pose additional layers of challenge. For GETx-CVD to move from proof-of-concept to routine practice, we will need reliable, scalable production of high-quality vectors or nanoparticles, robust assays to monitor editing outcomes in patients, and regulatory frameworks that can appropriately evaluate benefit–risk profiles for permanent genomic interventions.

4.4 Ethical considerations: from individual to civilization

The power to edit the human genome, even in somatic tissues such as the liver, carries profound ethical implications that extend beyond any single target or disease. At the individual level, the central ethical questions include informed consent, understanding of long-term risks, and the patient's tolerance for irreversible changes. Unlike conventional drugs, which can be stopped or adjusted, most *in vivo* gene editing interventions are essentially permanent for the targeted cells. Patients must therefore make decisions under uncertainty about long-term outcomes, including rare adverse events that may appear many years later. Clear communication, transparent risk–benefit assessment, and respect for patient autonomy are essential.

At the family and community levels, issues of access, equity, and justice are prominent. If GETx-CVD therapies are expensive and initially available only to a small subset of patients, we risk widening existing health disparities, both within and between countries. Cardiovascular disease is already strongly influenced by socioeconomic conditions, diet, and access to medical care. Introducing a powerful but costly gene editing therapy could concentrate benefits among the most privileged, while leaving behind those who carry the greatest burden of disease. Thoughtful policy design, global collaboration, and innovative payment models will be needed to avoid turning genomic medicine into a new form of inequality.

At the population level, widespread use of somatic gene editing could gradually alter the distribution of risk alleles in the human gene pool, even if germline editing is prohibited. For example, if millions of people receive permanent inactivation of PCSK9 or ASGR1 in their livers, the biological landscape of lipid metabolism in the human population will gradually change. This change may be beneficial in terms of reducing myocardial infarction and stroke, but it may also have unexpected consequences on infections, immune responses, or other traits that

are tightly coupled to lipid metabolism. From an evolutionary perspective, human beings have always been subject to natural selection and random genetic drift. Now we are entering an era where deliberate, large-scale, directional changes to gene function become possible at the species level, even if we do not directly edit germ cells.

At the level of human civilization, the advent of GETx-CVD is one chapter in a larger story: humanity's increasing ability to rewrite its own biology. From a philosophical point of view, cardiovascular gene editing is not only about preventing heart attacks; it is about how much we are willing to intervene in our own genetic "destiny," and who will decide what counts as disease, enhancement, or acceptable risk. If we use gene editing primarily to reduce premature death and severe disability, many people will view it as a natural extension of medicine's traditional mission. However, if in the future we begin to use similar technologies to extend lifespan far beyond current limits, or to confer traits that are closer to enhancement than to therapy, society will face deep questions about fairness, identity, and the meaning of being human.

Furthermore, there is a collective responsibility to manage the risks associated with powerful technologies. Inappropriate use, inadequate oversight, or premature deployment of GETx technologies could lead to catastrophic outcomes that might damage public trust not only in gene editing but in biomedical science as a whole. In my personal view, gene editing technologies should be developed with humility, with careful respect for the complexity of biological systems, and with compassion for patients whose needs motivate this research in the first place.

4.5 Lessons learned and future directions, the next 5, 10, and 20 years from 2026

From the ASGR1 and IDOL projects, I have learned several scientific and personal lessons. Scientifically, I learned that technical success in editing, as indicated by high on-target efficiency, good vector performance, and clean safety signals, does not guarantee therapeutic efficacy. Biology can be surprising, and even a "negative" result such as the lack of LDLR upregulation in *Idol*-edited mice carries valuable information about pathway redundancy and species-specific regulation. I also learned that target selection must be guided not only by molecular logic but also by rigorous human genetic evidence and cross-species validation. For ASGR1, the convergence of human loss-of-function data, pig and mouse studies, and my own adenoviral-Cas9 experiments provides a robust foundation for further translational work.

Personally, I have come to appreciate the importance of patience and long-term vision in translational science. Gene editing therapy is a field where experiments take time, where unexpected results are common, and where each step must be built carefully on the last one. In this sense, the thesis is not an end, but a starting point. Below, I outline my aspirations and plans for the next 5, 10, and 20 years, recognizing that real life will be more complex than any plan I write today.

In the next five years, I hope to deepen and refine the ASGR1 work and related liver targets. One immediate goal is to move from conventional Cas9 nucleases to base editors and prime editors for ASGR1, designing strategies to disrupt splice sites or recreate protective intronic deletions in a more precise and potentially safer manner. Another goal is to perform more comprehensive off-target and structural variant analyses, such as long-read sequencing and high-coverage unbiased assays, to better characterize the genomic consequences of *in vivo* editing. I also plan to investigate how ASGR1 editing interacts with existing lipid-lowering drugs

and with metabolic regulators such as GLP-1 receptor agonists, both in preclinical models and, if possible, in early translational collaborations.

Looking ahead to ten years, I envision that the field will have progressed to more clinical trials of liver-directed gene editing therapies targeting cardiovascular risk factors. By that time, I hope to be actively involved in the design and interpretation of such trials, helping to bridge basic science, preclinical modeling, and clinical decision-making. Scientifically, I would like to expand beyond the liver and explore editing strategies that target vascular endothelium, smooth muscle cells, and possibly macrophages in atherosclerotic plaque, using emerging delivery systems such as engineered viral-like particles or ligand-decorated nanoparticles. I also foresee increasing integration between gene editing and other modalities, such as RNA therapeutics, cell therapies, and immunomodulation. My aim is to participate in building a more comprehensive "toolbox" for cardiovascular disease, where gene editing is one powerful instrument among many, used in a thoughtful and individualized way.

Over a 20-year horizon, it is possible that GETx-CVD will become part of standard care for high-risk patients, perhaps delivered in specialized centers with strong genetic counseling and long-term follow-up. By that time, we may also see more ambitious interventions aimed at multi-trait risk reduction, combining edits that address lipids, blood pressure, inflammation, and perhaps even cardiac regeneration. In such a future, the role of scientists and physicians will not only be to design and deliver the therapies, but also to guide society in making wise choices about how far to go in editing the human genome. Personally, I hope that after 20 years I will still maintain the curiosity and humility that I have now, and that I will have trained younger scientists who can carry the field forward with both technical excellence and ethical sensitivity.

4.6 Concluding remarks

Looking back at the path from ASGR1 to IDOL, from plasmid construction to mouse phenotyping, and from individual experiments to this concluding chapter, I feel that this thesis represents a small but meaningful contribution to the emerging story of gene editing therapy for cardiovascular disease. The work is far from complete, but the direction is clear. With continued effort from many people around the world, I believe that, step by step, we can move closer to a future in which severe cardiovascular events become much less common, and where carefully designed gene editing therapies help more people live longer and healthier lives.

Bibliography

1. Crispr Developers Win 2020 Nobel Prize for Chemistry. *Am J Med Genet A* **185**, 8-9 (2021).
2. WHO, Cardiovascular diseases. Available online: https://www.who.int/health-topics/cardiovascular-diseases#tab=tab_1. (accessed on 11/20/2025).
3. T. Gordon, W. B. Kannel, W. P. Castelli, T. R. Dawber, Lipoproteins, cardiovascular disease, and death. The Framingham study. *Arch Intern Med* **141**, 1128-1131 (1981).
4. M. Miller *et al.*, Triglycerides and Cardiovascular Disease. *Circulation* **123**, 2292-2333 (2011).
5. M. El Shahawy *et al.*, Efficacy and Safety of Alirocumab Versus Ezetimibe Over 2 Years (from ODYSSEY COMBO II). *Am J Cardiol* **120**, 931-939 (2017).
6. M. Farnier, Alirocumab for the treatment of hyperlipidemia in high-risk patients: an updated review. *Expert Rev Cardiovasc Ther* **15**, 923-932 (2017).
7. P. A. McCullough *et al.*, Efficacy and Safety of Alirocumab in High-Risk Patients With Clinical Atherosclerotic Cardiovascular Disease and/or Heterozygous Familial Hypercholesterolemia (from 5 Placebo-Controlled ODYSSEY Trials). *Am J Cardiol* **121**, 940-948 (2018).
8. R. M. Gupta, One-shot, one cure with genome editing for dyslipidemia. *Circ Cardiovasc Genet* **7**, 967-968 (2014).
9. M. Nishiga, L. S. Qi, J. C. Wu, Therapeutic genome editing in cardiovascular diseases. *Adv Drug Deliv Rev*, (2020).
10. J. Zhou, Z. Ren, J. Xu, J. Zhang, Y. E. Chen, Gene editing therapy ready for cardiovascular diseases: opportunities, challenges, and perspectives. *Med Rev (2021)* **1**, 6-9 (2021).
11. A. King, A CRISPR edit for heart disease. *Nature* **555**, S23-S25 (2018).
12. F. V. Jacinto, W. Link, B. I. Ferreira, CRISPR/Cas9-mediated genome editing: From basic research to translational medicine. *J Cell Mol Med* **24**, 3766-3778 (2020).
13. S. Huang *et al.*, Research progress in gene editing technology. *FBL* **26**, 916-927 (2021).
14. D. Liu, D. Cao, R. Han, Recent advances in therapeutic gene-editing technologies. *Molecular Therapy* **33**, 2619-2644 (2025).
15. J. Boch *et al.*, Breaking the code of DNA binding specificity of TAL-type III effectors. *Science* **326**, 1509-1512 (2009).
16. M. J. Moscou, A. J. Bogdanove, A simple cipher governs DNA recognition by TAL effectors. *Science* **326**, 1501 (2009).
17. Y. G. Kim, J. Cha, S. Chandrasegaran, Hybrid restriction enzymes: zinc finger fusions to Fok I cleavage domain. *Proc Natl Acad Sci U S A* **93**, 1156-1160 (1996).
18. J. C. Miller *et al.*, A TALE nuclease architecture for efficient genome editing. *Nat Biotechnol* **29**, 143-148 (2011).

19. M. Christian *et al.*, Targeting DNA double-strand breaks with TAL effector nucleases. *Genetics* **186**, 757-761 (2010).
20. C. D. Yeh, C. D. Richardson, J. E. Corn, Advances in genome editing through control of DNA repair pathways. *Nat Cell Biol* **21**, 1468-1478 (2019).
21. A. C. Komor, Y. B. Kim, M. S. Packer, J. A. Zuris, D. R. Liu, Programmable editing of a target base in genomic DNA without double-stranded DNA cleavage. *Nature* **533**, 420-+ (2016).
22. N. M. Gaudelli *et al.*, Programmable base editing of A*T to G*C in genomic DNA without DNA cleavage. *Nature* **551**, 464-471 (2017).
23. A. C. Komor *et al.*, Improved base excision repair inhibition and bacteriophage Mu Gam protein yields C:G-to-T:A base editors with higher efficiency and product purity. *Sci Adv* **3**, eaao4774 (2017).
24. L. W. Koblan *et al.*, Improving cytidine and adenine base editors by expression optimization and ancestral reconstruction. *Nat Biotechnol* **36**, 843-846 (2018).
25. D. Zhao *et al.*, Glycosylase base editors enable C-to-A and C-to-G base changes. *Nat Biotechnol* **39**, 35-40 (2021).
26. L. Chen *et al.*, Adenine transversion editors enable precise, efficient A•T-to-C•G base editing in mammalian cells and embryos. *Nature Biotechnology* **42**, 638-650 (2024).
27. H. Tong *et al.*, Programmable A-to-Y base editing by fusing an adenine base editor with an N-methylpurine DNA glycosylase. *Nature Biotechnology* **41**, 1080-1084 (2023).
28. P. J. Chen, D. R. Liu, Prime editing for precise and highly versatile genome manipulation. *Nat Rev Genet* **24**, 161-177 (2023).
29. D. Liu, D. Cao, R. Han, Recent advances in therapeutic gene-editing technologies. *Mol Ther* **33**, 2619-2644 (2025).
30. D. Wang, F. Zhang, G. Gao, CRISPR-Based Therapeutic Genome Editing: Strategies and In Vivo Delivery by AAV Vectors. *Cell* **181**, 136-150 (2020).
31. P. Tebas *et al.*, Gene Editing of CCR5 in Autologous CD4 T Cells of Persons Infected with HIV. *New England Journal of Medicine* **370**, 901-910 (2014).
32. E. A. Stadtmauer *et al.*, CRISPR-engineered T cells in patients with refractory cancer. *Science* **367**, eaba7365 (2020).
33. Y. Lu *et al.*, Safety and feasibility of CRISPR-edited T cells in patients with refractory non-small-cell lung cancer. *Nature Medicine* **26**, 732-740 (2020).
34. A. A. Sousa *et al.*, Systematic optimization of prime editing for the efficient functional correction of CFTR F508del in human airway epithelial cells. *Nat Biomed Eng* **9**, 7-21 (2025).
35. N. E. King *et al.*, Correction of Airway Stem Cells: Genome Editing Approaches for the Treatment of Cystic Fibrosis. *Hum Gene Ther* **31**, 956-972 (2020).
36. K. A. Everette *et al.*, Ex vivo prime editing of patient haematopoietic stem cells rescues sickle-cell disease phenotypes after engraftment in mice. *Nat Biomed Eng* **7**, 616-628 (2023).
37. J. T. Stack *et al.*, DNA-PKcs inhibition improves sequential gene insertion of the full-length CFTR cDNA in airway stem cells. *Mol Ther Nucleic Acids* **35**, 102339 (2024).
38. X. Wang *et al.*, Long sequence insertion via CRISPR/Cas gene-editing with transposase, recombinase, and integrase. *Curr Opin Biomed Eng* **28**, (2023).
39. X. Chen *et al.*, Recent advances in CRISPR-Cas9-based genome insertion technologies. *Molecular Therapy Nucleic Acids* **35**, 102138 (2024).

40. M. F. Naso, B. Tomkowicz, W. L. Perry, W. R. Strohl, Adeno-Associated Virus (AAV) as a Vector for Gene Therapy. *BioDrugs* **31**, 317-334 (2017).
41. M. Watanabe, Y. Nishikawaji, H. Kawakami, K. I. Kosai, Adenovirus Biology, Recombinant Adenovirus, and Adenovirus Usage in Gene Therapy. *Viruses* **13**, (2021).
42. X. Wang *et al.*, Recent advances in lentiviral vectors for gene therapy. *Science China Life Sciences* **64**, 1842-1857 (2021).
43. H. P. Mandalawatta, K. C. Rajendra, K. Fairfax, A. W. Hewitt, Emerging trends in virus and virus-like particle gene therapy delivery to the brain. *Mol Ther Nucleic Acids* **35**, 102280 (2024).
44. C. Hald Albertsen *et al.*, The role of lipid components in lipid nanoparticles for vaccines and gene therapy. *Adv Drug Deliv Rev* **188**, 114416 (2022).
45. J.-Y. Dong, P.-D. Fan, R. A. Frizzell, Quantitative analysis of the packaging capacity of recombinant adeno-associated virus. *Human gene therapy* **7**, 2101-2112 (1996).
46. F. Sonntag, K. Schmidt, J. A. Kleinschmidt, A viral assembly factor promotes AAV2 capsid formation in the nucleolus. *Proceedings of the National Academy of Sciences of the United States of America* **107**, 10220-10225 (2010).
47. P. J. Ogden, E. D. Kelsic, S. Sinai, G. M. Church, Comprehensive AAV capsid fitness landscape reveals a viral gene and enables machine-guided design. *Science* **366**, 1139-1143 (2019).
48. S. Russell *et al.*, Efficacy and safety of voretigene neparvovec (AAV2-hRPE65v2) in patients with RPE65-mediated inherited retinal dystrophy: a randomised, controlled, open-label, phase 3 trial. *Lancet* **390**, 849-860 (2017).
49. D. Wang, P. W. L. Tai, G. Gao, Adeno-associated virus vector as a platform for gene therapy delivery. *Nature Reviews Drug Discovery* **18**, 358-378 (2019).
50. C. Schmelas, D. Grimm, Split Cas9, Not Hairs - Advancing the Therapeutic Index of CRISPR Technology. *Biotechnol J* **13**, e1700432 (2018).
51. J. M. Levy *et al.*, Cytosine and adenine base editing of the brain, liver, retina, heart and skeletal muscle of mice via adeno-associated viruses. *Nature Biomedical Engineering* **4**, 97-110 (2020).
52. N. E. Bengtsson, H. Tasfaout, J. S. Chamberlain, The road toward AAV-mediated gene therapy of Duchenne muscular dystrophy. *Mol Ther* **33**, 2035-2051 (2025).
53. H. Nishimasu *et al.*, Crystal Structure of Staphylococcus aureus Cas9. *Cell* **162**, 1113-1126 (2015).
54. A. Edraki *et al.*, A Compact, High-Accuracy Cas9 with a Dinucleotide PAM for In Vivo Genome Editing. *Molecular Cell* **73**, 714-726.e714 (2019).
55. E. Kim *et al.*, In vivo genome editing with a small Cas9 orthologue derived from Campylobacter jejuni. *Nat Commun* **8**, 14500 (2017).
56. Z. Hu *et al.*, A compact Cas9 ortholog from Staphylococcus Auricularis (SauriCas9) expands the DNA targeting scope. *PLoS Biol* **18**, e3000686 (2020).
57. D. Duan, Lethal immunotoxicity in high-dose systemic AAV therapy. *Molecular Therapy* **31**, 3123-3126 (2023).
58. Y. S. Tseng, M. Agbandje-McKenna, Mapping the AAV Capsid Host Antibody Response toward the Development of Second Generation Gene Delivery Vectors. *Front Immunol* **5**, 9 (2014).

59. H. T. Le, Q.-C. Yu, J. M. Wilson, M. A. Croyle, Utility of PEGylated recombinant adeno-associated viruses for gene transfer. *Journal of Controlled Release* **108**, 161-177 (2005).
60. D. Wang *et al.*, A rationally engineered capsid variant of AAV9 for systemic CNS-directed and peripheral tissue-detargeted gene delivery in neonates. *Molecular Therapy Methods & Clinical Development* **9**, 234-246 (2018).
61. L. V. Tse *et al.*, Structure-guided evolution of antigenically distinct adeno-associated virus variants for immune evasion. *Proceedings of the National Academy of Sciences of the United States of America* **114**, E4812-e4821 (2017).
62. F. Locatelli *et al.*, Betibeglogene Autotemcel Gene Therapy for Non–β0/β0 Genotype β-Thalassemia. *New England Journal of Medicine* **386**, 415-427 (2022).
63. A. I. Scott, K. K. Mallhi, J. Ganesh, W.-L. Chen, Elivaldogene autotemcel approved for treatment of cerebral adrenoleukodystrophy (CALD) in males: A therapeutics bulletin of the American College of Medical Genetics and Genomics (ACMG). *Genetics in Medicine Open* **1**, (2023).
64. R. N. Gangji, Q. A. Ali, R. Dhamija, A. M. Corado, S. Kharbanda, Lenmeldy (atidarsagene autotemcel) for individuals with early metachromatic leukodystrophy (MLD): A therapeutics bulletin of the American College of Medical Genetics and Genomics (ACMG). *Genet Med Open* **3**, 103432 (2025).
65. J. Kanter *et al.*, Biologic and Clinical Efficacy of LentiGlobin for Sickle Cell Disease. *New England Journal of Medicine* **386**, 617-628 (2022).
66. S. L. Maude *et al.*, Tisagenlecleucel in children and young adults with B-cell lymphoblastic leukemia. *New England Journal of Medicine* **378**, 439-448 (2018).
67. P. Sharma *et al.*, FDA Approval Summary: Axicabtagene Ciloleucel for Second-Line Treatment of Large B-Cell Lymphoma. *Clin Cancer Res* **29**, 4331-4337 (2023).
68. N. Bouchkouj *et al.*, FDA Approval Summary: Brexucabtagene Autoleucel for Treatment of Adults With Relapsed or Refractory B-Cell Precursor Acute Lymphoblastic Leukemia. *Oncologist* **27**, 892-899 (2022).
69. K. Britton *et al.*, FDA Approval Summary: Lisocabtagene Maraleucel for Relapsed or Refractory Follicular Lymphoma. *Clin Cancer Res* **31**, 3830-3833 (2025).
70. K. Wanisch, R. J. Yáñez-Muñoz, Integration-deficient lentiviral vectors: a slow coming of age. *Molecular therapy* **17**, 1316-1332 (2009).
71. H. Kymäläinen *et al.*, Long-term episomal transgene expression from mitotically stable integration-deficient lentiviral vectors. *Human gene therapy* **25**, 428-442 (2014).
72. H. Jaffe *et al.*, Adenovirus–mediated in vivo gene transfer and expression in normal rat liver. *Nature genetics* **1**, 372-378 (1992).
73. M. A. Rosenfeld *et al.*, In vivo transfer of the human cystic fibrosis transmembrane conductance regulator gene to the airway epithelium. *Cell* **68**, 143-155 (1992).
74. S. E. Raper *et al.*, Fatal systemic inflammatory response syndrome in a ornithine transcarbamylase deficient patient following adenoviral gene transfer. *Molecular Genetics and Metabolism* **80**, 148-158 (2003).
75. K. Kumahara *et al.*, Suppression of inflammation by dexamethasone prolongs adenoviral vector-mediated transgene expression in murine nasal mucosa. *Acta oto-laryngologica* **125**, 1301-1306 (2005).

76. C. R. O'Riordan *et al.*, PEGylation of adenovirus with retention of infectivity and protection from neutralizing antibody in vitro and in vivo. *Hum Gene Ther* **10**, 1349-1358 (1999).
77. M. A. Morsy *et al.*, An adenoviral vector deleted for all viral coding sequences results in enhanced safety and extended expression of a leptin transgene. *Proceedings of the National Academy of Sciences* **95**, 7866-7871 (1998).
78. P. Kazemian *et al.*, Lipid-Nanoparticle-Based Delivery of CRISPR/Cas9 Genome-Editing Components. *Molecular Pharmaceutics* **19**, 1669-1686 (2022).
79. G. Sahay *et al.*, Efficiency of siRNA delivery by lipid nanoparticles is limited by endocytic recycling. *Nature Biotechnology* **31**, 653-658 (2013).
80. T. Asai *et al.*, Cell-penetrating peptide-conjugated lipid nanoparticles for siRNA delivery. *Biochem Biophys Res Commun* **444**, 599-604 (2014).
81. B. Huang, S. C. De Smedt, W. H. De Vos, K. Braeckmans, Light-triggered nanocarriers for nucleic acid delivery. *Drug Deliv* **32**, 2502346 (2025).
82. I. Urits *et al.*, A Review of Patisiran (ONPATTRO®) for the Treatment of Polyneuropathy in People with Hereditary Transthyretin Amyloidosis. *Neurol Ther* **9**, 301-315 (2020).
83. P. Polack Fernando *et al.*, Safety and Efficacy of the BNT162b2 mRNA Covid-19 Vaccine. *New England Journal of Medicine* **383**, 2603-2615 (2020).
84. R. Baden Lindsey *et al.*, Efficacy and Safety of the mRNA-1273 SARS-CoV-2 Vaccine. *New England Journal of Medicine* **384**, 403-416 (2021).
85. M. Farzaneh *et al.*, The Lentiviral Vector Pseudotyped by Modified Rabies Glycoprotein Does Not Cause Reactive Gliosis and Neurodegeneration in Rat Hippocampus. *Iran Biomed J* **23**, 324-329 (2019).
86. K. M. Frietze, D. S. Peabody, B. Chackerian, Engineering virus-like particles as vaccine platforms. *Current Opinion in Virology* **18**, 44-49 (2016).
87. S. Banskota *et al.*, Engineered virus-like particles for efficient in vivo delivery of therapeutic proteins. *Cell* **185**, 250-265.e216 (2022).
88. M. An *et al.*, Engineered virus-like particles for transient delivery of prime editor ribonucleoprotein complexes in vivo. *Nature Biotechnology* **42**, 1526-1537 (2024).
89. A. Raguram, M. An, P. Z. Chen, D. R. Liu, Directed evolution of engineered virus-like particles with improved production and transduction efficiencies. *Nature Biotechnology*, (2024).
90. R. Gupta *et al.*, Platforms, advances, and technical challenges in virus-like particles-based vaccines. *Front Immunol* **14**, 1123805 (2023).
91. R. Tang *et al.*, Engineering PEG10-assembled endogenous virus-like particles with genetically encoded neoantigen peptides for cancer vaccination. *eLife* **13**, RP98579 (2024).
92. T. Horie, K. Ono, VERVE-101: a promising CRISPR-based gene editing therapy that reduces LDL-C and PCSK9 levels in HeFH patients. *European Heart Journal - Cardiovascular Pharmacotherapy* **10**, 89-90 (2023).
93. P. Flight *et al.*, † VERVE-102, a clinical stage in vivo base editing medicine, leads to potent and precise inactivation of PCSK9 in preclinical studies. *Journal of Clinical Lipidology* **19**, e68 (2025).

94. World's First: In Vivo Gene Editing Product ART002 Achieves Saturation of Pharmacological Effect in Humans and Reduces LDL-C Safely and Effectively. Available online: https://www.accuredit.com/46/63. (accessed on 11/16/2025).
95. Clinical Exploration Trial of YOLT-101 in the Treatment of Familial Hypercholesterolemia (FH). Available online: https://clinicaltrials.gov/study/NCT06461702. (accessed on 11/16/2025).
96. Phase 1b Study of VERVE-201 in Patients With Refractory Hyperlipidemia. Available online: https://clinicaltrials.gov/study/NCT06451770. (accessed on 11/16/2025).
97. P. K. Morrow *et al.*, Abstract 16908: CTX310: An Investigational in vivo CRISPR-Based Therapy Efficiently and Durably Reduces ANGPTL3 Protein and Triglyceride Levels in Non-Human Primates After a Single Dose. *Circulation* **148**, A16908-A16908 (2023).
98. The World's First Gene-Editing Therapy Targeting APOC3 for Hyperlipidemia. Available online: https://www.prnewswire.com/news-releases/the-worlds-first-gene-editing-therapy-targeting-apoc3-for-hyperlipidemia-302606367.html. (accessed on 11/16/2025).
99. P. K. Morrow *et al.*, Abstract 17013: CTX320: An Investigational in vivo CRISPR-Based Therapy Efficiently and Durably Reduces Lipoprotein (a) Levels in Non-Human Primates After a Single Dose. *Circulation* **148**, A17013-A17013 (2023).
100. N. Nassoury *et al.*, The cellular trafficking of the secretory proprotein convertase PCSK9 and its dependence on the LDLR. *Traffic* **8**, 718-732 (2007).
101. Y.-W. Qian *et al.*, Secreted PCSK9 downregulates low density lipoprotein receptor through receptor-mediated endocytosis. *Journal of lipid research* **48**, 1488-1498 (2007).
102. F.-H. Meng *et al.*, New Loss-of-Function Mutations in PCSK9 Reduce Plasma LDL Cholesterol. *Arteriosclerosis, Thrombosis, and Vascular Biology* **43**, 1219-1233 (2023).
103. J. C. Cohen, E. Boerwinkle, T. H. Mosley, H. H. Hobbs, Sequence Variations in PCSK9, Low LDL, and Protection against Coronary Heart Disease. *New England Journal of Medicine* **354**, 1264-1272 (2006).
104. Q. Ding *et al.*, Permanent alteration of PCSK9 with in vivo CRISPR-Cas9 genome editing. *Circ Res* **115**, 488-492 (2014).
105. X. Wang *et al.*, CRISPR-Cas9 Targeting of PCSK9 in Human Hepatocytes In Vivo-Brief Report. *Arterioscler Thromb Vasc Biol* **36**, 783-786 (2016).
106. A. C. Chadwick, X. Wang, K. Musunuru, In Vivo Base Editing of PCSK9 (Proprotein Convertase Subtilisin/Kexin Type 9) as a Therapeutic Alternative to Genome Editing. *Arterioscler Thromb Vasc Biol* **37**, 1741-1747 (2017).
107. F. A. Ran *et al.*, In vivo genome editing using Staphylococcus aureus Cas9. *Nature* **520**, 186-191 (2015).
108. Q. Li *et al.*, In vivo PCSK9 gene editing using an all-in-one self-cleavage AAV-CRISPR system. *Molecular Therapy - Methods & Clinical Development* **20**, 652-659 (2021).
109. M. A. Cappelluti *et al.*, Durable and efficient gene silencing in vivo by hit-and-run epigenome editing. *Nature* **627**, 416-423 (2024).
110. F. Tremblay *et al.*, A potent epigenetic editor targeting human PCSK9 for durable reduction of low-density lipoprotein cholesterol levels. *Nature Medicine* **31**, 1329-1338 (2025).

111. L. Wang *et al.*, Long-term stable reduction of low-density lipoprotein in nonhuman primates following in vivo genome editing of PCSK9. *Molecular Therapy* **29**, 2019-2029 (2021).
112. K. Musunuru *et al.*, In vivo CRISPR base editing of PCSK9 durably lowers cholesterol in primates. *Nature* **593**, 429-434 (2021).
113. T. Rothgangl *et al.*, In vivo adenine base editing of PCSK9 in macaques reduces LDL cholesterol levels. *Nat Biotechnol* **39**, 949-957 (2021).
114. R. G. Lee *et al.*, Efficacy and Safety of an Investigational Single-Course CRISPR Base-Editing Therapy Targeting PCSK9 in Nonhuman Primate and Mouse Models. *Circulation* **147**, 242-253 (2023).
115. R. Wei *et al.*, Improved split prime editors enable efficient in vivo genome editing. *Cell Rep* **44**, 115144 (2025).
116. J. G. Robinson *et al.*, Efficacy and safety of alirocumab in reducing lipids and cardiovascular events. *N Engl J Med* **372**, 1489-1499 (2015).
117. D. J. Blom *et al.*, A 52-week placebo-controlled trial of evolocumab in hyperlipidemia. *N Engl J Med* **370**, 1809-1819 (2014).
118. K. K. Ray *et al.*, Two Phase 3 Trials of Inclisiran in Patients with Elevated LDL Cholesterol. *N Engl J Med* **382**, 1507-1519 (2020).
119. J. Lin *et al.*, Efficacy and safety of ongericimab in Chinese patients with heterozygous familial hypercholesterolemia: A randomized, double-blind, placebo-controlled phase 3 trial. *Atherosclerosis* **403**, 119120 (2025).
120. S. Yan *et al.*, Pharmacokinetic/LDL-C and exposure-response analysis of tafolecimab in Chinese hypercholesterolemia patients: Results from phase I, II, and III studies. *Clin Transl Sci* **16**, 2791-2803 (2023).
121. Y. Zhang *et al.*, Ebronucimab in Chinese patients with hypercholesterolemia---A randomized double-blind placebo-controlled phase 3 trial to evaluate the efficacy and safety of ebronucimab. *Pharmacological Research* **207**, 107340 (2024).
122. Y. Sun *et al.*, Recaticimab as Add-On Therapy to Statins for Nonfamilial Hypercholesterolemia: The Randomized, Phase 3 REMAIN-2 Trial. *J Am Coll Cardiol* **84**, 2037-2047 (2024).
123. A. Hofherr *et al.*, ETESIAN: A phase 2B study of the efficacy, safety and tolerability of AZD8233, a PCSK9-targeted antisense oligonucleotide, in patients with dyslipidemia. *Atherosclerosis* **355**, 28 (2022).
124. Ribo Showcases New Clinical Data from Leading siRNA Programs at ESC 2025, Underscoring Significant Progress and Achievements in Advancing Cardiovascular Therapies. Available online: https://www.ribolia.com/en/media-center/our-products-news/50?utm_source. (accessed on 11/16/2025).
125. E. Q. Klug *et al.*, Efficacy and Safety of Lerodalcibep in Patients With or at High Risk of Cardiovascular Disease: A Randomized Clinical Trial. *JAMA Cardiol* **9**, 800-807 (2024).
126. J. R. Burnett, A. J. Hooper, MK-0616: An oral PCSK9 inhibitor for hypercholesterolemia treatment. *Expert Opinion on Investigational Drugs* **32**, 873-878 (2023).
127. M. J. Koren *et al.*, PCSK9 inhibition with orally administered NNC0385-0434 in hypercholesterolaemia: a randomised, double-blind, placebo-controlled and active-controlled phase 2 trial. *The Lancet Diabetes & Endocrinology* **12**, 174-183 (2024).

128. R. Vega *et al.*, AZD0780, the first oral small molecule PCSK9 inhibitor for the treatment of hypercholesterolemia: Results from a randomized, single-blind, placebo-controlled phase 1 trial. *Atherosclerosis* **395**, (2024).
129. Verve Therapeutics Announces Positive Initial Data from the Heart-2 Phase 1b Clinical Trial of VERVE-102, an In Vivo Base Editing Medicine Targeting PCSK9. Available online: https://vervetx.gcs-web.com/news-releases/news-release-details/verve-therapeutics-announces-positive-initial-data-heart-2-phase. (accessed on 11/16/2025).
130. L. Da Dalt *et al.*, PCSK9 deficiency reduces insulin secretion and promotes glucose intolerance: the role of the low-density lipoprotein receptor. *Eur Heart J* **40**, 357-368 (2019).
131. H. Fang *et al.*, PCSK9 potentiates innate immune response to RNA viruses by preventing AIP4-mediated polyubiquitination and degradation of VISA/MAVS. *Proceedings of the National Academy of Sciences of the United States of America* **122**, e2412206122 (2025).
132. E. M. O'Connell, F. W. Lohoff, Proprotein Convertase Subtilisin/Kexin Type 9 (PCSK9) in the Brain and Relevance for Neuropsychiatric Disorders. *Front Neurosci* **14**, 609 (2020).
133. J. Liu, H. Afroza, D. J. Rader, W. Jin, Angiopoietin-like protein 3 inhibits lipoprotein lipase activity through enhancing its cleavage by proprotein convertases. *J Biol Chem* **285**, 27561-27570 (2010).
134. F. E. Dewey *et al.*, Genetic and Pharmacologic Inactivation of ANGPTL3 and Cardiovascular Disease. *N Engl J Med* **377**, 211-221 (2017).
135. N. O. Stitziel *et al.*, ANGPTL3 Deficiency and Protection Against Coronary Artery Disease. *J Am Coll Cardiol* **69**, 2054-2063 (2017).
136. A. C. Chadwick, N. H. Evitt, W. Lv, K. Musunuru, Reduced Blood Lipid Levels With In Vivo CRISPR-Cas9 Base Editing of ANGPTL3. *Circulation* **137**, 975-977 (2018).
137. M. Qiu *et al.*, Lipid nanoparticle-mediated codelivery of Cas9 mRNA and single-guide RNA achieves liver-specific in vivo genome editing of Angptl3. *Proceedings of the National Academy of Sciences of the United States of America* **118**, (2021).
138. Y. Zuo *et al.*, Liver-specific in vivo base editing of Angptl3 via AAV delivery efficiently lowers blood lipid levels in mice. *Cell & Bioscience* **13**, 109 (2023).
139. J. R. Davis *et al.*, Efficient in vivo base editing via single adeno-associated viruses with size-optimized genomes encoding compact adenine base editors. *Nature Biomedical Engineering* **6**, 1272-1283 (2022).
140. J. Khirallah *et al.*, In vivo base editing of Angptl3 via lipid nanoparticles to treat cardiovascular disease. *Molecular Therapy Nucleic Acids* **36**, (2025).
141. B. M. Kuehn, Evinacumab Approval Adds a New Option for Homozygous Familial Hypercholesterolemia With a Hefty Price Tag. *Circulation* **143**, 2494-2496 (2021).
142. F. J. Raal *et al.*, Evinacumab for Homozygous Familial Hypercholesterolemia. *N Engl J Med* **383**, 711-720 (2020).
143. R. S. Rosenson *et al.*, Efficacy of evinacumab in patients with severe hypertriglyceridemia and a history of severe hypertriglyceridemia-related acute pancreatitis: A phase 2b trial. *Journal of Clinical Lipidology*.
144. R. S. Rosenson *et al.*, Zodasiran, an RNAi Therapeutic Targeting ANGPTL3, for Mixed Hyperlipidemia. *N Engl J Med* **391**, 913-925 (2024).
145. K. K. Ray *et al.*, Durability and efficacy of solbinsiran, a GalNAc-conjugated siRNA targeting ANGPTL3, in adults with mixed dyslipidaemia (PROLONG-

ANG3): a double-blind, randomised, placebo-controlled, phase 2 trial. *The Lancet* **405**, 1594-1607 (2025).
146. D. Gaudet *et al.*, Vupanorsen, an N-acetyl galactosamine-conjugated antisense drug to ANGPTL3 mRNA, lowers triglycerides and atherogenic lipoproteins in patients with diabetes, hepatic steatosis, and hypertriglyceridaemia. *Eur Heart J* **41**, 3936-3945 (2020).
147. L. J. Laffin *et al.*, Phase 1 Trial of CRISPR-Cas9 Gene Editing Targeting ANGPTL3. *N Engl J Med*, (2025).
148. P. Tarugi, S. Bertolini, S. Calandra, Angiopoietin-like protein 3 (ANGPTL3) deficiency and familial combined hypolipidemia. *J Biomed Res* **33**, 73-81 (2019).
149. A. Kumari *et al.*, ANGPTL3/8 is an atypical unfoldase that regulates intravascular lipolysis by catalyzing unfolding of lipoprotein lipase. *Proceedings of the National Academy of Sciences of the United States of America* **122**, e2420721122 (2025).
150. A. R. Tall, Plasma cholesteryl ester transfer protein. *J Lipid Res* **34**, 1255-1274 (1993).
151. P. J. Barter, S. J. Nicholls, J. J. Kastelein, K.-A. Rye, Is cholesteryl ester transfer protein inhibition an effective strategy to reduce cardiovascular risk? CETP inhibition as a strategy to reduce cardiovascular risk: the pro case. *Circulation* **132**, 423-432 (2015).
152. L. T. Nordestgaard *et al.*, Long-term Benefits and Harms Associated With Genetic Cholesteryl Ester Transfer Protein Deficiency in the General Population. *JAMA Cardiol* **7**, 55-64 (2022).
153. I. Y. Millwood *et al.*, Association of CETP Gene Variants With Risk for Vascular and Nonvascular Diseases Among Chinese Adults. *JAMA Cardiol* **3**, 34-43 (2018).
154. J. Zhang *et al.*, Deficiency of Cholesteryl Ester Transfer Protein Protects Against Atherosclerosis in Rabbits. *Arteriosclerosis, Thrombosis, and Vascular Biology* **37**, 1068-1075 (2017).
155. M. Sugano *et al.*, Effect of antisense oligonucleotides against cholesteryl ester transfer protein on the development of atherosclerosis in cholesterol-fed rabbits. *Journal of Biological Chemistry* **273**, 5033-5036 (1998).
156. P. J. Barter *et al.*, Effects of Torcetrapib in Patients at High Risk for Coronary Events. *New England Journal of Medicine* **357**, 2109-2122 (2007).
157. G. G. Schwartz *et al.*, Effects of Dalcetrapib in Patients with a Recent Acute Coronary Syndrome. *New England Journal of Medicine* **367**, 2089-2099 (2012).
158. Effects of Anacetrapib in Patients with Atherosclerotic Vascular Disease. *New England Journal of Medicine* **377**, 1217-1227 (2017).
159. A. M. Lincoff *et al.*, Evacetrapib and Cardiovascular Outcomes in High-Risk Vascular Disease. *New England Journal of Medicine* **376**, 1933-1942 (2017).
160. S. J. Nicholls *et al.*, Safety and Efficacy of Obicetrapib in Patients at High Cardiovascular Risk. *New England Journal of Medicine* **393**, 51-61 (2025).
161. G. K. Hovingh, K. K. Ray, S. M. Boekholdt, Is Cholesteryl Ester Transfer Protein Inhibition an Effective Strategy to Reduce Cardiovascular Risk? *Circulation* **132**, 433-440 (2015).
162. T. Ebara, R. Ramakrishnan, G. Steiner, N. S. Shachter, Chylomicronemia due to apolipoprotein CIII overexpression in apolipoprotein E-null mice. Apolipoprotein CIII-induced hypertriglyceridemia is not mediated by effects on apolipoprotein E. *J Clin Invest* **99**, 2672-2681 (1997).

163. D. A. Lambert *et al.*, Hydrolysis of phospholipids by purified milk lipoprotein lipase. Effect of apoprotein CII, CIII, A and E, and synthetic fragments. *Clin Chim Acta* **291**, 19-33 (2000).
164. F. M. Sacks, The crucial roles of apolipoproteins E and C-III in apoB lipoprotein metabolism in normolipidemia and hypertriglyceridemia. *Curr Opin Lipidol* **26**, 56-63 (2015).
165. M. Sundaram *et al.*, Expression of apolipoprotein C-III in McA-RH7777 cells enhances VLDL assembly and secretion under lipid-rich conditions. *J Lipid Res* **51**, 150-161 (2010).
166. J. Crosby *et al.*, Loss-of-function mutations in APOC3, triglycerides, and coronary disease. *N Engl J Med* **371**, 22-31 (2014).
167. G. Reyes-Soffer *et al.*, Effects of APOC3 Heterozygous Deficiency on Plasma Lipid and Lipoprotein Metabolism. *Arterioscler Thromb Vasc Biol* **39**, 63-72 (2019).
168. M. Guo *et al.*, Inactivation of ApoC3 by CRISPR/Cas9 protects against atherosclerosis in hamsters. *Circulation Research* **127**, 1456-1458 (2020).
169. Y. Zha *et al.*, CRISPR/Cas9-mediated knockout of APOC3 stabilizes plasma lipids and inhibits atherosclerosis in rabbits. *Lipids in Health and Disease* **20**, 180 (2021).
170. S. Karanth *et al.*, Abstract 4146303: A Single-Dose of a Novel CasX-Editor Lowers APOC3 Levels In Vivo. *Circulation* **150**, A4146303-A4146303 (2024).
171. J. L. Witztum *et al.*, Volanesorsen and Triglyceride Levels in Familial Chylomicronemia Syndrome. *N Engl J Med* **381**, 531-542 (2019).
172. I. Gouni-Berthold *et al.*, Efficacy and safety of volanesorsen in patients with multifactorial chylomicronaemia (COMPASS): a multicentre, double-blind, randomised, placebo-controlled, phase 3 trial. *Lancet Diabetes Endocrinol* **9**, 264-275 (2021).
173. E. S. G. Stroes *et al.*, Olezarsen, Acute Pancreatitis, and Familial Chylomicronemia Syndrome. *N Engl J Med* **390**, 1781-1792 (2024).
174. G. F. Watts *et al.*, Plozasiran for Managing Persistent Chylomicronemia and Pancreatitis Risk. *N Engl J Med* **392**, 127-137 (2025).
175. Phase 2 Trial Evaluating the Efficacy and Safety of RBD5044 in Patients With Mixed Dyslipidemia. Available online: https://clinicaltrials.gov/study/NCT06797401. (accessed on 11/16/2025).
176. Study of RN0361 in Adult Healthy Subjects and Adult Hypertriglyceridemic Subjects. Available online: https://www.clinicaltrials.gov/study/NCT06471543?term=AREA%5BConditionSearch%5D(%22Familial%20Chylomicronemia%20Syndrome%22)&rank=6. (accessed on 11/16/2025).
177. A First in Human Study of STT-5058, an Antibody That Binds ApoC3. Available online: https://clinicaltrials.gov/study/NCT04419688. (accessed on 11/16/2025).
178. S. A. Khetarpal *et al.*, A human APOC3 missense variant and monoclonal antibody accelerate apoC-III clearance and lower triglyceride-rich lipoprotein levels. *Nat Med* **23**, 1086-1094 (2017).
179. C. Kiyose, Absorption, transportation, and distribution of vitamin E homologs. *Free Radic Biol Med* **177**, 226-237 (2021).
180. P. L. Gordts *et al.*, ApoC-III inhibits clearance of triglyceride-rich lipoproteins through LDL family receptors. *J Clin Invest* **126**, 2855-2866 (2016).

181. G. Ashwell, A. G. Morell, The role of surface carbohydrates in the hepatic recognition and transport of circulating glycoproteins. *Adv Enzymol Relat Areas Mol Biol* **41**, 99-128 (1974).
182. G. Ashwell, J. Harford, Carbohydrate-specific receptors of the liver. *Annu Rev Biochem* **51**, 531-554 (1982).
183. J.-Q. Wang *et al.*, Inhibition of ASGR1 decreases lipid levels by promoting cholesterol excretion. *Nature* **608**, 413-420 (2022).
184. P. Nioi *et al.*, Variant ASGR1 Associated with a Reduced Risk of Coronary Artery Disease. *N Engl J Med* **374**, 2131-2141 (2016).
185. B. Xie *et al.*, Deficiency of ASGR1 in pigs recapitulates reduced risk factor for cardiovascular disease in humans. *PLoS Genet* **17**, e1009891 (2021).
186. Z. Zhang *et al.*, Deficiency of ASGR1 promotes liver injury by increasing GP73-mediated hepatic endoplasmic reticulum stress. *Nature Communications* **15**, 1908 (2024).
187. B. G. Nordestgaard *et al.*, Lipoprotein(a) as a cardiovascular risk factor: current status. *Eur Heart J* **31**, 2844-2853 (2010).
188. S. Burgess *et al.*, Association of LPA Variants With Risk of Coronary Disease and the Implications for Lipoprotein(a)-Lowering Therapies: A Mendelian Randomization Analysis. *JAMA Cardiol* **3**, 619-627 (2018).
189. R. Clarke *et al.*, Causal Relevance of Lp(a) for Coronary Heart Disease and Stroke Types in East Asian and European Ancestry Populations: A Mendelian Randomization Study. *Circulation* **151**, 1699-1711 (2025).
190. A. M. Doerfler *et al.*, LPA disruption with AAV-CRISPR potently lowers plasma apo(a) in transgenic mouse model: A proof-of-concept study. *Mol Ther Methods Clin Dev* **27**, 337-351 (2022).
191. D. A. Garcia *et al.*, Lipid nanoparticle delivery of TALEN mRNA targeting LPA causes gene disruption and plasma lipoprotein(a) reduction in transgenic mice. *Mol Ther* **33**, 90-103 (2025).
192. N. J. Viney *et al.*, Antisense oligonucleotides targeting apolipoprotein(a) in people with raised lipoprotein(a): two randomised, double-blind, placebo-controlled, dose-ranging trials. *Lancet* **388**, 2239-2253 (2016).
193. A randomized double-blind, placebo-controlled, multicenter trial assessing the impact of lipoprotein(a) lowering with pelacarsen (TQJ230) on the progression of calcific aortic valve stenosis [Lp(a)FRONTIERS CAVS]. Available online: https://clinicaltrials.gov/study/NCT05646381. (accessed on 11/16/2025).
194. A phase 3, randomized, double-blind, placebo-controlled study to investigate the effect of lepodisiran on the reduction of major adverse cardiovascular events in adults with elevated lipoprotein(a) who have established atherosclerotic cardiovascular disease or are at risk for a first cardiovascular event—ACCLAIM-Lp(a). Available online: https://clinicaltrials.gov/study/NCT06292013. (accessed on 11/16/2025).
195. S. E. Nissen *et al.*, Zerlasiran-A Small-Interfering RNA Targeting Lipoprotein(a): A Phase 2 Randomized Clinical Trial. *Jama* **332**, 1992-2002 (2024).
196. A double-blind, randomized, placebo-controlled, multicenter study assessing the impact of olpasiran on major cardiovascular events in participants with atherosclerotic cardiovascular disease and elevated lipoprotein(a). Available online: https://clinicaltrials.gov/study/NCT05581303. (accessed on 11/16/2025).

197. L. Michael *et al.*, Discovery and preclinical development of LY3473329, a potent small molecule inhibitor of lipoprotein(a) formation. *European Heart Journal* **44**, (2023).
198. S. J. Nicholls *et al.*, Oral Muvalaplin for Lowering of Lipoprotein(a): A Randomized Clinical Trial. *Jama* **333**, 222-231 (2025).
199. E. Anglés-Cano, A. de la Peña Díaz, S. Loyau, Inhibition of fibrinolysis by lipoprotein(a). *Ann N Y Acad Sci* **936**, 261-275 (2001).
200. N. Zelcer, C. Hong, R. Boyadjian, P. Tontonoz, LXR regulates cholesterol uptake through Idol-dependent ubiquitination of the LDL receptor. *Science* **325**, 100-104 (2009).
201. J. K. Nelson *et al.*, Deubiquitylase Inhibition Reveals Liver X Receptor-independent Transcriptional Regulation of the E3 Ubiquitin Ligase IDOL and Lipoprotein Uptake. *J Biol Chem* **291**, 4813-4825 (2016).
202. C. Hong *et al.*, The E3 ubiquitin ligase IDOL induces the degradation of the low density lipoprotein receptor family members VLDLR and ApoER2. *J Biol Chem* **285**, 19720-19726 (2010).
203. E. Scotti *et al.*, Targeted disruption of the idol gene alters cellular regulation of the low-density lipoprotein receptor by sterols and liver x receptor agonists. *Mol Cell Biol* **31**, 1885-1893 (2011).
204. J. K. Liao, U. Laufs, Pleiotropic effects of statins. *Annu Rev Pharmacol Toxicol* **45**, 89-118 (2005).
205. D. I. Chasman *et al.*, Forty-three loci associated with plasma lipoprotein size, concentration, and cholesterol content in genome-wide analysis. *PLoS Genet* **5**, e1000730 (2009).
206. T. M. Teslovich *et al.*, Biological, clinical and population relevance of 95 loci for blood lipids. *Nature* **466**, 707-713 (2010).
207. D. Weissglas-Volkov *et al.*, The N342S MYLIP polymorphism is associated with high total cholesterol and increased LDL receptor degradation in humans. *J Clin Invest* **121**, 3062-3071 (2011).
208. V. Sorrentino *et al.*, Identification of a loss-of-function inducible degrader of the low-density lipoprotein receptor variant in individuals with low circulating low-density lipoprotein. *Eur Heart J* **34**, 1292-1297 (2013).
209. C. Hong *et al.*, The LXR-Idol axis differentially regulates plasma LDL levels in primates and mice. *Cell Metab* **20**, 910-918 (2014).
210. T. Koike *et al.*, IDOL Deficiency Inhibits Cholesterol-Rich Diet-Induced Atherosclerosis in Rabbits. *Arterioscler Thromb Vasc Biol* **45**, 669-671 (2025).
211. S. D. Lee *et al.*, IDOL regulates systemic energy balance through control of neuronal VLDLR expression. *Nat Metab* **1**, 1089-1100 (2019).
212. J. Gao *et al.*, The E3 ubiquitin ligase IDOL regulates synaptic ApoER2 levels and is important for plasticity and learning. *eLife* **6**, e29178 (2017).
213. M. Di Cesare *et al.*, The Heart of the World. *Glob Heart* **19**, 11 (2024).
214. D. Susan-Resiga *et al.*, Asialoglycoprotein receptor 1 is a novel PCSK9-independent ligand of liver LDLR cleaved by furin. *Journal of Biological Chemistry* **297**, 101177 (2021).
215. M. Svecla *et al.*, ASGR1 deficiency diverts lipids toward adipose tissue but results in liver damage during obesity. *Cardiovasc Diabetol* **23**, 42 (2024).
216. M. Svecla *et al.*, ASGR1 deficiency improves atherosclerosis but alters liver metabolism in ApoE(-/-) mice. *Cardiovasc Diabetol* **23**, 428 (2024).

217. Y. Xu *et al.*, Hypomorphic ASGR1 modulates lipid homeostasis via INSIG1-mediated SREBP signaling suppression. *JCI Insight* **6**, (2021).
218. Y. Zhang *et al.*, ASGR1 Deficiency Inhibits Atherosclerosis in Western Diet–Fed ApoE−/− Mice by Regulating Lipoprotein Metabolism and Promoting Cholesterol Efflux. *Arteriosclerosis, Thrombosis, and Vascular Biology* **44**, 2428-2449 (2024).
219. M. Abifadel *et al.*, Mutations in PCSK9 cause autosomal dominant hypercholesterolemia. *Nat Genet* **34**, 154-156 (2003).
220. L. Ma *et al.*, MiCas9 increases large size gene knock-in rates and reduces undesirable on-target and off-target indel edits. *Nat Commun* **11**, 6082 (2020).
221. C. T. Rueden *et al.*, ImageJ2: ImageJ for the next generation of scientific image data. *BMC Bioinformatics* **18**, 529 (2017).
222. S. H. Zhang, R. L. Reddick, J. A. Piedrahita, N. Maeda, Spontaneous hypercholesterolemia and arterial lesions in mice lacking apolipoprotein E. *Science* **258**, 468-471 (1992).
223. M. S. Popoviciu, L. Paduraru, G. Yahya, K. Metwally, S. Cavalu, Emerging Role of GLP-1 Agonists in Obesity: A Comprehensive Review of Randomised Controlled Trials. *Int J Mol Sci* **24**, (2023).
224. M. Taghdiri, C. Mussolino, Viral and Non-Viral Systems to Deliver Gene Therapeutics to Clinical Targets. *Int J Mol Sci* **25**, (2024).
225. L. K. Tsai *et al.*, Promotion or inhibition? This is a question in gene editing. *Mol Ther* **33**, 444-446 (2025).
226. J. Frostegård, Immunity, atherosclerosis and cardiovascular disease. *BMC Medicine* **11**, 117 (2013).
227. N. J. Stone *et al.*, 2013 ACC/AHA guideline on the treatment of blood cholesterol to reduce atherosclerotic cardiovascular risk in adults: a report of the American College of Cardiology/American Heart Association Task Force on Practice Guidelines. *J Am Coll Cardiol* **63**, 2889-2934 (2014).
228. J. L. Goldstein, M. S. Brown, A century of cholesterol and coronaries: from plaques to genes to statins. *Cell* **161**, 161-172 (2015).
229. F. Taylor *et al.*, Statins for the primary prevention of cardiovascular disease. *Cochrane Database Syst Rev*, CD004816 (2013).
230. S. U. Khan *et al.*, A Bayesian network meta-analysis of PCSK9 inhibitors, statins and ezetimibe with or without statins for cardiovascular outcomes. *Eur J Prev Cardiol*, 2047487318766612 (2018).
231. R. P. Giugliano *et al.*, Clinical Efficacy and Safety of Evolocumab in High-Risk Patients Receiving a Statin: Secondary Analysis of Patients With Low LDL Cholesterol Levels and in Those Already Receiving a Maximal-Potency Statin in a Randomized Clinical Trial. *JAMA Cardiol* **2**, 1385-1391 (2017).
232. K. K. Ray *et al.*, Reductions in Atherogenic Lipids and Major Cardiovascular Events: A Pooled Analysis of 10 ODYSSEY Trials Comparing Alirocumab With Control. *Circulation* **134**, 1931-1943 (2016).
233. A. M. Doerfler *et al.*, LPA disruption with AAV-CRISPR potently lowers plasma apo(a) in transgenic mouse model: A proof-of-concept study. *Molecular Therapy - Methods & Clinical Development* **27**, 337-351 (2022).
234. C. Therapeutics, A Safety and Tolerability Study Evaluating CTX320 in Subjects With Elevated Lipoprotein(a) and a History of Atherosclerotic Cardiovascular Disease or

Calcific Aortic Valve Stenosis. https://anzctr.org.au/Trial/Registration/TrialReview.aspx?ACTRN=12623001095651, (2023).
235. C. Hong *et al.*, The E3 Ubiquitin Ligase IDOL Induces the Degradation of the Low Density Lipoprotein Receptor Family Members VLDLR and ApoER2 *. *Journal of Biological Chemistry* **285**, 19720-19726 (2010).
236. D. Weissglas-Volkov *et al.*, The N342S MYLIP polymorphism is associated with high total cholesterol and increased LDL receptor degradation in humans. *J Clin Invest* **121**, 3062-3071 (2011).
237. C. Hong *et al.*, The LXR-Idol axis differentially regulates plasma LDL levels in primates and mice. *Cell Metab* **20**, 910-918 (2014).
238. T. Koike *et al.*, IDOL Deficiency Inhibits Cholesterol-Rich Diet–Induced Atherosclerosis in Rabbits. *Arteriosclerosis, Thrombosis, and Vascular Biology* **45**, 669-671 (2025).
239. L. Trapani, M. Segatto, V. Pallottini, Regulation and deregulation of cholesterol homeostasis: The liver as a metabolic "power station". *World J Hepatol* **4**, 184-190 (2012).
240. V. T. Chu *et al.*, Efficient generation of Rosa26 knock-in mice using CRISPR/Cas9 in C57BL/6 zygotes. *BMC Biotechnology* **16**, 4 (2016).
241. J. K. Hoober, ASGR1 and its enigmatic relative, CLEC10A. *International journal of molecular sciences* **21**, 4818 (2020).
242. N. M. van Loon *et al.*, Inactivation of the E3 Ubiquitin Ligase IDOL Attenuates Diet-Induced Obesity and Metabolic Dysfunction in Mice. *Arterioscler Thromb Vasc Biol* **38**, 1785-1795 (2018).
243. M. Kosicki, K. Tomberg, A. Bradley, Repair of double-strand breaks induced by CRISPR-Cas9 leads to large deletions and complex rearrangements. *Nat Biotechnol* **36**, 765-771 (2018).
244. H. Jiang *et al.*, Effects of transient immunosuppression on adenoassociated, virus-mediated, liver-directed gene transfer in rhesus macaques and implications for human gene therapy. *Blood* **108**, 3321-3328 (2006).
245. S. R. Ferdosi *et al.*, Multifunctional CRISPR-Cas9 with engineered immunosilenced human T cell epitopes. *Nat Commun* **10**, 1842 (2019).
246. Y. Yan *et al.*, Non-viral vectors for RNA delivery. *J Control Release* **342**, 241-279 (2022).
247. M. von Scheidt *et al.*, Applications and Limitations of Mouse Models for Understanding Human Atherosclerosis. *Cell Metab* **25**, 248-261 (2017).